Fair and Risk-Averse Resource Allocation in Transportation Systems under Uncertainties

Luying Sun

Dissertation submitted to the Faculty of the
Virginia Polytechnic Institute and State University
in partial fulfillment of the requirements for the degree of

Doctor of Philosophy
in
Industrial and Systems Engineering

Weijun Xie, Chair
Peng Wei
Xiaowei Yue
Haibo Zeng

May 31, 2023
Blacksburg, Virginia

Keywords: Resource Allocation, Mixed-Integer Programming, Valid Inequalities, Fairness, Risk-Averse

Copyright 2023, Luying Sun

Fair and Risk-Averse Resource Allocation in Transportation Systems under Uncertainties

Luying Sun

ABSTRACT

Addressing fairness among users and risk mitigation in the context of resource allocation in transportation systems under uncertainties poses a crucial challenge yet to be satisfactorily resolved. This dissertation attempts to address this challenge, focusing on achieving a balance between system-wide efficiency and individual fairness in stochastic transportation resource allocation problems.

To study complicated fair and risk-averse resource allocation problems - from public transit to urban air mobility and multi-stage infrastructure maintenance - we develop three models: DrFRAM, FairUAM, and FCMDP. Each of these models, despite being proven NP-hard even in a simplistic case, inspires us to develop efficient solution algorithms. We derive mixed-integer linear programming (MILP) formulations for these models, leveraging the unique properties of each model and linearizing non-linear terms. Additionally, we strengthen these models with valid inequalities. To efficiently solve these models, we design exact algorithms and approximation algorithms capable of obtaining near-optimal solutions.

We numerically validate the effectiveness of our proposed models and demonstrate their capability to be applied to real-world case studies to adeptly address the uncertainties and risks arising from transportation systems. This dissertation provides a foundational platform for future inquiries of risk-averse resource allocation strategies under uncertainties for more efficient, equitable, and resilient decision-making. Our adaptable framework can address a variety of transportation-related challenges and can be extended beyond the transportation domain to tackle resource allocation problems in a broader setting.

Fair and Risk-Averse Resource Allocation in Transportation Systems under Uncertainties

Luying Sun

GENERAL AUDIENCE ABSTRACT

In transportation systems, decision-makers constantly strive to devise the optimal plan for the most beneficial outcomes when facing future uncertainties. When optimizing overall efficiency, individual fairness has often been overlooked. Besides, the uncertainties in the transportation systems raise serious questions about the adaptability of the allocation plan. In response to these issues, we introduce the concept of fair and risk-averse resource allocation under uncertainties in this dissertation. Our goal is to formulate the optimal allocation plan that is both fair and risk-averse amid uncertainties.

To tackle the complexities of fair and risk-averse resource allocation problems, we propose innovative methods and practical algorithms, including creating novel formulations as well as deriving super-fast algorithms. These solution approaches are designed to accommodate the fairness, uncertainties, and risks typically in transportation systems. Beyond theoretical results, we apply our frameworks and algorithms to real-world case studies, thus demonstrating our approaches' adaptability to various transportation systems and ability to achieve various optimization goals. Ultimately, this dissertation aims to contribute to fairer, more efficient, and more robust transportation systems. We believe our research findings can help decision-makers with well-informed choices about resource allocation in transportation systems, which, in turn, lead to the development of more equitable and reliable systems, benefiting all the stakeholders.

Dedication

To my parents and partner.

Acknowledgments

I would like to convey my gratitude to my advisor, Dr. Weijun Xie, for his patience and enlightening guidance throughout my Ph.D. journey. My hearty thanks also extend to Dr. Peng Wei for his consistent support and scholarly insight into my research projects. In addition, I hold a deep appreciation for my academic committee, Dr. Xiaowei Yue and Dr. Haibo Zeng, for their invaluable suggestions, which shaped my graduate studies.

My years at Virginia Tech were memorable by collaborating with many talented colleagues. I extend my sincere thanks to Tim Witten for his invaluable support of my research pertaining to Blacksburg Transit. As part of my Ph.D. studies, I had a unique learning opportunity to spend my summer at Metron. I am especially thankful to my mentors, Robert Hoffman, Bert Hackney, and Rafal Kicinger, for their thoughtful discussions and input, which greatly inspired my understanding of urban air mobility.

Ultimately, I wish to express my deepest gratitude to my parents and partner, whose unwavering support has been my strength during this journey. Equally, I am incredibly thankful for the support and engagement of my friends. The journey to this point has been challenging, but knowing I had their support made the journey worthwhile.

Contents

List of Figures xi

List of Tables xiii

1 Introduction 1

1.1 Background and Motivation 1

1.2 Research Objectives 2

1.3 Dissertation Organization 3

2 Literature Review 4

2.1 Public Transit 4

2.2 Urban Air Mobility 5

2.3 Constrained Markovian Decision Processes 6

2.4 Stochastic and Robust Optimization 8

2.5 Fairness and Risk-Aversion 9

3 Distributionally Robust Fair Transit Resource Allocation During a Pandemic 11

3.1 Introduction 11

3.1.1 Summary of Main Contributions 12

3.2 Model Formulation 14
3.2.1 Wasserstein Ambiguity Set 20
3.3 Model Properties 22
3.3.1 Computational Complexity of DrFRAM (3.5) 22
3.3.2 Theoretical Sensitivity Analyses and Model Simplification 24
3.4 Linearizing the Second-stage Problem 27
3.4.1 Linearizing Constraints (3.2b) 28
3.4.2 Linearizing the Second-stage Objective Function (3.2a) 29
3.4.3 An Exact Mixed-Integer Linear Programming (MILP) Reformulation for DrFRAM (3.7) 30
3.5 Stronger Formulations and Valid Inequalities 37
3.5.1 Convexification of Set X_i^1 38
3.5.2 Convexification of Set $X_{ij\ell}^2$ 39
3.5.3 Valid Inequalities 43
3.6 Approximation Algorithms Based on No-One-Left Policy 45
3.6.1 Enhancing No-one-left Policy 47
3.7 Numerical Study 48
3.7.1 Results of Small Instances 48
3.7.2 Results of Larger Instances 55
3.7.3 Out-of-sample Performance 58

3.7.4 Blacksburg Transit Case Study 61

3.8 Conclusion 66

4 On a Fair and Risk-averse Urban Air Mobility Resource Allocation Problem Under Demand and Capacity Uncertainties 68

4.1 Introduction 68

4.1.1 Summary of Main Contribution 70

4.2 Model Formulation 72

4.3 Model Properties 79

4.3.1 Computational Complexity of FairUAM (4.1) 79

4.3.2 Sensitivity Analyses 82

4.3.3 Model Simplification and Integrality of Decision Variables 84

4.4 Valid Inequalities and A Solution Method 87

4.4.1 Valid Inequalities 87

4.4.2 A Decomposition Algorithm 92

4.5 Numerical Study 96

4.5.1 Results on Random Instances 97

4.5.2 Case Study on a Real-World Network 102

4.6 Conclusion 110

5 Fair Constrained Markovian Decision Processes Problems 111

5.1 Introduction . . . 111
5.1.1 Summary of Main Contributions . . . 112
5.2 Fair Budget-Constrained MDP under a Finite Horizon . . . 113
5.2.1 Model Formulation . . . 114
5.2.2 An MILP Formulation . . . 116
5.3 Linearization and Relaxation Schemes . . . 117
5.3.1 Continuous Relaxation . . . 118
5.3.2 Lagrangian Relaxation . . . 121
5.4 An Effective Heuristic Solution Algorithm . . . 125
5.5 An extension: Fair Budget-Constrained MDP under Infinite Horizon . . . 127
5.6 Numerical Study . . . 130
5.6.1 Results on Hypothetical Instances . . . 130
5.6.2 Case Study on A Bridge Maintenance Problem . . . 135
5.7 Conclusion . . . 136

6 Conclusion **138**

Bibliography **140**

Appendices **159**

Appendix A Appendix of Chapter 3 **160**

A.1 Summary Statistics of Data 160

A.2 Testing Integrality of L_{ij} 161

A.3 Reformulation of the Model (3.1) with Moment Ambiguity Set 161

List of Figures

3.1 Tuning the Wasserstein Radius and Comparing the DrFRAM, RO and SAA Solutions. 61

3.2 Confidence Intervals of DrFRAM Objective Values and Mean-Risk Objective Values 64

3.3 A Comparison of Risk-Neutral Objective Values for Four Different Methods with Different Noise Levels 65

3.4 Sensitivity Analysis on Model Parameters 65

3.5 A Comparison of Route-based Weighted Sum of Bus Utilization Rate and Passenger Abandon Rate Among Four Different Results. Here, xticks are route names of Blacksburg Transit and route-based objective represents the weighted sum of bus utilization rate and passenger abandon rate for each route. 66

3.6 A Comparison of Routed-based Total Bus Capacity Between the Current Assignment and DrFRAM Result 67

3.7 Illustration of Route HWA/HWB and Route MSA 67

4.1 An illustration of the FairUAM network and its components 73

4.2 An illustration of one OD pair and two routes with different bottleneck visiting sequences 91

4.3 Comparison of Lower Bound and Optimality Gap with and without the Valid Inequalities 100

4.4 Evaluation of the Objective Value when Airspace Capacity Decreases or Demand Increases . . . 101

4.5 Trade-off between Fairness and Efficiency . . . 102

4.6 Map of 13 airports within 50 miles from KSEA . . . 103

4.7 Evaluation of Total Operation Cost when Passenger Demand Increases . . . 106

4.8 Impact on Total Operation Cost and Fairness while Increasing Total Capacity of Busy Bottleneck Points (KSEA, KBFI, 2S1, KTIW) or Taking Detours to Avoid Them . . . 109

4.9 Evaluation of Total Operation Cost and Largest Average Company Cost when Airspace Capacity Changes . . . 109

5.1 Impact of Discount Factor α and Weighted Scalar ρ . . . 134

List of Tables

3.1 Results of Different MILP Formulations 50

3.2 Results of Continuous Relaxations of Different MILP Models 51

3.3 Results of Four Scenario Decomposition Algorithm 1 Based on Four Different MILP Formulations and Two Approximate Methods (i.e., Algorithm 3, Algorithm 4) 53

3.4 Results of Instances with a Larger Objective Value 54

3.5 Results of MILP.B and MILP.VI for Solving Larger Instances 56

3.6 Results of MILP.CONV and MILP.VI.CONV for Solving Larger Instances . 57

3.7 Results of Continuous Relaxations of Four Different MILP Formulations for Solving Larger Instances 58

3.8 Results of Three Scenario Decomposition Algorithm 1 Based on Three Different MILP Formulations (i.e., MILP.B, MILP.CONV, MILP.CONV.VI) for Solving Larger Instances 59

3.9 Results of the Scenario Decomposition Algorithm 1 Based on MILP.VI, Denoted by Algorithm 1.VI, Scenario Decomposition with Grouping Algorithm 2 Based on MILP.VI, Denoted by Algorithm 2.VI, and Two Approximate Methods (i.e., Algorithm 3, Algorithm 4) for Solving Larger Instances 60

3.10 Cross Validation Results of Blacksburg Transit Data 63

4.1 Random Instance Setting and Results of Different Formulations and Algorithm 5 . . . 99

4.2 Results of Case Study on A Real-World Network . . . 106

4.3 Airspace Utilization Rate . . . 108

5.1 Results of MILP (5.10) and Continuous Relaxation/Randomized Policy . . . 132

5.2 Results of Algorithm 6 . . . 132

5.3 Impact of Discount Factor . . . 133

5.4 Impact of Weighted Scalar . . . 134

5.5 Results of Case Study on Bridge Maintenance . . . 136

A.1 Summary of Statistics of the Blacksburg Transit Data . . . 160

A.2 Objective Value of MILP with Integer $\boldsymbol{L}$ and MILP with Continuous $\boldsymbol{L}$ . . . 162

A.3 Bus assignment of MILP with Integer $\boldsymbol{L}$ and MILP with Continuous $\boldsymbol{L}$ . . . 162

Chapter 1

Introduction

1.1 Background and Motivation

Resource allocation is one of the classic problems in a centralized decision-making environment, especially with the application to transportation. The centralized decision-makers are interested in finding the most preferred allocation plans to satisfy the overall goal across the different stakeholders. In the meantime, the allocation plan must be successfully adapted to possible scenarios when the resource demand or capacity is not deterministic, since transportation problems are typically characterized by highly dynamic information processes. For example, in public transit, actual passenger demands are hard to estimate, even with historical data. In urban air mobility, passengers request the service a few days or even hours in advance. Furthermore, to better align with the highly dynamic nature of various systems, sequential decision-making processes are employed across many domains, including infrastructure maintenance, vehicle path planning, communication, and so on. Under these circumstances, deterministic models, ignoring the inherent uncertainties, may not be realistic and may generate inferior decision-making; on the other hand, stochastic programming is an effective way of evolving those uncertainties in resource allocation problems in transportation to take advantage of accounting for multiple scenarios of uncertainties. Furthermore, when the decision-makers and stakeholders prefer low risk in the outcomes among all the scenarios, besides optimizing the overall goal of minimum cost, a risk-averse allocation plan

is reliable for all scenarios and is also of vital importance to hedge against future uncertainties. To achieve the best overall goal, the most efficient way is to minimize the total cost collaboratively among all the stakeholders. However, this framework may not consider the individual benefits, and may only benefit few individuals by sacrificing others to achieve the best overall systematic outcome. This motivates us to consider fairness among different stakeholders.

1.2 Research Objectives

The presence of risk-aversion and fairness among different stakeholders brings in severe modeling challenges to resource allocation problems, especially when only limited data on uncertainties is available for decision-making. Based on different problem structures, the nonlinear terms of the models, as a result of incorporating the features of risk-aversion and fairness, as well as stochasticity, further complicate the models. This dissertation aims to develop mathematical tools to address these challenges. In particular, we would like to address the following main research questions:

i When only limited data is available, and the estimation of the underlying distribution of the uncertainties is subject to error, how to find the best fair allocation plan that also hedges against future uncertainties?

ii If both the capacity and demand are dynamically evolving, how to balance the uncertainties between them in a fair and risk-averse way?

iii If the decision process is multistage, what is the best fair resource allocation plan?

1.3 Dissertation Organization

This dissertation will be organized in a multiple-chapter format. Chapter 2 briefly reviews the related literature and recent advancements. Chapter 3 derives a Distributionally robust Fair transit Resource Allocation model (DrFRAM) under a data-driven ambiguity set to hedge against future uncertainties with limited data. In Chapter 4, a Fair and Risk-averse Urban Air Mobility resource allocation model (FairUAM) is proposed to coordinate multiple service providers while achieving both efficiency and fairness. Chapter 5 presented a fair budget-constrained Markovian Decision Processes model (FCMDP) to address the fairness among multiple agents in multistage decision processes. Chapter 6 concludes this dissertation and discusses the potential future research directions.

Chapter 2

Literature Review

2.1 Public Transit

Transit system design and optimization have been widely studied in the literature (Daganzo and Ouyang [1], Ceder [2]). The works in transit are mainly on optimal scheduling and routing to serve the public better. Chien and Schonfeld [3] incorporated spatial characteristics and demand patterns of urban areas into their optimization model. Other important earlier works can be found in De Cea and Fernández [4], Quadrifoglio et al. [5], Guan et al. [6], Jeihani et al. [7] or in the review papers Guihaire and Hao [8], Hörcher and Tirachini [9]. Recently, Nourbakhsh and Ouyang [10] focused on the flexible transit design in the low-demand areas, and Ouyang et al. [11] proposed a continuum approximation approach for bus design under heterogeneous demand. Chen and Nie [12] attempted to integrate an e-hailing system with public transit. Iliopoulou and Kepaptsoglou [13] jointly optimized network design and charging infrastructure locations for the electric buses. Abdolmaleki et al. [14] built a new model for synchronizing timetables in a transit network that minimizes the total transfer waiting time. There are a lot more interesting works in the literature focusing on different optimization problems (Román-De la Sancha et al. [15], Matisziw et al. [16], Jin et al. [17], Agarwal and Ergun [18], Mahéo et al. [19]). The study of transit design during a pandemic, especially the COVID-19 pandemic, is rather limited. The COVID-19 pandemic caused a major transit demand decline for many public transit systems in the United States

due to the fear of contracting the disease, practicing social distancing, and lockdown policy, which has also been observed by many social workers (Liu et al. [20]). Mo et al. [21] studied the epidemic spreading model in the time-varying transit network. Chen et al. [22] redesigned the campus bus systems by shortening the routes and enforcing social distancing. Gkiotsalitis and Cats [23] and Yang and Nie [24] optimized metro service frequency during the COVID-19 pandemic.

2.2 Urban Air Mobility

Vascik and Hansman [25] addressed key operational constraints anticipated to impact on-demand air mobility were proposed and addressed. For selecting appropriate vertiport locations, Fadhil [26] used a geographic information-based analysis to find suitable sites, Daskilewicz et al. [27] studied an integer programming model to maximize the population-cumulative potential time savings, Rajendran and Zack [28] developed an iterative constrained clustering method to recommend potential facility locations and Rath and Chow [29] proposed a mixed-integer linear programming (MILP) model to maximize the revenue and ridership. We refer interested readers to Garrow et al. [30] and Rajendran and Srinivas [31] for a comprehensive review on UAM, including its history, aircraft technology, demand prediction, infrastructure design, and operations. Thipphavong et al. [32] is among the first that expanded the NASA operational concepts for UAM. Mueller et al. [33] proposed a framework for on-demand mobility airspace, including demand-capacity balancing and trajectory planning. Kleinbekman et al. [34] introduced an energy-efficient trajectory optimization model for UAM arrival with route selection capability, proposing a mixed-integer linear program to determine aircraft arrival sequence and minimize total arrival delay. Bharadwaj et al. [35] presented a decentralized procedure for route planning on individual vehicles us-

ing Markov decision processes. Researchers also developed models and methods on flight scheduling and dispatching (Shihab et al. [36, 37], Roy et al. [38]). Bharadwaj et al. [39] designed a scalable planning framework with safety-oriented constraints and minimized the violations. Wu and Zhang [40] designed an integer programming model considering potential UAM travel demand to decide the optimal vertiport locations and user allocation to vertiports. Wang et al. [41] developed an aggregate three-dimension air traffic assignment framework to plan for future UAM operations.

2.3 Constrained Markovian Decision Processes

Traditional MDPs can be solved via value iteration or policy iteration (Puterman [42]), which can also be conveniently solved through linear programs with finite horizon (Golabi et al. [43]) or infinite horizon (Puterman [42]). In particular, it has been shown that these linear programs have an optimal solution corresponding to a deterministic policy (Puterman [42]). However, these solution methods become inadequate when dealing with general CMDPs in order to search for optimal deterministic policy under constraints (Altman [44], Hawkins [45], Adelman and Mersereau [46], Chen et al. [47]). As observed by many researchers (Adelman and Mersereau [46], Chen et al. [47], Dimitrov and Morton [48]), within a deterministic policy, each state will choose a particular action, which essentially is equivalent to the following integer program: define a binary vector for each state, this vector is feasible if and only if it has one nonzero component. This integer program reformulation exhibits a remarkably powerful modeling technique. One example is the multi-arm bandit (MAB) problem (Gittins [49], Whittle [50], Gittins and Jones [51], Hosseini et al. [52]), a classic sequential decision model used to optimize the resource allocation among multiple projects (or bandits) over time. The objective of an MAB is to find a policy for the sequential selection of active projects

based on the current states, such that the expected total discounted reward is maximized over an infinite time horizon. It is easy to see that an MAB is a special case of CMDPs with restrictions on the action space. Albeit important, many researches merely focus on the reformulation of CMDPs. Indeed, this class of problems involves significant modeling and algorithmic challenges. It is fundamentally important to analyze the model structure and develop computationally effective algorithms for these models.

Recently, there have been some efforts in solving CMDPs. Authors in Adelman and Mersereau [46], Hu et al. [53] proposed a Lagrangian relaxation approach, which has been demonstrated as an efficient solution algorithm to solve CMDPs. Alternatively, Caramanis et al. [54] suggested solving the CMDPs via a column generation procedure. Since it is known that the Lagrangian relaxation is equivalent to the column generation method, these two methods always output the same optimal value. A comprehensive survey of existing CMDP algorithms was conducted in De Nijs et al. [55], which outlined their advantages and disadvantages, as well as identified their applicable domains. Moreover, authors in de Nijs and Stuckey [56] developed a replanning framework that used a Lagrangian relaxation-based column generation procedure, thereby addressing the weaknesses in existing constraint relaxation algorithms for CMDPs. Furthermore, Shi et al. [57] studied an aerial-ground vehicle routing problem and transformed it into a CMDP problem to address the challenge in vehicle energy consumption. Considering long-term fairness within MDPs, Wen et al. [58] studied recommendation systems through a CMDP with fairness constraints. Chadha et al. [59] integrated a rigid fairness constraint in a battery-sharing problem and constructed a CMDP-based framework to maximize efficiency. Chen et al. [60] addressed a same-day delivery problem as a multi-objective MDP, aiming to maximize a weighted sum of overall expected performance and minimal individual service rate. However, for practically implementable decision-making, the deterministic policy is more desirable, and unfortunately, there is little work studying

fair CMDP with deterministic policy.

To bridge this gap, we study budget-constrained MDP with a deterministic policy, wherein multiple agents collaborate in the decision-making processes. An example of this can be seen in the infrastructure maintenance problem involving multiple bridges (Hu et al. [53]). We reveal the connection between a budget-constrained MDP and a mixed integer linear program (MILP). We first consider the budget-constrained MDP under a finite horizon. Based upon the observation that each agent chooses only one action for each state in a deterministic policy, we propose an MILP for the budget-constrained MDP. It turns out that the relaxation bound of this proposed MILP recovers the Lagrangian dual bound. In order to efficiently solve the problem, we propose an approximation solution algorithm and extend our model to accommodate an infinite-horizon case.

2.4 Stochastic and Robust Optimization

Stochastic programming has been widely used in resource allocation problems in transportation for decades (Powell and Topaloglu [61]). Recent advances in stochastic and robust optimization provide tools for resource allocation problems under uncertainty (Li et al. [62], Fernandes et al. [63], Li et al. [64], Fu and Lam [65], Hamdouch et al. [66], Hadas and Shnaiderman [67]). Shehadeh [68] proposed a distributionally robust optimization (DRO) model to plan fleet-sizing, routing, and scheduling for mobile facilities to minimize the conditional value at risk (CVaR) of the operational cost. Moug et al. [69] formulated a two-stage stochastic model to recruit drivers and optimize resource planning with constraints on the total number of unserved evacuees.

Regarding public transit, Kulshrestha et al. [70] developed a robust model for bus dispatching for evacuations to optimize the total travel time under demand uncertainty. An and

Lo [71] studied transit system design under demand uncertainty using two-stage stochastic programming. Liang et al. [72] proposed a two-step modeling framework for the bus transit network design considering an existing metro network and demand uncertainty. In Yoon and Chow [73], the authors provided a sequential learning framework to address the demand uncertainty when designing lines and routes in the transit system.

For urban air mobility, Mukherjee and Hansen [74] developed three stochastic air traffic flow management (ATFM) models with static ground delay and dynamic rerouting decisions. Ganji et al. [75] proposed a stochastic optimization model to assign ground delay and optimize rerouting decisions at the same time by considering the en-route capacity. Gupta and Bertsimas [76] presented a robust and adaptive ATFM framework under airspace capacity uncertainty, which was solved by piecewise affine policies. Wang and Jacquillat [77] proposed a two-stage stochastic integrated model to optimize aircraft scheduling and ground-holding operations under operating uncertainty and developed a decomposition algorithm with dual integer cuts to solve it. In volatile environments, instead of optimizing the average performance using risk-neutral objectives, risk aversion is commonly used to hedge against uncertainty and enforce safety in the worst case.

2.5 Fairness and Risk-Aversion

Gabrel et al. [78] and Rahimian and Mehrotra [79] surveyed the recent advances in robust optimization (RO), distributionally robust optimization (DRO), and the relationships therein. Hou et al. [80] worked on risk-averse stochastic UAM network design in a data-driven framework, considering vertiport location selection and aircraft route planning. Yan and Howe [81] briefly introduced equity in urban mobility. Bertsimas et al. [82] characterized the trade-off between efficiency and fairness and discussed different fairness considerations from manage-

rial prescriptions for different problems. Chen et al. [83] derived a chance-constrained model based on probabilistic airspace capacity and developed a polynomial approximation-based approach to solve a large-scale problem. Rodionova et al. [84] addressed fairness by adding the min-max fairness measure into their deterministic model. Hamdan et al. [85] developed an ATFM model with rerouting under deterministic capacity considering delay distribution and flight reversal fairness. Hamdan et al. [86] proposed a deterministic model with central authority considering path rerouting and options and inter-flight and inter-airline fairness. Pelegrín et al. [87] proposed a deconfliction model to minimize the total deviation from flight schedules in a fair way, and Wu et al. [88] introduced a path planning algorithm for multiple aircraft with fairness awareness to generate collision-free paths under the vehicle and environmental uncertainties. Chin et al. [89] focused on three fairness metrics for on-demand air mobility resource allocation in a rolling horizon to incorporate the dynamic demand. Bennaceur et al. [90] proposed a MILP model for the UAM air-taxi problem with fairness between the regular and premium classes. To efficiently solve the problem, they decomposed the original model into two subproblems, then used a beam-search algorithm to solve them.

Chapter 3

Distributionally Robust Fair Transit Resource Allocation During a Pandemic

3.1 Introduction

The recent outbreak of the SARS-CoV-2 (i.e., COVID-19 disease) has been profoundly influencing society. Many schools have been shut down and turned online; many restaurants and shopping malls have either been closed or significantly reduced capacity; many firms have required employees to work from home. On the other hand, as the vaccination process has been accelerated and the promise of the vaccines, the number of COVID-19 infection cases in the U.S. has been decreasing since January 2021. Therefore, many states are now re-opening the business as well as schools; for example, the Commonwealth of Virginia's public schools have been re-opened since March 2021. Starting from August 2021, as the viruses are constantly evolving into new variants which may be more infectious than the original ones, many states have restarted the mask mandates in public conveyances and indoor activities. Undoubtedly, these policies have tremendously influenced people's daily activities, which causes a significant demand uncertainty for public transit. Besides demand uncertainty, to keep passengers safe and prevent transmission of coronaviruses, it is of vital

importance to observe the social distancing within the public transit, which in turn will reduce the capacity of transit vehicles (e.g., buses) and thus affect the entire operations of the public transit systems. This chapter is trying to solve this issue. The results in this chapter are also useful for another wave of COVID-19 outbreaks or preparing for a future pandemic.

The authors collaborate with local Blacksburg Transit, a daily outdoor transportation tool used by many students and residents in the Town of Blacksburg. Blacksburg Transit collects daily operating data, including the number of passengers on each bus and a timestamp in the format of "mm/dd/yyyy hh:mm:ss," and the data are updated in minutes. Unfortunately, many Blacksburg Transit data have enormous missing values due to frequent sensor malfunctioning. During the COVID-19 pandemic, transit operators have noticed that the imbalance among routes often happens, and many residents change their daily commuting plans (e.g., working from home, virtual classes). Blacksburg Transit is eager to figure out an appropriate operation plan for the new travel activities. Since the training of employees and installation of bus stops can cause much longer delays and aggravate the under-staffing issue, the transit operators in Blacksburg Transit would like to keep the current routes and stops as they are but to optimize the transit resources, i.e., bus allocation, to minimize their highest utilization rates as well as social equity. This motivates us to study the fair transit resource allocation problem. As Blacksburg Transit shares with us the passenger alighting and boarding data, we are able to build a data-driven optimization model to leverage these available data to account for future uncertainties.

3.1.1 Summary of Main Contributions

The objective of this study, motivated by Blacksburg Transit, is to determine optimal transit resource allocation to minimize the highest bus utilization rate and the largest passenger

abandon rate with limited bus operation data given to achieve better social equity under stochastic passenger arrival and alighting rates and overcome the future uncertainties as much as we can to serve the passengers better. This gives rise to Distributionally robust Fair transit Resource Allocation model (DrFRAM) under a data-driven ambiguity set. The main contributions of DrFRAM are summarized below:

(i) We study DrFRAM under type-∞ Wasserstein ambiguity set. As far as we are concerned, our DrFRAM model is the first one focusing on fair multi-type transit resource allocation under passenger arrival and alighting rates uncertainty. We prove that DrFRAM cannot be solved in a polynomial time unless $P = NP$ even when the problem is deterministic and there are only two types of buses.

(ii) We derive the monotonicity properties of the DrFRAM, using which we can significantly simplify the DrFRAM and linearize the nonlinear components in the objective of DrFRAM.

(iii) We propose a mixed-integer linear programming (MILP) formulation for DrFRAM by binarizing integer variables and linearizing the nonlinear functions using McCormick inequalities. To strengthen the MILP formulation, we derive stronger ones and develop valid inequalities by exploiting the model structures. These formulations allow us to design efficient scenario decomposition methods.

(iv) Besides these exact methods, we develop an approximate scenario decomposition method using objective cuts to speed up the convergence and No-one-left based approximation algorithm for solving DrFRAM to near-optimality. Both approaches come with theoretical approximation guarantees, demonstrating the strengths of these approaches.

(v) We numerically demonstrate the effectiveness of the proposed approaches, outperforming the sampling average approximation method, and apply them to solve the real-world

instances using the data provided by Blacksburg Transit.

Notation. The following notation is used throughout the chapter. We use bold letters (e.g., $\boldsymbol{x}, \boldsymbol{A}$) to denote vectors and matrices and use corresponding non-bold letters to denote their components. Given a vector or matrix $\boldsymbol{x}$, its zero norm $\|\boldsymbol{x}\|_0$ denotes the number of its nonzero elements. We let $\mathbf{e}$ be the vector or matrix of all ones and let $\mathbf{e}_i$ be the ith standard basis vector. Given an integer n, we let $[n] := \{1, 2, \ldots, n\}$, and use $\mathbb{R}^n_+ := \{\mathbf{x} \in \mathbb{R}^n : x_i \geq 0, \forall i \in [n]\}$. Given a real number t, we let $(t)_+ := \max\{t, 0\}$. Given a finite set I, we let $|I|$ denote its cardinality. We let $\tilde{\boldsymbol{\xi}}$ denote a random vector and denote its realizations by $\boldsymbol{\xi}$. We use superscript $k \in [N]$ to denote the index of scenario k. For a matrix $\boldsymbol{A}$, we let $\boldsymbol{A}_{i:}$ denote ith row of $\boldsymbol{A}$ and $\boldsymbol{A}_{:j}$ denote jth column of $\boldsymbol{A}$. Additional notations will be introduced as needed.

Organization. The remainder of the chapter is organized as follows. In Section 3.2, we introduce the model formulation. Sections 3.3 and 3.4 show model properties and derive an equivalent mixed-integer linear programming formulation. Section 3.5 shows the convexification of two substructures and derivation of strong valid inequalities, and Section 3.6 develops approximation algorithms. Finally, Section 3.7 numerically demonstrates the effectiveness of the proposed solution approaches, and Section 3.8 concludes this chapter.

3.2 Model Formulation

We collaborate with Blacksburg Transit in this research. Since March 2020, Blacksburg Transit has been making efforts to prevent the spread of the pandemic and reduce the risk of exposure to COVID-19 in order to support the town better. In particular, they are curious about the optimal plan of bus resource allocation to minimize the highest bus utilization rate during the pandemic. They are willing to provide us with recent transit sensor

data about passengers' arrival and alighting information to support our research. However, due to various reasons, such as sensor malfunctioning, a lot of data has a large portion of missing values, and only a small subset of the data provided to us (less than 30 samples) can be useful in our research. Exploring these data and talking to Blacksburg Transit operators, we see that some buses are overcrowded while others are empty at most times. The routes connecting the residential areas to the campus have much fewer passengers on the bus than those connecting downtown Blacksburg to the campus (see a detailed summary of statistics of the Blacksburg Transit data in Appendix A.1). Those overcrowded buses may be difficult to enforce the social distancing requirement and increase the risk of virus exposure. Besides, the transit operators have little knowledge of underlying probability distribution nor moment information of the passenger arrival or alighting rates, especially during the pandemic. Therefore, motivated by Blacksburg Transit, we plan to formulate the problem as a Distributionally robust Fair transit Resource Allocation model (DrFRAM) using a data-driven ambiguity set, which allows us to leverage the collected dataset to its maximum extent and account for non-stationary uncertainties in the near future.

For the strategic planning purpose as well as considering the intrinsic problem structure of DrFRAM that passenger's arrival and alighting data are available, we adopt the modeling of a transit system based on the seminal work in Hadas and Shnaiderman [67] using aggregate arrival and alighting rates and not relying on the user-specific origin-destination data, since the former is easy to obtain and the latter is difficult to get access to in the transit data available to us. In DrFRAM, there are K different types of buses, where each bears a nominal capacity c_k for each $k \in [K]$, and there are η_k type-k buses. Note that during a pandemic, to observe social distancing strictly, the bus capacities will be decreased proportionally and strictly enforced to keep passengers safe and sound. Thus, we let a pandemic factor $\delta_k \in [0, 1]$ denote the percent of a type k bus capacity that allows being operated. That is, only $\lfloor \delta_k c_k \rfloor$

passengers will be allowed onto the bus during a pandemic. Suppose that there are I distinct bus routes, and for each bus route $i \in [i]$, there are J_i bus stops. Since passengers can alight and depart a bus at any bus stop for each $i \in [I]$ and $j \in [J_i]$, we let the random parameter $\tilde{a}_{ij} \in [0, 1]$ denote the proportion of passengers alighting from the bus and let the random variable $\tilde{\lambda}_{ij} \in \mathbb{Z}_+$ represent the passenger arrival rate during a unit time interval, i.e., the number of passengers arriving during that time. Note that $\tilde{\boldsymbol{a}}, \tilde{\boldsymbol{\lambda}}$ are both random since they can vary over time and change with the severeness of the pandemic. For notational convenience, we let $\tilde{\boldsymbol{\xi}} = (\tilde{\boldsymbol{a}}, \tilde{\boldsymbol{\lambda}})$. Since the historical data are available to us, in DrFRAM, we use the Wasserstein distance to characterize the random parameters, which can both ensure the model to data-driven and robust (see, e.g., Kuhn et al. [91]).

The transit operators would like to know that given the predetermined routes (so they should not re-train their employees), what is the fairest way to allocate buses so that the passengers will be the best serviced and the safety policies should be strictly enforced? To help them make a better decision, we let the integer variable $n_{ik} \in \mathbb{Z}_+$ denote the number of type $k \in [K]$ buses allocated to the $i \in [I]$th route. Due to consistency and for ease of management, the transit operators would like to ensure that each route is subject to the same type of bus whenever possible. Thus, we let the binary variable $x_{ik} \in \{0, 1\}$ denote whether type k buses will be assigned to route $i \in [I]$ or not. Using this notation, we see that $\sum_{k\in[K]} x_{ik}\lfloor \delta_k c_k \rfloor$ represents the bus capacity at route $i \in [I]$. In our model, given a realization $\boldsymbol{\xi}$ of the random parameters $\tilde{\boldsymbol{\xi}}$, we let $L_{ij}(\boldsymbol{\xi})$ denote the number of passengers remaining on a bus right after the jth stop at route $i \in [I]$. Due to its physical meaning and the fact that the arrival rates can be quite low during the pandemic, we keep the variable $L_{ij}(\boldsymbol{\xi})$ as an integer [1]. Next, to model the social equity among different routes, we introduce two important functions. We define the bus utilization rate as the ratio of the number of

[1] Our numerical result in Appendix A.2 shows that relaxing the integrality of $L_{ij}(\boldsymbol{\xi})$ can cause a much smaller objective value and may even lead to a misleading conclusion.

passengers on the bus to the bus capacity and the passenger abandon rate as the ratio of the number of passengers who cannot get on board due to limited bus capacity to the number of passengers arrived. The operation managers would like to know an optimal way to allocate the buses, which is fair to passengers from different routes. That is, they want to ensure that both the highest bus utilization rate and the largest passenger abandon rate due to limited bus capacity among all the routes are low.

In DrFRAM, as passenger arrival and alighting rates are often subject to change over time, and their joint probability distribution is difficult to estimate, these two parameters are supposed to be random. Besides, we assume that

(i) the bus routes are predetermined;

(ii) each route is subject to the same type of bus;

(iii) traffic conditions (for example, congestion and interaction with pedestrians and other vehicles), staffing are not considered in our model; and

(iv) limited passenger arrival and alighting data are available.

After talking to Blacksburg Transit operators, we were informed that these assumptions are consistent with the daily operations in Blacksburg Transit during the COVID-19 pandemic. With the notation introduced above, we are ready to present the mathematical formulation of DrFRAM as below:

$$\text{(DrFRAM)} \qquad v^* = \min_{\boldsymbol{n},\boldsymbol{x}} \sup_{\mathbb{P}\in\mathcal{P}} \mathbb{E}_{\mathbb{P}}\left[\mathcal{Q}\left(\boldsymbol{n},\boldsymbol{x},\tilde{\boldsymbol{\xi}}\right)\right], \tag{3.1a}$$

$$\text{s.t.} \quad \sum_{k\in[K]} x_{ik} = 1, \forall i \in [I], \tag{3.1b}$$

$$n_{ik} \le \eta_k x_{ik}, \forall i \in [I], \forall k \in [K], \tag{3.1c}$$

$$\sum_{i\in[I]} n_{ik} \leq \eta_k, \forall k \in [K], \tag{3.1d}$$

$$\sum_{k\in[K]} n_{ik} \geq 1, \forall i \in [I], \tag{3.1e}$$

$$x_{ik} \in \{0,1\}, n_{ik} \in \mathbb{Z}^+, \forall i \in [I], \forall k \in [K]. \tag{3.1f}$$

In DrFRAM (3.1), the objective is to minimize the worst-case resource planning outcomes, where ambiguity set $\mathcal{P}$ denotes a family of probability distributions, and $\mathcal{Q}(\boldsymbol{n}, \boldsymbol{x}, \tilde{\boldsymbol{\xi}})$ denotes the random recourse function which will be specified later. Constraints (3.1b) ensure that each route will commit to one type of bus. Constraints (3.1c) and (3.1d) jointly show that the number of buses allocated to a particular route is no larger than the number of available buses. Constraints (3.1e) show that each route should have at least one bus to achieve social equity. Constraints (3.1f) specify the boundaries of the decision variables. As far as the authors are concerned, this model is new by considering multi-type transit resources, minimizing the utilization rates, minimizing the abandon rates, and achieving fairness among different routes, and has not been studied in any literature.

Given a realization $\boldsymbol{\xi}$ of random parameters $\tilde{\boldsymbol{\xi}}$ and the values of first-stage decisions $(\boldsymbol{n}, \boldsymbol{x})$, we can express the recourse function in the following way:

$$\mathcal{Q}(\boldsymbol{n}, \boldsymbol{x}, \boldsymbol{\xi}) = \min_{\boldsymbol{L}(\boldsymbol{\xi})} Q(\boldsymbol{n}, \boldsymbol{x}, \boldsymbol{\xi}, \boldsymbol{L}(\boldsymbol{\xi})) := \left\{ \max_{i\in[I], j\in[J_i]} \underbrace{\frac{L_{ij}(\boldsymbol{\xi})}{\sum_{k\in[K]} n_{ik}\lfloor \delta_k c_k \rfloor}}_{\text{bus utilization rate}} \right.$$

$$\left. + \omega \max_{i\in[I], j\in[J_i]} \underbrace{\max\left[0, 1 + \frac{1}{\lambda_{ij}}\left(\lceil (1-a_{ij}) L_{i,j-1}(\boldsymbol{\xi}) \rceil - \sum_{k\in[K]} n_{ik}\lfloor \delta_k c_k \rfloor\right)\right]}_{\text{passenger abandon rate}} \right\}, \tag{3.2a}$$

$$\text{s.t.} \quad L_{ij}(\boldsymbol{\xi}) = \min\left\{\sum_{k\in[K]} n_{ik}\lfloor\delta_k c_k\rfloor, \lceil(1-a_{ij})L_{i,j-1}(\boldsymbol{\xi})\rceil + \lambda_{ij}\right\}, \forall i \in [I], \forall j \in [J_i], \tag{3.2b}$$

$$L_{i0}(\boldsymbol{\xi}) = 0, L_{ij}(\boldsymbol{\xi}) \in \mathbb{Z}^+, \forall i \in [I], \forall j \in [J_i], \tag{3.2c}$$

where $\omega \geq 0$ is the weight that balances the importance of the highest bus utilization rate and the largest passenger abandon rate. The objective (3.2a) is to minimize the weighted highest bus utilization rate and the largest passenger abandon rate to enhance social equity. Note that we choose the min-max fairness measure in (3.2), widely used in the fairness-related literature Radunovic and Le Boudec [92], Du et al. [93]. Constraints (3.2b) postulate the number of passengers on board at each stop, which follows the convention from the existing transit literature (see, e.g., Hadas and Shnaiderman [67]). Constraints (3.2c) specify the boundary conditions of the recourse decisions, i.e., the initialization and integrality of variables $\boldsymbol{L}(\boldsymbol{\xi})$.

As mentioned at the beginning of the model formulation, the moment information is not available to us, and the limited data we obtain may not be sufficient for us to estimate the moments accurately. Besides, since the recourse function is nonlinear and nonconvex with respect to the random parameters, the separation of constraints in the dual reformulation of moment ambiguity set could be computationally challenging (see Appendix A.3 for the detailed derivation). Thus, we decide not to use a moment-based ambiguity set in this research. Instead, to fully exploit the limited data, we plan to focus on the more appropriate Wasserstein ambiguity set due to its consistency, tractability, computational advantages, as well as its flexibility to account for non-stationary uncertainties in the near future. In our numerical study, we compare the proposed Wasserstein ambiguity set with the conventional sampling average approximation approach and the robust model with the box uncertainty set.

Our results show that by tuning the Wasserstein radius, the proposed method outperforms the other two.

3.2.1 Wasserstein Ambiguity Set

In this subsection, we briefly introduce the notion of the Wasserstein ambiguity set and its attractive properties, which are suitable for DrFRAM. In this work, we were provided with historical data collected during the operations. Thus, given an empirical distribution $\mathbb{P}_{\tilde{\boldsymbol{\zeta}}}$ constructed using i.i.d. historical data $Z = \{\bar{\boldsymbol{\zeta}}^\ell = (\bar{\boldsymbol{a}}^\ell, \bar{\boldsymbol{\lambda}}^\ell)\}_{\ell\in[N]}$ such that $\mathbb{P}_{\tilde{\boldsymbol{\zeta}}}\{\tilde{\boldsymbol{\zeta}} = \bar{\boldsymbol{\zeta}}^\ell\} = 1/N$, this chapter considers the data-driven Wasserstein ambiguity set (see, e.g., Kuhn et al. [91], Gao and Kleywegt [94], Blanchet et al. [95], Esfahani and Kuhn [96], Blanchet and Murthy [97], Hanasusanto and Kuhn [98], Chen et al. [99], Xie [100], Abadeh et al. [101], Blanchet et al. [102], Chen and Xie [103]) as below:

$$\mathcal{P}_q = \left\{\mathbb{P} : W_q\left(\mathbb{P}, \mathbb{P}_{\tilde{\boldsymbol{\zeta}}}\right) \leq \theta\right\}, \tag{3.3}$$

where $\theta \geq 0$ denotes the Wasserstein radius and for any $q \in [1, \infty]$, the Wasserstein distance $W_q(:,:)$ is defined as

$$W_q\left(\mathbb{P}_1, \mathbb{P}_2\right) = \inf\left\{\sqrt[q]{\int_{\Xi\times\Xi} \|\boldsymbol{\xi}_1 - \boldsymbol{\xi}_2\|^q \mathbb{Q}(d\boldsymbol{\xi}_1, d\boldsymbol{\xi}_2)} : \begin{array}{l}\mathbb{Q} \text{ is a joint distribution of } \tilde{\boldsymbol{\xi}}_1 \text{ and } \tilde{\boldsymbol{\xi}}_2 \\ \text{with marginals } \mathbb{P}_1 \text{ and } \mathbb{P}_2, \text{ respectively}\end{array}\right\}.$$

where the support

$$\Xi = \{(\boldsymbol{a}, \boldsymbol{\lambda}) : a_{ij} \in [0,1], \lambda_{ij} \in \mathbb{Z}_+, \forall i \in [I], \forall j \in [J_i]\}.$$

When $q = \infty$, it reduces to the $\infty-$Wasserstein distance

$$W_\infty(\mathbb{P}_1, \mathbb{P}_2) = \inf \left\{ \mathbb{Q} - \operatorname{ess\,sup} \|\tilde{\boldsymbol{\xi}}_1 - \tilde{\boldsymbol{\xi}}_2\| : \begin{array}{l} \mathbb{Q} \text{ is a joint distribution of } \tilde{\boldsymbol{\xi}}_1 \text{ and } \tilde{\boldsymbol{\xi}}_2 \\ \text{with marginals } \mathbb{P}_1 \text{ and } \mathbb{P}_2, \text{ respectively} \end{array} \right\}.$$

Above, $\mathbb{Q}$-ess sup $\|\cdot\|$ is the essential supreme of $\|\cdot\|$ with respect to the joint distribution $\mathbb{Q}$, which is formally defined as

$$\mathbb{Q} - \operatorname{ess\,sup} \|\tilde{\xi}_1 - \tilde{\xi}_2\| = \inf \left\{ \Delta : \mathbb{Q}[\|\tilde{\xi}_1 - \tilde{\xi}_2\| > \Delta] = 0 \right\}.$$

It has been shown in Bertsimas et al. [104] that its corresponding type $\infty-$Wasserstein ambiguity set $\mathcal{P}_\infty$ has the following equivalent form

$$\mathcal{P}_\infty = \left\{ \frac{1}{N} \sum_{\ell \in [N]} \chi(\tilde{\boldsymbol{\xi}} - \boldsymbol{\xi}^\ell) : \exists \boldsymbol{\xi}^\ell \in \Xi, \|\boldsymbol{\xi}^\ell - \bar{\boldsymbol{\zeta}}^\ell\| \leq \theta, \forall \ell \in [N] \right\}, \tag{3.4}$$

where $\chi(\cdot)$ is the Dirac delta function. This neat representation has a straightforward interpretation, i.e., the worst-case distribution is also supported by N points, and each support point can only deviate at most θ amount from one of the empirical data $Z = \{\bar{\boldsymbol{\zeta}}^k\}_{k \in [N]} \subset \Xi$.

Since $W_\infty(\cdot, \cdot)$ has a similar statistical performance as $W_q(\cdot, \cdot)$ with $q \in [1, \infty)$ (Fournier and Guillin [105], Trillos and Slepčev [106], Xie [107], Xie et al. [108]) but has more attractive computational properties, we focus on $\infty-$Wasserstein ambiguity set, i.e., throughout this chapter, we suppose that $\mathcal{P} = \mathcal{P}_\infty$.

3.3 Model Properties

This section explores the properties of DrFRAM (3.1) and shows its computational complexity.

According to the worst-case characterization in (3.4) of type-∞ Wasserstein ambiguity set $\mathcal{P} = \mathcal{P}_\infty$. DrFRAM (3.1) can be equivalently represented as the following deterministic counterpart:

$$\text{(DrFRAM)} \qquad v^* = \min_{\boldsymbol{n},\boldsymbol{x}} \left\{ \frac{1}{N} \sum_{\ell\in[N]} \sup_{\boldsymbol{\xi}^\ell\in\Xi, \|\boldsymbol{\xi}^\ell - \boldsymbol{\zeta}^\ell\|\le\theta} \mathcal{Q}\left(\boldsymbol{n}, \boldsymbol{x}, \boldsymbol{\xi}^\ell\right) : (3.1b) - (3.1f) \right\}. \tag{3.5}$$

Model (3.5) can be interpreted as a robustification of Sampling Average Approximation (SAA) by choosing the worst-case perturbation for each empirical sample. Our model properties are based on this reformulation, and we finally choose a particular norm $\|\cdot\|$ in Section 3.3.2 to further simplify DrFRAM (3.5).

3.3.1 Computational Complexity of DrFRAM (3.5)

We observe that DrFRAM (3.5) is a mixed-integer nonlinear program and thus expect that it is an NP-hard problem. This motivates us to derive mixed-integer programming techniques and approximation algorithms to solve it.

The NP-hardness of DrFRAM (3.5) is established upon the well-known NP-complete problem – partition problem.

Proposition 3.1. *Solving DrFRAM (3.5) is NP-hard even when $N = 1, K = 2, \theta = 0$.*

Proof: Let us consider the following NP-complete problem.

(Partition Problem) Given an integer $T \in \mathbb{Z}_+$, consider n positive numbers $\{\alpha_i\}_{i\in[T]} \subseteq \mathbb{Z}_{++}$ having an even sum, is there a partition S_1, S_2 such that $\sum_{i\in S_1} \alpha_i = \sum_{i\in S_2} \alpha_i = \beta, S_1 \cap S_2 = \emptyset, S_1 \cup S_2 = [T]$?

We show that finding a feasible solution for a special case of DrFRAM (3.5) can be reduced to the partition problem. First of all, suppose there is only $N = 1$ empirical sample and the Wasserstein radius $\theta = 0$. We also assume that there are $K = 2$ types of buses, there are $\eta_k = \beta$ buses for each $k \in [K]$ and the reduced bus capacity is $\lfloor \delta_k c_k \rfloor = C > \max_{i\in[T]} a_i$. Suppose that there are $I = T$ routes and for each route $i \in [I]$, there is only $J_i = 1$ stop and the empirical alight rate $\bar{a}_{i1} = 1$ and arrival rate $\bar{\lambda}_{i1} = a_i$. Under this setting, DrFRAM (3.5) can be reduced to the following optimization problem:

$$v^* = \min_{\boldsymbol{n},\boldsymbol{x}} \max_{i\in[T]} \frac{a_i}{C \sum_{k\in[2]} n_{ik}}, \tag{3.6a}$$

$$\text{s.t.} \quad \sum_{k\in[2]} x_{ik} = 1, \forall i \in [T], \tag{3.6b}$$

$$n_{ik} \le \beta x_{ik}, \forall i \in [T], \forall k \in [2], \tag{3.6c}$$

$$\sum_{i\in[T]} n_{ik} \le \beta, \forall k \in [2], \tag{3.6d}$$

$$\sum_{k\in[2]} n_{ik} \ge 1, \forall i \in [T], \tag{3.6e}$$

$$x_{ik} \in \{0, 1\}, n_{ik} \in \mathbb{Z}^+, \forall i \in [T], \forall k \in [2]. \tag{3.6f}$$

Thus, in the model (3.6), the optimal value $v^* \le \frac{1}{C}$ if and only if there exists a feasible solution $(\boldsymbol{n}, \boldsymbol{x})$ satisfying the $\sum_{k\in[2]} n_{ik} \ge a_i$ for all $i \in [T]$. Or equivalently, the following set is nonempty

$$\mathcal{T} := \{(\boldsymbol{n}, \boldsymbol{x}) : n_{ik} \ge a_i x_{ik}, \forall i \in [T], \forall k \in [2], (3.6b) - (3.6f)\}.$$

Note that $2\beta = \sum_{i\in[T]} a_i$. Thus, in set $\mathcal{T}$, we must have $n_{ik} = a_i x_{ik}$. Hence, set $\mathcal{T}$ is nonempty if and only if the following integer program is nonempty:

$$\sum_{i\in[T]} a_{ik} x_{ik} = \beta, \sum_{k\in[2]} x_{ik} = 1, x_{ik} \in \{0,1\}, \forall i \in [T], \forall k \in [2],$$

which is exactly equivalent to the partition problem.

Hence, checking the special case (3.6) having a feasible solution with its objective value no larger than $1/C$ is equivalent to solving the partition problem. This proves the NP-hardness of DrFRAM (3.5). □

Proposition 3.1 shows that even under simple settings, DrFRAM (3.5) may not be polynomial-time solvable. This motivates us to develop exact and approximation algorithms to solve it, which serve different purposes. For example, exact algorithms can be useful to verify the correctness of approximation algorithms and can solve many instances to optimality, while approximation algorithms, usually more scalable, can provide high-quality initial solutions to speed up the exact ones.

3.3.2 Theoretical Sensitivity Analyses and Model Simplification

In this subsection, we analyze the properties of the recourse function $\mathcal{Q}(\boldsymbol{n}, \boldsymbol{x}, \boldsymbol{\xi})$ and the second-stage objective function $Q(\boldsymbol{n}, \boldsymbol{x}, \boldsymbol{\xi}, \boldsymbol{L}(\boldsymbol{\xi}))$. These properties allow us to simplify DrFRAM (3.5) by linearizing the nonlinear objective function.

We begin with the results for the second-stage objective function $Q(\boldsymbol{n}, \boldsymbol{x}, \boldsymbol{\xi}, \boldsymbol{L}(\boldsymbol{\xi}))$.

Proposition 3.2. *For the second-stage objective function $Q(\boldsymbol{n}, \boldsymbol{x}, \boldsymbol{\xi}, \boldsymbol{L}(\boldsymbol{\xi}))$, we have the following sensitivity results:*

3.3. Model Properties

- *Function* $Q(\boldsymbol{n}, \boldsymbol{x}, \boldsymbol{\xi}, \boldsymbol{L}(\boldsymbol{\xi}))$ *is monotone non-decreasing as the recourse decision* $L_{ij}(\boldsymbol{\xi})$ *increases for some* $i \in [I]$ *and* $j \in [J_i]$*;*

- *Function* $Q(\boldsymbol{n}, \boldsymbol{x}, \boldsymbol{\xi}, \boldsymbol{L}(\boldsymbol{\xi}))$ *is monotone non-increasing as the first-stage decision* n_{ik} *increases for some* $i \in [I]$ *and* $k \in [K]$*;*

- *Function* $Q(\boldsymbol{n}, \boldsymbol{x}, \boldsymbol{\xi}, \boldsymbol{L}(\boldsymbol{\xi}))$ *is monotone non-decreasing as the passenger arrival rate* λ_{ij} *increases for some* $i \in [I]$ *and* $j \in [J_i]$*; and*

- *Function* $Q(\boldsymbol{n}, \boldsymbol{x}, \boldsymbol{\xi}, \boldsymbol{L}(\boldsymbol{\xi}))$ *is monotone non-decreasing as the passenger alighting rate* a_{ij} *increases for some* $i \in [I]$ *and* $j \in [J_i]$.

Proof: We prove the results according to their orders.

- The first monotonicity result is simply because when the number of passengers on the buses increases, both bus utilization rate and passenger abandon rate grow or stay the same.

- The second monotonicity result is because when the number of buses allocated to a particular route increases, both its bus utilization rate and passenger abandon rate decrease or stay the same.

- The third and the fourth monotonicity results are because when more passengers arrive at a bus stop of a particular route, the route's bus utilization rate and passenger abandon rate increase or stay the same.

□

Since the minimization operator does not change the monotonicity of a function, results in Parts (ii)-(iv) still hold for the recourse function $\mathcal{Q}(\boldsymbol{n}, \boldsymbol{x}, \boldsymbol{\xi})$.

Corollary 3.3. *For the recourse function $\mathcal{Q}(\boldsymbol{n}, \boldsymbol{x}, \boldsymbol{\xi})$, we have the following sensitivity results:*

- *Recourse function $\mathcal{Q}(\boldsymbol{n}, \boldsymbol{x}, \boldsymbol{\xi})$ is monotone non-increasing as the first-stage decision n_{ik} increases for some $i \in [I]$ and $k \in [K]$;*
- *Recourse function $\mathcal{Q}(\boldsymbol{n}, \boldsymbol{x}, \boldsymbol{\xi})$ is monotone non-decreasing as the passenger arrival rate λ_{ij} increases for some $i \in [I]$ and $j \in [J_i]$; and*
- *Recourse function $\mathcal{Q}(\boldsymbol{n}, \boldsymbol{x}, \boldsymbol{\xi})$ is monotone non-decreasing as the passenger alighting rate a_{ij} increases for some $i \in [I]$ and $j \in [J_i]$.*

The results in Corollary 3.3 inspire us to choose a proper norm $\|\cdot\|$ in the type-∞ Wasserstein ambiguity set. Specifically, since random parameters $\tilde{\boldsymbol{a}}$ and $\tilde{\boldsymbol{\lambda}}$ have different magnitudes, we choose the weighted ℓ_∞ norm as $\|\boldsymbol{\xi}\| = \max\{\gamma\|\boldsymbol{a}\|_\infty, \|\boldsymbol{\lambda}\|_\infty\}$ (recall that we let $\boldsymbol{\xi} = (\boldsymbol{a}, \boldsymbol{\lambda})$), where the positive weight $\gamma > 0$ is to demonstrate the balance of the importance of both parameters. In practice, one can choose a proper γ such that the scaled vector $\gamma\boldsymbol{a}$ and vector $\boldsymbol{\lambda}$ have a similar order of magnitude.

In the spirit of Corollary 3.3 and the weighted ℓ_∞ norm, DrFRAM (3.5) admits the following equivalent representation.

Proposition 3.4. *Suppose $\|\boldsymbol{\xi}\| = \max\{\gamma\|\boldsymbol{a}\|_\infty, \|\boldsymbol{\lambda}\|_\infty\}$ for some $\gamma > 0$, then we have*

$$\text{(DrFRAM)} \qquad v^* = \min_{\boldsymbol{n},\boldsymbol{x}} \left\{ \frac{1}{N} \sum_{\ell \in [N]} \mathcal{Q}\left(\boldsymbol{n}, \boldsymbol{x}, \hat{\boldsymbol{\xi}}^\ell\right) : (3.1b) - (3.1f) \right\}, \tag{3.7}$$

where $\hat{\boldsymbol{\xi}}^\ell = (\hat{\boldsymbol{a}}^\ell, \hat{\boldsymbol{\lambda}}^\ell)$ with $\hat{a}^\ell_{ij} = \max\{0, \bar{a}^\ell_{ij} - \theta/\gamma\}$ and $\hat{\lambda}^\ell_{ij} = \max\{0, \bar{\lambda}^\ell_{ij} + \lfloor\theta\rfloor\}$.

Proof: The simplification of the inner supremum in DrFRAM (3.5) follows the monotonicity results in Corollary 3.3 and the definition of the weighted ℓ_∞ norm. □

Proposition 3.4 removes an obstacle in DrFRAM (3.5) by finding a closed-form worst-case representation for each scenario. Thus, we will mainly focus on addressing the second obstacle, which is the nonlinearity and non-convexity in the second-stage problem.

3.4 Linearizing the Second-stage Problem

As mentioned in the previous section, the difficulty of DrFRAM (3.7) resides in the second-stage problem (3.2) (i.e., the representation of the recourse function). The linearization technique is mainly based on the fact that the product of a binary variable $x \in \{0,1\}$ and a bounded continuous variable $y \in \{l,u\}$ can be linearized using the well-known McCormick inequalities (McCormick [109]), i.e.,

$$\{xy : x \in \{0,1\}, y \in [l,u]\} = \{z : y - u(1-x) \leq z \leq y - l(1-x), lx \leq z \leq ux, x \in \{0,1\}, y \in [l,u]\}.$$

Hence, to begin with, we first binarize the first-stage integer variables $\boldsymbol{n}$ as

$$n_{ik} = \sum_{r \in [R_k]} 2^{r-1} u_{ikr}, \forall i \in [I], \forall k \in [K], \tag{3.8a}$$

$$u_{ikr} \in \{0,1\}, \forall i \in [I], \forall k \in [K], \forall r \in [R_k], \tag{3.8b}$$

where we let $R_k = \lceil \log(\eta_k) \rceil$ for each $k \in [K]$ denote the largest possible bit when representing integer variable n_{ik}.

3.4.1 Linearizing Constraints (3.2b)

In this subsection, we focus on linearizing the constraints (3.2b) when $\boldsymbol{\xi} = \hat{\boldsymbol{\xi}}^\ell$ for each $\ell \in [N]$. First, to suppress the notation, we let $\boldsymbol{L}^\ell := \boldsymbol{L}(\hat{\boldsymbol{\xi}}^\ell)$.

Before we linearize the constraints (3.2b), we observe that due to the monotonicity results in Part (i) of Proposition 3.2, constraints (3.2b) are equivalent to

$$L_{ij}^\ell \geq \min \left\{ \sum_{k\in[K]} n_{ik} \lfloor \delta_k c_k \rfloor, \lceil (1-\hat{a}_{ij}^\ell) L_{i,j-1}^\ell \rceil + \lambda_{ij} \right\}, \forall i \in [I], \forall j \in [J_i]. \tag{3.9}$$

Since the ceiling function is lower semi-continuous, we can replace $\lceil (1-a_{ij}) L_{i,j-1}^\ell \rceil$ by its epigraph variable $\bar{L}_{i,j-1}^\ell$ such that

$$\bar{L}_{i,j-1}^\ell \geq (1-\hat{a}_{ij}^\ell) L_{i,j-1}^\ell, \bar{L}_{i,j-1}^\ell \in \mathbb{Z}_+, \forall i \in [I], \forall j \in [J_i]. \tag{3.10}$$

In this way, constraints (3.9) can be further reformulated as

$$L_{ij}^\ell \geq \min \left\{ \sum_{k\in[K]} n_{ik} \lfloor \delta_k c_k \rfloor, \bar{L}_{i,j-1}^\ell + \hat{\lambda}_{ij}^\ell \right\}, \forall i \in [I], \forall j \in [J_i],$$

Above, the piecewise minimum function can be linearized using binary variables $\boldsymbol{y}^\ell$, indicating whether each stop is fully occupied or not:

$$\begin{aligned} &L_{ij}^\ell \geq \textstyle\sum_{k\in[K]} n_{ik} \lfloor \delta_k c_k \rfloor - M y_{ij}^\ell, L_{ij}^\ell \geq \bar{L}_{i,j-1}^\ell + \hat{\lambda}_{ij}^\ell - M(1-y_{ij}^\ell), y_{ij}^\ell \in \{0,1\}, \forall i \in [I], \forall j \in [J_i], \\ &L_{ij}^\ell \geq \textstyle\sum_{k\in[K]} n_{ik} \lfloor \delta_k c_k \rfloor - (M-\hat{\lambda}_{ij}^\ell) y_{ij}^\ell, L_{ij}^\ell \geq \bar{L}_{i,j-1}^\ell + \hat{\lambda}_{ij}^\ell y_{ij}^\ell, y_{ij}^\ell \in \{0,1\}, \forall i \in [I], \forall j \in [J_i], \end{aligned} \tag{3.11}$$

where we choose $M = \max_{k\in[K]} \eta_k \lfloor \delta_k c_k \rfloor$ to be the maximum number of passengers that a route can carry at the same time. The equivalence of (3.9) and (3.11) is due to the fact that

$\bar{L}^{\ell}_{i,j-1} \leq L^{\ell}_{i,j-1}$.

3.4.2 Linearizing the Second-stage Objective Function (3.2a)

For each $\ell \in [N]$, let us use E^{ℓ}_1, E^{ℓ}_2 to denote the first and second parts of the objective function (3.2a). Then, according to constraints (3.10), equivalently, the second-stage objective function can be rewritten as

$$Q(\boldsymbol{n}, \boldsymbol{x}, \hat{\boldsymbol{\xi}}^{\ell}, \hat{\boldsymbol{L}}^{\ell}) = E^{\ell}_1 + \omega E^{\ell}_2$$

where

$$E^{\ell}_1 \left(\sum_{k\in[K]} n_{ik} \lfloor \delta_k c_k \rfloor \right) \geq L^{\ell}_{ij}, \forall i \in [I], \forall j \in [J_i], E^{\ell}_1 \in [0,1], \tag{3.12a}$$

$$E^{\ell}_2 \geq (\hat{\lambda}^{\ell}_{ij})^{-1} \left(\bar{L}^{\ell}_{i,j-1} + \hat{\lambda}^{\ell}_{ij} - \sum_{k\in[K]} n_{ik} \lfloor \delta_k c_k \rfloor \right), \forall i \in [I], \forall j \in [J_i], E^{\ell}_2 \in [0,1]. \tag{3.12b}$$

Now it remains to linearize the bilinear terms in (3.12a). According to (3.8), we can represent variables $\boldsymbol{n}$ using binary variables $\boldsymbol{u}$. Therefore, constraints (3.12a) are equivalent to

$$\sum_{k\in[K]} \sum_{r\in[R_k]} 2^{r-1} \lfloor \delta_k c_k \rfloor E^{\ell}_1 u_{ikr} \geq L^{\ell}_{ij}, \forall i \in [I], \forall j \in [J_i], E^{\ell}_1 \in [0,1],$$

Introducing McCormick inequalities to linearize the bilinear terms, we have

$$\sum_{k\in[K]} \sum_{r\in[R_k]} 2^{r-1} \lfloor \delta_k c_k \rfloor w^{\ell}_{ikr} \geq L^{\ell}_{ij}, \forall i \in [I], \forall j \in [J_i], E^{\ell}_1 \in [0,1], \tag{3.12c}$$

$$w^{\ell}_{ikr} \geq 0, w^{\ell}_{ikr} \geq E^{\ell}_1 + u_{ikr} - 1, w^{\ell}_{ikr} \leq E^{\ell}_1, w^{\ell}_{ikr} \leq u_{ikr}, \forall k \in [K], \forall i \in [I], \forall r \in [R]. \tag{3.12d}$$

3.4.3 An Exact Mixed-Integer Linear Programming (MILP) Reformulation for DrFRAM (3.7)

Let us put all the linearized pieces together, and we are ready to present an exact MILP reformulation for DrFRAM (3.7). In particular, DrFRAM (3.7) is equivalent to the following MILP:

$$\text{(DrFRAM)} \qquad v^* = \min_{\boldsymbol{n},\boldsymbol{x},\boldsymbol{u}} \left\{ \frac{1}{N} \sum_{\ell\in[N]} \mathcal{Q}\left(\boldsymbol{n},\boldsymbol{x},\boldsymbol{u},\hat{\boldsymbol{\xi}}^\ell\right) : (3.1b)-(3.1f), (3.8a), (3.8b) \right\}, \tag{3.13a}$$

where for simplicity, we slightly abuse the notation by redefining $\mathcal{Q}(\boldsymbol{n},\boldsymbol{x},\boldsymbol{u},\hat{\boldsymbol{\xi}}^\ell)$ as

$$\mathcal{Q}(\boldsymbol{n},\boldsymbol{x},\boldsymbol{u},\hat{\boldsymbol{\xi}}^\ell) = \min_{\boldsymbol{L}^\ell,\bar{\boldsymbol{L}}^\ell,\boldsymbol{w}^\ell,\boldsymbol{y}^\ell,\boldsymbol{E}^\ell} \left\{ E_1^\ell + \omega E_2^\ell : (3.2c), (3.10), (3.11), (3.12b)-(3.12d) \right\}. \tag{3.13b}$$

Note that we can encode the entire DrFRAM (3.13) into the off-the-shelf solvers such as Gurobi, CPLEX, MOSEK. However, our numerical study shows that, albeit effective, model (3.13) has difficulty solving large-scale instances, remaining large optimality gaps within an hour. Thus, we will develop valid inequalities and strong formulations based on the knapsack polytope and the disjunctive programming (Balas [110]) in the next section.

Finally, we remark that one can adopt the scenario decomposition method proposed by Ahmed [111] to solve the DrFRAM (3.13) in a decomposed way. The general idea is to completely decompose MILP (3.13) into N subproblems, i.e., for each $\ell \in [N]$, we solve

$$v^\ell := \min_{\boldsymbol{n},\boldsymbol{x},\boldsymbol{u}} \left\{ \mathcal{Q}\left(\boldsymbol{n},\boldsymbol{x},\boldsymbol{u},\hat{\boldsymbol{\xi}}^\ell\right) : (3.1b)-(3.1f), (3.8a), (3.8b) \right\}. \tag{3.14}$$

Subproblem (3.14) can be accelerated with the valid inequalities and stronger formulations

developed in the next section. Note that the average of their objective functions provides a lower bound of DrFRAM, and the first-stage decision obtained in each subproblem is also feasible to the original MILP (3.13). Hence, we can evaluate these decisions and choose the best one as an upper bound. Next, we cut off the obtained decisions from their corresponding subproblems using the no-good cut (Ahmed [111]), i.e., for a scenario ℓ, given a first-stage binary solution $(\bar{\boldsymbol{x}}^\ell, \bar{\boldsymbol{u}}^\ell)$ (we do not need to include $\bar{\boldsymbol{n}}^\ell$ since it can be represented by $\bar{\boldsymbol{u}}^\ell$), we add the following no-good cut

$$\sum_{i\in[I],k\in[K]} \left((1-\bar{x}_{ik}^\ell)x_{ik} + \sum_{r\in[R_k]} (1-\bar{u}_{ikr}^\ell)u_{ikr} \right) \geq 1$$

into the ℓth subproblem; and repeat the same procedure. We terminate the solution procedure when invoking a stopping criterion. The detailed implementation can be found in Algorithm 1.

Algorithm 1: Scenario Decomposition for Solving DrFRAM

Initialization: Set $\tau = 0, \epsilon > 0$, $\mathcal{X}^\ell = \{(\boldsymbol{n}, \boldsymbol{x}, \boldsymbol{u}) : (3.1b) - (3.1f), (3.8a), (3.8b)\}$ for all $\ell \in [N]$, $LB = -\infty$, $UB = \infty$;
while $UB - LB > \epsilon$ **do**
  for $\ell \in [N]$ **do**
    $(\bar{\boldsymbol{n}}^\ell, \bar{\boldsymbol{x}}^\ell, \bar{\boldsymbol{u}}^\ell) \in \arg\min\{\mathcal{Q}(\boldsymbol{n}, \boldsymbol{x}, \boldsymbol{u}, \hat{\boldsymbol{\xi}}^\ell) : (\boldsymbol{n}, \boldsymbol{x}, \boldsymbol{u}) \in \mathcal{X}^\ell\}$;
  $LB = \max\{LB, \frac{1}{N}\sum_{\ell\in[N]} \mathcal{Q}(\bar{\boldsymbol{n}}^\ell, \bar{\boldsymbol{x}}^\ell, \bar{\boldsymbol{u}}^\ell, \hat{\boldsymbol{\xi}}^\ell)\}$;
  $UB = \min\{UB, \min_{t\in[N]} \frac{1}{N}\sum_{\ell\in[N]} \mathcal{Q}(\bar{\boldsymbol{n}}^t, \bar{\boldsymbol{x}}^t, \bar{\boldsymbol{u}}^t, \hat{\boldsymbol{\xi}}^\ell)\}$;
  $\mathcal{X}^\ell \to \mathcal{X}^\ell \setminus \{(\bar{\boldsymbol{n}}^\ell, \bar{\boldsymbol{x}}^\ell, \bar{\boldsymbol{u}}^\ell)\}$ for each $\ell \in [N]$;
  $\tau \leftarrow \tau + 1$

We can further extend the scenario decomposition by bundling the scenarios (see, e.g., Ryan et al. [112]). Instead of solving N subproblems for each scenario $\ell \in [N]$, we group similar scenarios into disjoint subsets $G_\nu \subset [N], \nu \in [\mathcal{N}]$ using K-means clustering algorithm, and the subsets consist of a partition of $[N]$. We follow the same procedure that completely

decomposes MILP (3.13) into $\mathcal{N}$ subproblems, i.e., for each $\nu \in [\mathcal{N}]$, we solve

$$v^{\nu} := \min_{\boldsymbol{n},\boldsymbol{x},\boldsymbol{u}} \left\{ \frac{1}{|G_\nu|} \sum_{\ell \in G_\nu} \mathcal{Q}\left(\boldsymbol{n}, \boldsymbol{x}, \boldsymbol{u}, \hat{\boldsymbol{\xi}}^{\ell}\right) : (3.1b) - (3.1f), (3.8a), (3.8b) \right\}. \tag{3.15}$$

The detailed implementation can be found in Algorithm 2.

Algorithm 2: Scenario Decomposition with Grouping for Solving DrFRAM

Initialization: Set $\tau = 0, \epsilon > 0$, integer $\mathcal{N}$ (divisible of N), cluster G_ν, and set $\mathcal{X}^{\nu} = \bigcap_{\ell \in G_\nu} \{(\boldsymbol{n}, \boldsymbol{x}, \boldsymbol{u}) : (3.1b) - (3.1f), (3.8a), (3.8b)\}$ for all $\nu \in [\mathcal{N}]$, $LB = -\infty$, $UB = \infty$;
while $UB - LB > \epsilon$ **do**
  for $\nu \in [\mathcal{N}]$ **do**
    $(\bar{\boldsymbol{n}}^{\nu}, \bar{\boldsymbol{x}}^{\nu}, \bar{\boldsymbol{u}}^{\nu}) \in \arg\min \left\{ v^{\nu} = \frac{1}{|G_\nu|} \sum_{\ell \in G_\nu} \mathcal{Q}(\boldsymbol{n}, \boldsymbol{x}, \boldsymbol{u}, \hat{\boldsymbol{\xi}}^{\ell}) : (\boldsymbol{n}, \boldsymbol{x}, \boldsymbol{u}) \in \mathcal{X}^{\nu} \right\}$;
  $LB = \max\{LB, \frac{1}{\mathcal{N}} \sum_{\nu \in [\mathcal{N}]} v^{\nu}\}$;
  $UB = \min\{UB, \min_{t \in [\mathcal{N}]} \frac{1}{N} \sum_{\ell \in [N]} \mathcal{Q}(\bar{\boldsymbol{n}}^{t}, \bar{\boldsymbol{x}}^{t}, \bar{\boldsymbol{u}}^{t}, \hat{\boldsymbol{\xi}}^{\ell})\}$;
  $\mathcal{X}^{\nu} \to \mathcal{X}^{\nu} \setminus \{(\bar{\boldsymbol{n}}^{\nu}, \bar{\boldsymbol{x}}^{\nu}, \bar{\boldsymbol{u}}^{\nu})\}$ for each $\ell \in [\mathcal{N}]$;
  $\tau \leftarrow \tau + 1$

Note that to accelerate the algorithm, we can add an objective cut rather than the no-good cut to each subproblem to force the objective function to increase by at least a positive step, that is, for each $\ell \in [N]$, we add the following inequality

$$E_1^{\ell} + \omega E_2^{\ell} \geq \mathcal{Q}\left(\bar{\boldsymbol{n}}^{\ell}, \bar{\boldsymbol{x}}^{\ell}, \bar{\boldsymbol{u}}^{\ell}\right) + \hat{\epsilon}^{\ell} \tag{3.16}$$

into the ℓth subproblem, where $(\bar{\boldsymbol{n}}^{\ell}, \bar{\boldsymbol{x}}^{\ell}, \bar{\boldsymbol{u}}^{\ell})$ denotes an optimal solution of ℓth subproblem and $\hat{\epsilon}^{\ell} > 0$. Instead of solving the problem to optimal, the accelerated scenario decomposition can obtain a suboptimal solution. The detailed implementation can be found in Algorithm 3.

Finally, we conclude this section by showing that if the data from distributionally robust counterparts (i.e., $\{\hat{\boldsymbol{\xi}}^{\ell}\}_{\ell \in [N]}$) have a small variability, then the naive scenario decomposition

Algorithm 3: Accelerated Scenario Decomposition for Solving DrFRAM

Initialization: Set $\tau = 0, \epsilon > 0$, $\mathcal{X}^\ell = \{(\boldsymbol{n}, \boldsymbol{x}, \boldsymbol{u}) : (3.1b) - (3.1f), (3.8a), (3.8b)\}$ for all $\ell \in [N]$, $\{\hat{\epsilon}^\ell\}_{\ell \in [N]}$, $LB = -\infty$, $UB = \infty$;
while $UB - LB > \epsilon$ **do**
  for $\ell \in [N]$ **do**
    $(\bar{\boldsymbol{n}}^\ell, \bar{\boldsymbol{x}}^\ell, \bar{\boldsymbol{u}}^\ell) \in \arg\min\{\mathcal{Q}(\boldsymbol{n}, \boldsymbol{x}, \boldsymbol{u}, \hat{\boldsymbol{\xi}}^\ell) : (3.16), (\boldsymbol{n}, \boldsymbol{x}, \boldsymbol{u}) \in \mathcal{X}^\ell\}$;
  $LB = \max\{LB, \frac{1}{N}\sum_{\ell \in [N]} \mathcal{Q}(\bar{\boldsymbol{n}}^\ell, \bar{\boldsymbol{x}}^\ell, \bar{\boldsymbol{u}}^\ell, \hat{\boldsymbol{\xi}}^\ell)\}$;
  $UB = \min\{UB, \min_{t \in [N]} \frac{1}{N}\sum_{\ell \in [N]} \mathcal{Q}(\bar{\boldsymbol{n}}^t, \bar{\boldsymbol{x}}^t, \bar{\boldsymbol{u}}^t, \hat{\boldsymbol{\xi}}^\ell)\}$;
  $\tau \leftarrow \tau + 1$

lower bound (i.e., $1/N \sum_{\ell \in [N]} v^\ell$ will not be faraway from the true optimal v^*.

Proposition 3.5. *Suppose that the weight $\omega = 0$ (i.e., the passenger abandon rate for each bus stop is negligible), and there exists a matrix $\boldsymbol{\mu} = (\boldsymbol{\mu}^a, \boldsymbol{\mu}^\lambda) \in \Xi$ and a positive integer $\hat{\alpha} \in \mathbb{Z}_{++}$ such that*

$$\hat{a}_{ij}^\ell = \mu_{ij}^a, \mu_{ij}^\lambda \leq |\hat{\lambda}_{ij}^\ell| \leq \hat{\alpha}\mu_{ij}^\lambda, \forall i \in [I], \forall j \in [J_i].$$

Then the following approximation ratio holds for the naive scenario decomposition lower bound (without any no good cut or objective cut)

$$\frac{1}{\hat{\alpha}} v^* \leq \frac{1}{N} \sum_{\ell \in [N]} v^\ell \leq v^*.$$

Proof: We split the proof into three steps.

Step 1. The second inequality holds true since we drop the nonanticipactivity constraints when computing the naive scenario decomposition lower bound.

Step 2. Next, to prove the first inequality, let us use v^D to denote the optimal value of the

following nominal problem as

$$v^D(\alpha) = \min_{\boldsymbol{n},\boldsymbol{x},\boldsymbol{u}} \{\mathcal{Q}(\boldsymbol{n},\boldsymbol{x},\boldsymbol{u},\alpha\boldsymbol{\mu}) : (3.1b) - (3.1f), (3.8a), (3.8b)\} \tag{3.17}$$

for some positive integer $\alpha \in \mathbb{Z}_{++}$. In model (3.17), the function $\mathcal{Q}(\boldsymbol{n},\boldsymbol{x},\boldsymbol{u},\alpha\boldsymbol{\mu})$ is defined in (3.13b) by letting $\hat{\boldsymbol{\xi}}^\ell = \alpha\boldsymbol{\mu}$.

According to the monotonicity results in Corollary 3.3, we have

$$\mathcal{Q}(\boldsymbol{n},\boldsymbol{x},\boldsymbol{u},\hat{\boldsymbol{\xi}}^\ell) \leq \mathcal{Q}(\boldsymbol{n},\boldsymbol{x},\boldsymbol{u},\hat{\alpha}\boldsymbol{\mu})$$

for all $\ell \in [N]$ and any feasible $(\boldsymbol{n},\boldsymbol{x},\boldsymbol{u})$. Thus, aggregating the above inequalities for all $\ell \in [N]$, we have

$$\frac{1}{N}\sum_{\ell\in[N} \mathcal{Q}(\boldsymbol{n},\boldsymbol{x},\boldsymbol{u},\hat{\boldsymbol{\xi}}^\ell) \leq \mathcal{Q}(\boldsymbol{n},\boldsymbol{x},\boldsymbol{u},\hat{\alpha}\boldsymbol{\mu})$$

for any feasible $(\boldsymbol{n},\boldsymbol{x},\boldsymbol{u})$. This implies that $v^* \leq v^D(\hat{\alpha})$.

Similarly, we also have $v^\ell \geq v^D(1)$ for each $\ell \in [N]$. That is, $\frac{1}{N}\sum_{\ell\in[N]} v^\ell \geq v^D(1)$. Now it remains to show that $v^D(\hat{\alpha}) \leq \hat{\alpha} v^D(1)$.

Step 3. We observe that

Claim 1. For any real number $q \in \mathbb{R}_+$ and positive integer number $\alpha \in \mathbb{Z}_{++}$, the following inequality must hold $\alpha\lceil q\rceil \geq \lceil \alpha q\rceil$.

Proof: This is simply because $\alpha\lceil q\rceil \geq \alpha q$ and the former is an integer. ◇

Suppose that $(\boldsymbol{n}^*,\boldsymbol{x}^*,\boldsymbol{u}^*)$ is an optimal first-stage solution and $(\boldsymbol{L}^1,\bar{\boldsymbol{L}}^1,\boldsymbol{w}^1,\boldsymbol{y}^1,\boldsymbol{E}^1)$ is an optimal second-stage decision to model (3.17) with $\alpha = 1$.

Now let us define

$$
\begin{aligned}
L_{ij}^{\hat{\alpha}} &= \min\left\{\sum_{k\in[K]} n_{ik}^{*}\lfloor\delta_k c_k\rfloor, \hat{\alpha}L_{ij}^{1}\right\}, \forall i\in[I], \forall j\in[J_i],\\
\bar{L}_{ij-1}^{\hat{\alpha}} &= \lceil(1-\mu_{ij}^{a})L_{i,j-1}^{\hat{\alpha}}\rceil, \forall i\in[I], \forall j\in[J_i],\\
y_{ij}^{\hat{\alpha}} &= \mathbb{I}\left(L_{ij}^{\hat{\alpha}} < \sum_{k\in[K]} n_{ik}^{*}\lfloor\delta_k c_k\rfloor\right), \forall i\in[I], \forall j\in[J_i],\\
E_1^{\hat{\alpha}} &= \max_{i\in[I],j\in[J_i]} \frac{L_{ij}^{\hat{\alpha}}}{\sum_{k\in[K]} n_{ik}^{*}\lfloor\delta_k c_k\rfloor},\\
E_2^{\hat{\alpha}} &= \max_{i\in[I],j\in[J_i]} (\hat{\alpha}\mu_{ij}^{\lambda})^{-1}\left(\bar{L}_{i,j-1}^{\hat{\alpha}} + \hat{\alpha}\mu_{ij}^{\lambda} - \sum_{k\in[K]} n_{ik}^{*}\lfloor\delta_k c_k\rfloor\right)_{+},\\
w_{ikr}^{\hat{\alpha}} &= E_1^{\hat{\alpha}} u_{ikr}^{*}, \forall i\in[I], \forall k\in[K], \forall r\in[R_k].
\end{aligned}
$$

According to the definition of the model (3.17) with $\alpha = \hat{\alpha}$, we see that $(\boldsymbol{n}^*, \boldsymbol{x}^*, \boldsymbol{u}^*)$ is a feasible first-stage solution and $(\boldsymbol{L}^{\hat{\alpha}}, \bar{\boldsymbol{L}}^{\hat{\alpha}}, \boldsymbol{w}^{\hat{\alpha}}, \boldsymbol{y}^{\hat{\alpha}}, \boldsymbol{E}^{\hat{\alpha}})$ satisfies constraints (3.2c), (3.10), (3.12b)–(3.12d). It remains to show that constraints (3.11) also hold.

Before proceeding, we observe the following fact:

Claim 2. For any $i\in[I], j\in[J_i]$, we must have $\bar{L}_{ij-1}^{\hat{\alpha}} \le \hat{\alpha}\bar{L}_{ij-1}^{1}$.

Proof: Note that

$$
\bar{L}_{ij-1}^{\hat{\alpha}} = \lceil(1-\mu_{ij}^{a})L_{i,j-1}^{\hat{\alpha}}\rceil \le \lceil(1-\mu_{ij}^{a})\hat{\alpha}L_{i,j-1}^{1}\rceil \le \hat{\alpha}\lceil(1-\mu_{ij}^{a})L_{i,j-1}^{1}\rceil := \hat{\alpha}\bar{L}_{ij-1}^{1},
$$

where the first inequality is due to the definition of $L_{i,j-1}^{\hat{\alpha}}$ and the second one is due to Claim 3. ◇

There are two cases:

- When $L_{ij}^{\hat{\alpha}} < \sum_{k\in[K]} n_{ik}^* \lfloor \delta_k c_k \rfloor$, it is sufficient to show that $L_{ij}^{\hat{\alpha}} \geq \bar{L}_{ij-1}^{\hat{\alpha}} + \hat{\alpha}\mu_{ij}^{\lambda}$. This must be true since we have

$$L_{ij}^{\hat{\alpha}} = \hat{\alpha} L_{ij}^1, \bar{L}_{ij-1}^{\hat{\alpha}} \leq \hat{\alpha}\bar{L}_{ij-1}^1, L_{ij}^1 \geq \bar{L}_{ij-1}^1 + \mu_{ij}^{\lambda}$$

  where the first inequality is due to Claim 2 and the second one is due to the fact that $(\boldsymbol{L}^1, \bar{\boldsymbol{L}}^1, \boldsymbol{w}^1, \boldsymbol{y}^1, \boldsymbol{E}^1)$ is an optimal (and of course feasible) second-stage decision to the model (3.17) with $\alpha = 1$.

- When $L_{ij}^{\hat{\alpha}} = \sum_{k\in[K]} n_{ik}^* \lfloor \delta_k c_k \rfloor$, we have $y_{ij}^{\alpha} = 0$. It is sufficient to show that $L_{ij}^{\hat{\alpha}} \geq \bar{L}_{ij-1}^{\hat{\alpha}}$. This is true since

$$\bar{L}_{ij-1}^{\hat{\alpha}} = \lceil (1-\mu_{ij}^a) L_{i,j-1}^{\hat{\alpha}} \rceil \leq \sum_{k\in[K]} n_{ik}^* \lfloor \delta_k c_k \rfloor := L_{ij}^{\hat{\alpha}}$$

  where the inequality is due to the fact that $L_{i,j-1}^{\hat{\alpha}} \leq \sum_{k\in[K]} n_{ik}^* \lfloor \delta_k c_k \rfloor$.

□

Finally, we observe that the objective function is

$$\begin{aligned} E_1^{\hat{\alpha}} + \omega E_2^{\hat{\alpha}} &= \max_{i\in[I], j\in[J_i]} \frac{L_{ij}^{\hat{\alpha}}}{\sum_{k\in[K]} n_{ik}^* \lfloor \delta_k c_k \rfloor} + \omega \max_{i\in[I], j\in[J_i]} (\hat{\alpha}\mu_{ij}^{\lambda})^{-1} \left(\bar{L}_{i,j-1}^{\hat{\alpha}} + \hat{\alpha}\mu_{ij}^{\lambda} - \sum_{k\in[K]} n_{ik}^* \lfloor \delta_k c_k \rfloor \right)_+ \\ &= \max_{i\in[I], j\in[J_i]} \frac{\min\left\{ \sum_{k\in[K]} n_{ik}^* \lfloor \delta_k c_k \rfloor, \hat{\alpha} L_{ij}^1 \right\}}{\sum_{k\in[K]} n_{ik}^* \lfloor \delta_k c_k \rfloor} \\ &\leq \max_{i\in[I], j\in[J_i]} \frac{\hat{\alpha}\min\left\{ \sum_{k\in[K]} n_{ik}^* \lfloor \delta_k c_k \rfloor, L_{ij}^1 \right\}}{\sum_{k\in[K]} n_{ik}^* \lfloor \delta_k c_k \rfloor} = \hat{\alpha} E_1^1 := \hat{\alpha} v^D(1) \end{aligned}$$

where the inequality is due to the fact that $\min\{a, \hat{\alpha}b\} \leq \hat{\alpha}\min\{a, b\}$ for any non-negative numbers a, b and positive integer $\hat{\alpha}$.

Since $(\boldsymbol{n}^*, \boldsymbol{x}^*, \boldsymbol{u}^*)$ is a feasible first-stage solution and $(\boldsymbol{L}^{\hat{\alpha}}, \bar{\boldsymbol{L}}^{\hat{\alpha}}, \boldsymbol{w}^{\hat{\alpha}}, \boldsymbol{y}^{\hat{\alpha}}, \boldsymbol{E}^{\hat{\alpha}})$ is a feasible second-stage solution to model (3.17) with the objective value at most $\hat{\alpha} v^D(1)$, this proves that $v^D(\hat{\alpha}) \leq \hat{\alpha} v^D(1)$. This completes the proof. □

Proposition 3.5 shows that not very surprisingly, if the alighting rate for each bus stop is deterministic, and the passenger demand does not vary too much from scenario to scenario, then the naive scenario decomposition lower bound tends to be very close to the true optimality. This is consistent with what we have found in the numerical study section. However, in general, Algorithm 1 suffers from slow convergence when being employed to find a global optimal solution. Therefore, in the next section, we will derive stronger formulations and valid inequalities to further strengthen MILP (3.13).

3.5 Stronger Formulations and Valid Inequalities

In this section, we strengthen the MILP model (3.13) by developing different families of valid inequalities. Our results and strong formulations are based on studying the mixed-integer substructures of model (3.13). Specifically, we consider convexifying the following two substructures to derive stronger formulations. First of all, for each $i \in [I]$, we consider the substructure of variables $(\boldsymbol{x}_{i:}, \boldsymbol{u}_{i::})$ by projecting out variables $\boldsymbol{n}$. That is, for each $i \in [I]$, let us define

$$X_i^1 = \{(\boldsymbol{x}_{i:}, \boldsymbol{u}_{i::}) : \exists \boldsymbol{n}_{i:}, (3.1b) - (3.1c), (3.8a), (3.8b)\}. \tag{3.18a}$$

The second substructure is defined for each sample $\ell \in [N]$ and each $i \in [I]$ and $j \in [J_i]$ as

$$X_{ij\ell}^2 = \left\{(\boldsymbol{x}_{i:}, \boldsymbol{u}_{i::}, L_{ij}^{\ell}) \in X_i^1 \times \mathbb{R}_+ : (3.12c), (3.12d)\right\}. \tag{3.18b}$$

3.5.1 Convexification of Set X_i^1

We will first convexify X_i^1. According to (3.18a), set X_i^1 is equivalent to

$$X_i^1 = \left(\bigvee_{k\in[K]} \left(X_{ik}^1 \wedge \{x_{ik} = 1\}\right) \right) \bigwedge \left\{ \boldsymbol{x}_{i:} \in \{0,1\}^K : \sum_{k\in[K]} x_{ik} = 1 \right\}$$

where

$$X_{ik}^1 := \left\{ (\boldsymbol{x}_{i:}, \boldsymbol{u}_{i::}) : \sum_{r\in[R_k]} 2^{r-1} u_{ikr} \le \eta_k x_{ik}, u_{ikr} \in \{0,1\}, \forall r \in [R_k] \right\}.$$

Suppose that $\eta_k = 2^{i_{1k}-1} + \ldots + 2^{i_{sk}-1} + 2^{R_k-1}$ and set $\mathcal{I} := \{i_{1k}, \ldots, i_{sk}, R_k\}$. Since $\{2^{r-1}\}_{r\in[R_k]}$ are superincreasing, according to proposition 3.4 in Gupte et al. [113], the convex hull of $X_{ik}^1 \wedge \{x_{ik} = 1\}$ can be described as

$$\operatorname{conv}\left(X_{ik}^1 \wedge \{x_{ik} = 1\}\right) = \left\{ (\boldsymbol{x}_{i:}, \boldsymbol{u}_{i::}) : \begin{array}{l} \boldsymbol{x}_{i:} \in [0,1]^K, x_{ik} = 1, \boldsymbol{u}_{ik:} \in [0,1]^{R_k}, \\ u_{ikr} + \sum_{\tau\in\mathcal{I}_r} u_{ik\tau} \le |\mathcal{I}_r|, \forall r \in [R_k] \setminus \mathcal{I} \end{array} \right\}$$

where $\mathcal{I}_r := \{s \in \mathcal{I} : s > r\}$.

Our convex hull description of set X_i^1 relies on the well-known disjunctive programming (Balas [110]).

Lemma 3.6. *Suppose $\bar{s}$ polyhedra $\bar{X}^i = \{\bar{\boldsymbol{y}} \in \mathbb{R}^{\bar{n}} : \boldsymbol{A}^i \bar{\boldsymbol{y}} \le \boldsymbol{b}^i\}$ with $\boldsymbol{A}^i \in \mathbb{R}^{\bar{m}_i \times \bar{n}}$ and $\boldsymbol{b} \in \mathbb{R}^{\bar{m}_i}$ for each $i \in [\bar{s}]$ share the same recession cone. Then the following result holds*

$$\operatorname{conv}\left\{ \left(\bigvee_{s\in[\bar{s}]} \left(\bar{X}^i \wedge \{\lambda_i = 1\}\right) \right) \bigwedge \left\{ \boldsymbol{\lambda} \in \{0,1\}^{\bar{s}} : \sum_{i\in[\bar{s}]} \lambda_i = 1 \right\} \right\}$$

$$= \left\{ (\bar{\boldsymbol{y}}, \boldsymbol{\lambda}) \in \mathbb{R}^{\bar{n}} \times [0,1]^{\bar{s}} : \boldsymbol{A}^i \bar{\boldsymbol{y}}^i \leq \boldsymbol{b}^i \lambda_i, \forall i \in [\bar{s}], \sum_{i \in [\bar{s}]} \bar{\boldsymbol{y}}^i = \bar{\boldsymbol{y}} \right\}.$$

According to Lemma 3.6 and the fact that the convex hull of the union of sets is equal to the convex hull of the union of the convex hulls of sets, we arrive at the complete description of the convex hull of set X_i^1. This result is summarized below.

Proposition 3.7. *For each $i \in [I]$, the convex hull of the set X_i^1 is equal to*

$$\operatorname{conv}\left(X_i^1\right) = \left\{ (\boldsymbol{x}_{i:}, \boldsymbol{u}_{i::}) : \begin{array}{l} \boldsymbol{x}_{i:} \in [0,1]^K, \sum_{k \in [K]} x_{ik} = 1, \\ u_{ikr} + \sum_{\tau \in \mathcal{I}_r} u_{ik\tau} \leq |\mathcal{I}_r| x_{ik}, \forall r \in [R_k] \setminus \mathcal{I}, \forall k \in [K], \\ 0 \leq u_{ikr} \leq x_{ik}, \forall r \in [R_k], \forall k \in [K] \end{array} \right\}. \tag{3.19}$$

3.5.2 Convexification of Set $X_{ij\ell}^2$

Similarly, to convexify set $X_{ij\ell}^2$, we first rewrite it as a disjunction

$$X_{ij\ell}^2 = \left(\bigvee_{k \in [K]} \left(X_{ij\ell k}^2 \wedge \{x_{ik} = 1\} \right) \right) \bigwedge \left\{ \boldsymbol{x}_{i:} \in \{0,1\}^K : \sum_{k \in [K]} x_{ik} = 1 \right\}, \tag{3.20}$$

where

$$X_{ij\ell k}^2 \wedge \{x_{ik} = 1\} := \left\{ (\boldsymbol{x}_{i:}, \boldsymbol{u}_{i::}, L_{ij}^\ell, \boldsymbol{w}_{i::}^\ell, E_1^\ell) : \begin{array}{l} (\boldsymbol{x}_{i:}, \boldsymbol{u}_{i::}) \in X_{ik}^1, \sum_{r \in [R_k]} 2^{r-1} \lfloor \delta_k c_k \rfloor w_{ikr}^\ell \geq L_{ij}^\ell, \\ w_{ikr}^\ell = u_{ikr} E_1^\ell, L_{ij}^\ell \in \mathbb{R}_+, E_1^\ell \in [0,1], x_{ik} = 1 \end{array} \right\}.$$

We first observe that the convex hull of set $X_{ij\ell k}^2 \wedge \{x_{ik} = 1\}$ is equal to the intersection of the constraint $\sum_{r \in [R_k]} 2^{r-1} \lfloor \delta_k c_k \rfloor w_{ikr}^\ell \geq L_{ij}^\ell$ and the convex hull of the feasible region subject

to the remaining constraints.

Lemma 3.8. *The following characterization holds for* $\mathrm{conv}(X^2_{ij\ell k} \wedge \{x_{ik} = 1\})$*, i.e.,*

$$\mathrm{conv}(X^2_{ij\ell k} \wedge \{x_{ik} = 1\}) = \mathrm{conv}(\bar{X}^2_{ij\ell k}) \bigcap \left\{ (\boldsymbol{w}^\ell_{i::}, L^\ell_{ij}) : \sum_{r\in[R_k]} 2^{r-1} \lfloor \delta_k c_k \rfloor w^\ell_{ikr} \geq L^\ell_{ij} \right\},$$

where

$$\bar{X}^2_{ij\ell k} = \left\{ (\boldsymbol{x}_{i:}, \boldsymbol{u}_{i::}, L^\ell_{ij}, \boldsymbol{w}^\ell_{i::}, E^\ell_1) : \ (\boldsymbol{x}_{i:}, \boldsymbol{u}_{i::}) \in X^1_{ik}, w^\ell_{ikr} = u_{ikr} E^\ell_1, L^\ell_{ij} \in \mathbb{R}_+, E^\ell_1 \in [0,1], x_{ik} = 1 \right\}.$$

Proof: Since the convex hull of the intersection of two sets is contained in the intersection of the convex hulls of two sets, we must have

$$\mathrm{conv}(X^2_{ij\ell k} \wedge \{x_{ik} = 1\}) \subseteq \mathrm{conv}(\bar{X}^2_{ij\ell k}) \bigcap \left\{ (\boldsymbol{w}^\ell_{i::}, L^\ell_{ij}) : \sum_{r\in[R_k]} 2^{r-1} \lfloor \delta_k c_k \rfloor w^\ell_{ikr} \geq L^\ell_{ij} \right\}.$$

It remains to show that

$$\mathrm{conv}(X^2_{ij\ell k} \wedge \{x_{ik} = 1\}) \supseteq \mathrm{conv}(\bar{X}^2_{ij\ell k}) \bigcap \left\{ (\boldsymbol{w}^\ell_{i::}, L^\ell_{ij}) : \sum_{r\in[R_k]} 2^{r-1} \lfloor \delta_k c_k \rfloor w^\ell_{ikr} \geq L^\ell_{ij} \right\}.$$

Indeed, for any $(\boldsymbol{x}_{i:}, \boldsymbol{u}_{i::}, L^\ell_{ij}, \boldsymbol{w}^\ell_{i::}, E^\ell_1) \in \mathrm{conv}(\bar{X}^2_{ij\ell k}) \bigcap \left\{ (\boldsymbol{w}^\ell_{i::}, L^\ell_{ij}) : \sum_{r\in[R_k]} 2^{r-1} \lfloor \delta_k c_k \rfloor w^\ell_{ikr} \geq L^\ell_{ij} \right\}$. There exists a finite collection $\{(\boldsymbol{x}^\tau_{i:}, \boldsymbol{u}^\tau_{i::}, L^{\ell\tau}_{ij}, \boldsymbol{w}^{\ell\tau}_{i::}, E^{\ell\tau}_1)\}_{\tau\in[q]}$ and $\{\alpha_\tau\}_{\tau\in[q]} \subset [0,1]$ such that

$$\sum_{\tau\in[q]} \alpha_\tau (\boldsymbol{x}^\tau_{i:}, \boldsymbol{u}^\tau_{i::}, L^{\ell\tau}_{ij}, \boldsymbol{w}^{\ell\tau}_{i::}, E^{\ell\tau}_1) = (\boldsymbol{x}_{i:}, \boldsymbol{u}_{i::}, L^\ell_{ij}, \boldsymbol{w}^\ell_{i::}, E^\ell_1), \sum_{\tau\in[q]} \alpha_\tau = 1$$

and $\beta := \sum_{\tau\in[q]} \alpha_\tau \sum_{r\in[R_k]} 2^{r-1} \lfloor \delta_k c_k \rfloor w^{\ell\tau}_{ikr} \geq L^\ell_{ij}$.

Now let us define

$$\hat{L}_{ij}^{\ell\tau} = \frac{L_{ij}^{\ell}}{\beta} \sum_{r\in[R_k]} 2^{r-1} \lfloor \delta_k c_k \rfloor w_{ikr}^{\ell\tau}$$

for each $\tau \in [q]$. Clearly, we have

$$\sum_{\tau\in[q]} \alpha_\tau(\boldsymbol{x}_{i:}^{\tau}, \boldsymbol{u}_{i::}^{\tau}, \hat{L}_{ij}^{\ell\tau}, \boldsymbol{w}_{i::}^{\ell\tau}, E_1^{\ell\tau}) = (\boldsymbol{x}_{i:}, \boldsymbol{u}_{i::}, L_{ij}^{\ell}, \boldsymbol{w}_{i::}^{\ell}, E_1^{\ell}),$$

$$(\boldsymbol{x}_{i:}^{\tau}, \boldsymbol{u}_{i::}^{\tau}, \hat{L}_{ij}^{\ell\tau}, \boldsymbol{w}_{i::}^{\ell\tau}, E_1^{\ell\tau}) \in X_{ij\ell k}^2 \wedge \{x_{ik} = 1\}, \forall \tau \in [q].$$

Thus, $(\boldsymbol{x}_{i:}, \boldsymbol{u}_{i::}, L_{ij}^{\ell}, \boldsymbol{w}_{i::}^{\ell}, E_1^{\ell}) \in \text{conv}(X_{ij\ell k}^2 \wedge \{x_{ik} = 1\})$. □

It turns out that according to Lemma 3.8 and proposition 3.1. in Gupte et al. [113], sets $\text{conv}(\bar{X}_{ij\ell k}^2)$ and $\text{conv}(X_{ij\ell k}^2 \wedge \{x_{ik} = 1\})$ can be completely described using the result in Proposition 3.7 and the fact that variables $\boldsymbol{x}_{i:}$ are independent of others and constraint system with respect to $\boldsymbol{x}_{i:}$ are integral. These results are summarized below.

Proposition 3.9. *For each $i \in [I], j \in [J_i], k \in [K], \ell \in [N]$, the sets $\text{conv}(\bar{X}_{ij\ell k}^2)$ and $\text{conv}(X_{ij\ell k}^2 \wedge \{x_{ik} = 1\})$ admit the following complete descriptions:*

$$\text{conv}(\bar{X}_{ij\ell k}^2) = \left\{ (\boldsymbol{x}_{i:}, \boldsymbol{u}_{i::}, L_{ij}^{\ell}, \boldsymbol{w}_{i::}^{\ell}, E_1^{\ell}) : \begin{array}{l} \boldsymbol{x}_{i:} \in [0,1]^K, x_{ik} = 1, E_1^{\ell} \in [0,1], \\ w_{ikr} + \sum_{\tau\in\mathcal{I}_r} w_{ik\tau} \le |\mathcal{I}_r| E_1^{\ell}, \forall r \in [R_k] \setminus \mathcal{I}, \\ u_{ikr} + \sum_{\tau\in\mathcal{I}_r} u_{ik\tau} - w_{ikr} - \sum_{\tau\in\mathcal{I}_r} w_{ik\tau} \le \\ |\mathcal{I}_r|(1 - E_1^{\ell}), \forall r \in [R_k] \setminus \mathcal{I}, \\ 0 \le w_{ikr} \le E_1^{\ell}, \forall r \in [R_k], \\ 0 \le u_{ikr} - w_{ikr} \le (1 - E_1^{\ell}), \forall r \in [R_k] \end{array} \right\}; \tag{3.21}$$

and

$$\operatorname{conv}(X^2_{ij\ell k} \wedge \{x_{ik}=1\}) = \left\{ (\boldsymbol{x}_{i:}, \boldsymbol{u}_{i::}, L^\ell_{ij}, \boldsymbol{w}^\ell_{i::}, E^\ell_1) : \begin{array}{l} \boldsymbol{x}_{i:} \in [0,1]^K, x_{ik}=1, E^\ell_1 \in [0,1], \\ w_{ikr} + \sum_{\tau \in \mathcal{I}_r} w_{ik\tau} \le |\mathcal{I}_r| E^\ell_1, \forall r \in [R_k] \setminus \mathcal{I}, \\ u_{ikr} + \sum_{\tau \in \mathcal{I}_r} u_{ik\tau} - w_{ikr} - \sum_{\tau \in \mathcal{I}_r} w_{ik\tau} \le \\ |\mathcal{I}_r|(1-E^\ell_1), \forall r \in [R_k] \setminus \mathcal{I}, \\ 0 \le w_{ikr} \le E^\ell_1, \forall r \in [R_k], \\ 0 \le u_{ikr} - w_{ikr} \le (1-E^\ell_1), \forall r \in [R_k], \\ \sum_{r \in [R_k]} 2^{r-1} \lfloor \delta_k c_k \rfloor w^\ell_{ikr} \ge L^\ell_{ij} \end{array} \right\}. \tag{3.22}$$

Following Lemma 3.6 and the fact that the convex hull of a union of sets is equal to the convex hull of the union of convex hulls of sets, we arrive at the following complete description of the convex hull of set $X^2_{ij\ell}$.

Proposition 3.10. *For each $i \in [I], j \in [J_i]$, and $\ell \in [N]$, the set $\operatorname{conv}(X^2_{ij\ell})$ admits the*

following complete description:

$$\operatorname{conv}(X^2_{ij\ell}) = \left\{ (\boldsymbol{x}_{i:}, \boldsymbol{u}_{i::}, L^\ell_{ij}, \boldsymbol{w}^\ell_{i::}, E^\ell_1) : \begin{array}{l} \boldsymbol{x}_{i:} \in [0,1]^K, \sum_{k\in[K]} x_{ik} = 1, \sum_{k\in[K]} \hat{E}^\ell_{1ik} = E^\ell_1, \hat{E}^\ell_{1ik} \le x_{ik}, \\ w_{ikr} + \sum_{\tau\in\mathcal{I}_r} w_{ik\tau} \le |\mathcal{I}_r| \hat{E}^\ell_{1ik}, \forall r \in [R_k] \setminus \mathcal{I}, \forall k \in [K], \\ u_{ikr} + \sum_{\tau\in\mathcal{I}_r} u_{ik\tau} - w_{ikr} - \sum_{\tau\in\mathcal{I}_r} w_{ik\tau} \le \\ |\mathcal{I}_r|(1 - \hat{E}^\ell_{1ik}), \forall r \in [R_k] \setminus \mathcal{I}, \\ 0 \le w_{ikr} \le \hat{E}^\ell_{1ik}, \forall r \in [R_k], \forall k \in [K], \\ 0 \le u_{ikr} - w_{ikr} \le (1 - \hat{E}^\ell_{1ik}), \forall r \in [R_k], \forall k \in [K], \\ \sum_{r\in[R_k]} 2^{r-1} \lfloor \delta_k c_k \rfloor w^\ell_{ikr} \ge \hat{L}^\ell_{ijk}, \forall k \in [K], \\ \sum_{k\in[K]} \hat{L}^\ell_{ijk} = L^\ell_{ij}, 0 \le \hat{E}^\ell_{1ik} \le E^\ell_1 \le 1, \hat{L}^\ell_{ijk} \ge 0, \forall k \in [K] \end{array} \right\}. \tag{3.23}$$

3.5.3 Valid Inequalities

In this subsection, we develop valid inequalities to further strengthen the MILP model (3.13).

One-bus-per-route Inequalities: First, at-least-one-bus-per-route constraints (3.1e) together with the binarization constraints (3.8a) imply that at least one of the corresponding binary variables must be nonzero, i.e., the following valid inequalities must hold:

$$\sum_{r\in[R_k]} u_{ikr} \ge x_{ik}, \forall i \in [I], \forall k \in [K]. \tag{3.24}$$

Under-capacity Inequalities: Let us define $\underline{M} = \min_{k\in[K]} \lfloor \delta_k c_k \rfloor$ as the minimum route capacity at any route. Suppose each route has no capacity restriction, i.e., any passenger is supposed to get on board, then we can compute the ideal number of passengers remaining

on the bus using the following formula:

$$\iota_{ij}^{\ell} = \lceil (1 - \hat{a}_{ij}^{\ell}) \iota_{i,j-1}^{\ell} \rceil + \hat{\lambda}_{ij}^{\ell}, \forall i \in [I], \forall j \in [J_i], \forall \ell \in [N], \tag{3.25}$$

where we let $\iota_{i0}^{\ell} = 0$ for all $i \in [I]$ and $\ell \in [N]$. Now let us define $j_{i*}^{\ell} = \min\{J_i, \min_{j \in [J_i]}\{\iota_{i0}^{\ell} > \underline{M}\}$ to be the first bus stop such that the number of passengers planning to be on board is greater than the minimum capacity for each $i \in [I]$ and $\ell \in [N]$. Then, clearly, for any bus stop $j \in [j_{i*}^{\ell} - 1]$, it is under-capacity, i.e., we must have

$$y_{ij}^{\ell} = 1, \forall i \in [I], \forall j \in [j_{i*}^{\ell} - 1], \forall \ell \in [N]. \tag{3.26}$$

Utilization Rate when Being Fully Occupied: If one bus stop is fully occupied, the bus utilization rate must be one. Thus, we have the following valid inequalities:

$$1 - y_{ij}^{\ell} \leq E_1^{\ell}, \forall i \in [I], \forall j \in [J_i], \forall \ell \in [N]. \tag{3.27}$$

Tightening Big-M Coefficients: Note that in (3.11), we must have $L_{ij}^{\ell} \geq \hat{\lambda}_{ij}^{\ell}$ if $\hat{y}_{ij}^{\ell} = 1$ and $L_{ij}^{\ell} \geq \bar{L}_{i,j-1}^{\ell}$. Hence, in the first part of (3.11), we can reduce M by $M - \hat{\lambda}_{ij}^{\ell}$, and in the second part of (3.11), $\hat{\lambda}_{ij}^{\ell} - M(1 - y_{ij}^{\ell})$ can be tightened by $\hat{\lambda}_{ij}^{\ell} y_{ij}^{\ell}$. Therefore, we arrive at the following stronger inequalities

$$L_{ij}^{\ell} \geq \sum_{k \in [K]} n_{ik} \lfloor \delta_k c_k \rfloor - (M - \hat{\lambda}_{ij}^{\ell}) y_{ij}^{\ell}, L_{ij}^{\ell} \geq \bar{L}_{i,j-1}^{\ell} + \hat{\lambda}_{ij}^{\ell} y_{ij}^{\ell}, \forall i \in [I], \forall j \in [J_i], \forall \ell \in [N]. \tag{3.28}$$

Passengers Being Unserved when a Bus is Fully Occupied: We note that the passenger abandon rate becomes positive only when the bus is fully occupied at some moments,

i.e., a passenger will be allowed on board unless the bus is full. Thus, we must have

$$E_2^\ell \leq E_1^\ell, \forall \ell \in [N]. \tag{3.29}$$

Lower Bounding the Bus Utilization Rate: The disjunctive programming results in Section 3.5.2 implies that $\hat{E}_{1ik}^\ell \geq \hat{L}_{ijk}^\ell / (n_{ik} \lfloor \delta_k c_k \rfloor)$. Since $n_{ik} \leq \hat{M}_k := \min\{\eta_k, \sum_{\kappa \in [K]} \eta_\kappa - I + 1\}$, we must have

$$\hat{E}_{1ik}^\ell \geq \frac{\hat{L}_{ijk}^\ell}{\hat{M}_k \lfloor \delta_k c_k \rfloor}, \forall i \in [I], \forall j \in [J_i], \forall \ell \in [N]. \tag{3.30}$$

3.6 Approximation Algorithms Based on No-One-Left Policy

We observe that the intricacy of the MILP model (3.13) comes from the linearization of the first part of the objective function using binary variables $\boldsymbol{u}$ and the linearization of constraints (3.2b) using auxiliary variables $\boldsymbol{y}$. To avoid both, we propose an approximation scheme using the notion of the so-called No-one-left policy. Recall that in the previous section, we define $\boldsymbol{\iota}$ to be the ideal number of passengers at each bus stop when there is no capacity restriction. Our No-one-left policy follows the same concept.

Thus, we propose to solve the following simplified model as

$$\text{(No-one-left)} \qquad \min_{\boldsymbol{n}, \boldsymbol{x}} \left\{ \frac{1}{N} \sum_{\ell \in [N]} \overline{\mathcal{Q}} \left(\boldsymbol{n}, \boldsymbol{x}, \hat{\boldsymbol{\xi}}^\ell \right) : (3.1b) - (3.1f) \right\}, \tag{3.31a}$$

where we define $\overline{\mathcal{Q}}(\boldsymbol{n}, \boldsymbol{x}, \hat{\boldsymbol{\xi}}^\ell) = \max_{i \in [I], j \in [J_i]} \iota_{ij}^\ell / (\sum_{k \in [K]} n_{ik} \lfloor \delta_k c_k \rfloor)$. Note that $\overline{\mathcal{Q}}(\boldsymbol{n}, \boldsymbol{x}, \hat{\boldsymbol{\xi}}^\ell)$

admits a second-order conic representation as

$$\overline{\mathcal{Q}}(\boldsymbol{n},\boldsymbol{x},\hat{\boldsymbol{\xi}}^\ell)=\min_{\overline{E}^\ell\in\mathbb{R}_+}\left\{\overline{E}^\ell:\left\|\left(2\sqrt{\max_{j\in[J_i]}\iota_{ij}^\ell},\sum_{k\in[K]}n_{ik}\lfloor\delta_k c_k\rfloor-\overline{E}^\ell\right)\right\|_2\le\sum_{k\in[K]}n_{ik}\lfloor\delta_k c_k\rfloor+\overline{E}^\ell,\forall i\in[I]\right\}. \tag{3.31b}$$

After solving the No-one-left model (3.31), we can evaluate its objective value v^N by plugging in its optimal first-stage decision $(\bar{\boldsymbol{n}},\bar{\boldsymbol{x}})$ into DrFRAM (3.7), i.e.,

$$v^N=\frac{1}{N}\sum_{\ell\in[N]}\mathcal{Q}\left(\bar{\boldsymbol{n}},\bar{\boldsymbol{x}},\hat{\boldsymbol{\xi}}^\ell\right).$$

The following result shows the approximation bound of the No-one-left policy.

Proposition 3.11. *Suppose that* $(\bar{\boldsymbol{n}},\bar{\boldsymbol{x}},\overline{\boldsymbol{E}})$ *and* $(\boldsymbol{n}^*,\boldsymbol{x}^*,\boldsymbol{E}^*)$ *are optimal solutions to the No-one-left model* (3.31) *and DrFRAM* (3.13)*, respectively. Then we have*

$$v^*\le v^N\le v^*+\frac{\omega}{N}\|(\overline{\boldsymbol{E}}-\mathbf{e})_+\|_0+\frac{\overline{M}/\underline{M}-1}{N}\|\boldsymbol{E}_2^*\|_0,$$

where $\underline{M}:=\min_{k\in[K]}\lfloor\delta_k c_k\rfloor$ *and* $\overline{M}:=\max_{i\in[I],j\in[J_i],\ell\in[N]}\iota_{ij}^\ell$.

Proof: First of all, $v^*\le v^N$ is due to the feasibility of the first-stage decision $(\bar{\boldsymbol{n}},\bar{\boldsymbol{x}})$.

Next, we note that if $\overline{E}^\ell>1$, then we have $1\le\mathcal{Q}(\bar{\boldsymbol{n}},\bar{\boldsymbol{x}},\hat{\boldsymbol{\xi}}^\ell)\le 1+\omega$. Therefore, we must have

$$v^N-\frac{\omega}{N}\|(\overline{\boldsymbol{E}}-\mathbf{e})_+\|_0\le\frac{1}{N}\sum_{\ell\in[N]}\overline{E}^\ell. \tag{3.32}$$

According to the optimality of $(\bar{\boldsymbol{n}}, \bar{\boldsymbol{x}}, \overline{\boldsymbol{E}})$ to No-one-left model (3.31), we have

$$\frac{1}{N}\sum_{\ell\in[N]}\overline{E}^{\ell} \le \frac{1}{N}\sum_{\ell\in[N]}\frac{\max_{i\in[I],j\in[J_i]}\iota_{ij}^{\ell}}{\sum_{k\in[K]}n_{ik}^{*}\lfloor\delta_k c_k\rfloor} \le v^{*} + \frac{\overline{M}/\underline{M}-1}{N}\|\boldsymbol{E}_2^{*}\|_0. \tag{3.33}$$

Combining these two inequalities (3.32) and (3.33) together, we arrive at the conclusion. □

Proposition 3.11 shows that $(\bar{\boldsymbol{n}}, \bar{\boldsymbol{x}})$ is optimal to DrFRAM (3.7) if no passenger is being abandoned (i.e., $\boldsymbol{E}_2^{*} = \boldsymbol{0}$) in an optimal solution to the DrFRAM model and all the utilization rates are zero in the No-one-left model.

3.6.1 Enhancing No-one-left Policy

In this subsection, we propose to enhance the No-one-left policy by incorporating the abandon rate for each scenario that reaches a full utilization rate of some routes and resolving the problems again. Namely, suppose $(\bar{\boldsymbol{n}}, \bar{\boldsymbol{x}})$ denotes an optimal first-stage decision of the No-one-left model (3.31). Let us denote two subsets of scenarios, $\mathcal{N}_{-} = \{\ell \in [N] : \mathcal{Q}\left(\bar{\boldsymbol{n}}, \bar{\boldsymbol{x}}, \hat{\boldsymbol{\xi}}^{\ell}\right) \le 1\}$ and $\mathcal{N}_{+} = \{\ell \in [N] : \mathcal{Q}\left(\bar{\boldsymbol{n}}, \bar{\boldsymbol{x}}, \hat{\boldsymbol{\xi}}^{\ell}\right) > 1\}$. Then the enhanced model is defined as follows:

$$\textbf{(EnModel)} \qquad \min_{\boldsymbol{n},\boldsymbol{x}}\left\{\frac{1}{N}\left[\sum_{\ell\in\mathcal{N}_{-}}\overline{\mathcal{Q}}\left(\boldsymbol{n},\boldsymbol{x},\hat{\boldsymbol{\xi}}^{\ell}\right)+\sum_{\ell\in\mathcal{N}_{+}}\overline{\mathcal{Q}}^{E}\left(\boldsymbol{n},\boldsymbol{x},\hat{\boldsymbol{\xi}}^{\ell}\right)\right] : (3.1b)-(3.1f)\right\}, \tag{3.34a}$$

where $\overline{\mathcal{Q}}(\boldsymbol{n},\boldsymbol{x},\hat{\boldsymbol{\xi}}^{\ell})$ is defined in (3.31) and

$$\overline{\mathcal{Q}}^{E}(\boldsymbol{n},\boldsymbol{x},\hat{\boldsymbol{\xi}}^{\ell}) = \min_{\boldsymbol{L}^{\ell},\bar{\boldsymbol{L}}^{\ell},\boldsymbol{y}^{\ell},E_2^{\ell}}\left\{1+E_2^{\ell} : (3.10),(3.11),(3.12b),E_2^{\ell}\in[0,1]\right\}. \tag{3.34b}$$

Once solving the EnModel (3.34), we can repeat the procedure until invoking the stopping

criteria. This procedure is summarized in Algorithm 4.

Algorithm 4: Enhancing No-one-left Policy

Initialization: Solve the No-one-left model (3.31) with an optimal first-stage solution $(\bar{\boldsymbol{n}}, \bar{\boldsymbol{x}})$; set $t = 0, N_- = [N]$ and initialize $t_{\max}$;
while *Set* $\mathcal{N}_-$ *is changing and* $t < t_{\max}$ **do**
    Define $\mathcal{N}_- = \{\ell \in [N] : \mathcal{Q}(\bar{\boldsymbol{n}}, \bar{\boldsymbol{x}}, \hat{\boldsymbol{\xi}}^\ell) \leq 1\}$ and $\mathcal{N}_+ = \{\ell \in [N] : \mathcal{Q}(\bar{\boldsymbol{n}}, \bar{\boldsymbol{x}}, \hat{\boldsymbol{\xi}}^\ell) > 1\}$;
    Solve the EnModel (3.34);
    $t \leftarrow t + 1$.

3.7 Numerical Study

In this section, we present a set of numerical results to compare the strengths of different model formulations and test the effectiveness of distinct methods using both small and large random instances as well as real-world data provided by Blacksburg Transit. For the random instances, passenger arrival rates were generated from uniform distributions with the minimum value ranging from 2 to 20 and maximum value ranging from 22 to 40, and the proportion of passengers alighting from the bus was randomly generated from triangular distributions with the lower limit ranging from 0 to 0.2, the upper limit range from 0.6 to 1, and the mode ranging from 0.45 to 0.55. A time limit of 3600 seconds was set for solving each instance. All the instances were coded in Python 3.7.0 with calls to Gurobi 9.0.3 on a personal computer with a 1.9 GHz Intel Core i7 processor and 16G memory.

3.7.1 Results of Small Instances

In this section, we tested five small instances to compare the performances of MILP formulations as well as their continuous relaxations, where the number of bus routes I is 5 or 6 and the number of scenarios N is 5, and $K = 3$ types of buses with nominal capacities

$c_1 = 60, c_2 = 80, c_3 = 120$. Each route has 10 to 40 stops. We generated 50 cases based on these instances using different parameter combinations (i.e., different values of $I, \boldsymbol{\eta}, \delta, \omega, \theta$). Particularly, cases 1-25, 26-35, 36-40, 41-45, 46-50 correspond to instances 1,2,3,4,5, respectively. For all the cases, we fixed the normalized parameter $\gamma = 100$.

The numerical results of exactly solving different MILP formulations are reported in Table 3.1, where $a - b$ in the "Case" column means instance $\#a$ and case $\#b$, "MILP.B" represents MILP (3.13), "OPT" represents the optimal objective value obtained, "MILP.VI" represents MILP (3.13) with (3.24)-(3.29), "MILP.CONV" represents MILP (3.13) with (3.19), (3.23), (3.28), and (3.30), "MILP.VI.CONV" represents MILP (3.13) with (3.19), (3.23), (3.24)-(3.30). Without a doubt, we see that all the formulations are able to find an optimal solution. MILP.VI improves MILP.B's solution time on average but introduces more nodes to explore. This is probably because the valid inequalities introduced may force the solver to explore different branches before reaching an optimal solution. MILP.CONV requires fewer nodes to explore, but it usually takes more time to solve. This is possible because of additional variables introduced to describe the convex hulls. The running time of MILP.VI.CONV is in between that of MILP.VI and MILP.CONV, but it has the least number of nodes to explore. Hence, MILP.VI is the best among these methods.

We see that if the Wasserstein radius θ increases, the objective value increases and solution time does not change too much, since any increase in θ may result in larger passenger arrival rates and lower passenger alighting rates. As the pandemic factor δ or the total number of buses increases and other parameters stay the same, both objective value and solution time decrease, since larger δ or larger $\boldsymbol{\eta}$ implies larger capacities for some routes and thus more passengers to get onto the bus. Weight ω does not affect the objective value and solution time too much when the objective value is less than 1. When the objective value exceeds 1, a larger ω results in a larger objective value while the solution time stays the same. Since

the problem size grows as the number of routes I increases, the solution time also increases.

Table 3.1: Results of Different MILP Formulations

Case	I	$\boldsymbol{\eta}$	δ	ω	θ	OPT	MILP.B		MILP.VI		MILP.CONV		MILP.VI.CONV	
							Time	Nodes	Time	Nodes	Time	Nodes	Time	Nodes
1 - 1					0	0.885	40	2624	27	3547	85	4221	44	2241
1 - 2					0.25	0.920	56	5123	30	3689	203	5284	77	2452
1 - 3	5	(4,6,2)	0.25	0.25	0.5	0.930	36	3781	14	10032	104	3308	99	3081
1 - 4					1	0.940	67	7065	40	7375	99	4823	79	2889
1 - 5					1.5	0.972	45	5870	28	6732	160	4912	112	2732
			Average				49	4893	28	6275	130	4510	82	2679
1 - 6					0	0.885	24	3646	20	3841	69	2936	50	1611
1 - 7					0.25	0.920	30	2421	26	2588	64	2449	66	1905
1 - 8	5	(4,6,2)	0.25	0.5	0.5	0.930	21	2448	11	7222	63	2121	93	2667
1 - 9					1	0.940	36	2542	32	2984	87	2548	96	2173
1 - 10					1.5	0.982	49	5110	14	3126	86	2516	107	2348
			Average				32	3233	21	3952	74	2514	82	2141
1 - 11					0	0.885	23	1955	39	4716	85	3691	55	1455
1 - 12					0.25	0.920	24	3101	21	2496	43	1402	57	1782
1 - 13	5	(4,6,2)	0.25	1	0.5	0.930	16	1682	6	3285	49	1786	76	2161
1 - 14					1	0.940	18	2186	46	4333	47	1363	106	2953
1 - 15					1.5	1.000	26	2598	18	4093	82	2668	118	2264
			Average				21	2304	26	3785	61	2182	82	2123
1 - 16					0	0.572	20	3610	18	9968	37	6979	43	6797
1 - 17					0.25	0.596	8	5566	15	7568	92	2279	49	3650
1 - 18	5	(6,9,3)	0.25	0.5	0.5	0.600	24	2818	25	14153	126	14562	51	2210
1 - 19					1	0.609	32	4904	27	17539	116	2651	51	2930
1 - 20					1.5	0.632	36	4601	17	9853	92	2308	56	4023
			Average				24	4300	20	11816	93	5756	50	3922
1 - 21					0	0.286	3	1856	2	1224	32	2649	17	1364
1 - 22					0.25	0.298	6	2965	3	3141	34	3712	16	2123
1 - 23	5	(6,9,3)	0.5	0.5	0.5	0.300	6	1514	6	2484	37	3381	50	4174
1 - 24					1	0.304	18	1809	2	1305	34	2573	27	1720
1 - 25					1.5	0.316	10	1705	2	2968	34	5101	76	21284
			Average				9	1970	3	2224	34	3483	37	6133
2 - 26					0	0.389	53	7363	37	11959	164	28193	90	12605
2 - 27					0.25	0.404	111	12592	31	15186	440	8294	124	15668
2 - 28	6	(10,15,5)	0.25	0.5	0.5	0.404	75	6496	23	9392	334	31837	132	14800
2 - 29					1	0.408	47	5636	16	6465	338	33053	73	6650
2 - 30					1.5	0.427	37	4858	35	13029	415	28730	121	8573
			Average				64	7389	28	11206	338	26021	108	11659
2 - 31					0	0.389	66	10349	18	7355	242	35119	67	9443
2 - 32					0.25	0.404	61	7711	27	11740	283	5371	95	12051
2 - 33	6	(10,15,5)	0.25	1	0.5	0.404	58	7054	24	9935	317	6177	76	7333
2 - 34					1	0.408	53	5675	23	8398	113	19688	62	8379
2 - 35					1.5	0.427	136	17187	28	13626	481	28128	198	11008
			Average				75	9595	24	10211	287	18897	100	9643

Results of continuous relaxations of different MILP formulations are reported in Table 3.2, where we use "C.MILP.B," "C.MILP.VI," "C.MILP.CONV," "C.MILP.VI.CONV" to denote the continuous relaxations of MILP.B, MILP.VI, MILP.CONV, MILP.VI.CONV, respectively. We also define "Gap" as the percentage of the difference between the objective value and OPT divided by OPT. It is evident that both C.MILP.VI and C.MILP.CONV are better than C.MILP. This demonstrates the effectiveness of the proposed valid inequalities and the proposed convexification results. Clearly, the integration of valid inequalities and convexifi-

cation results is the best, i.e., C.MILP.VI.CONV yields the smallest optimality gap, which is around 90% on average. Such results indicate that the MILP.VI.CONV model is the most effective in improving the root gap. We also notice that valid inequalities contribute more than convexification results in improving the optimality gap since C.MILP.VI is consistently better than C.MILP.CONV. Besides, C.MILP.CONV takes more time than C.MILP.VI. This also explains why MILP.VI performs better than MILP.CONV in Table 3.1. Regarding both solution time and formulation strength, among the four different MILP formulations, MILP.VI tends to be the best. Since the continuous relaxation values of MILP.B are nearly 0, deriving stronger MILP formulations is of necessity.

Table 3.2: Results of Continuous Relaxations of Different MILP Models

Case	C.MILP.B			C.MILP.VI			C.MILP.CONV			C.MILP.VI.CONV		
	Obj.Val	Time	Gap(%)	Obj.Val	Time	Gap(%)	Obj.Val	Time	Gap(%)	Obj.Val	Time	Gap(%)
1 - 1	0.000	0.02	100.0	0.089	0.06	89.9	0.088	0.09	90.0	0.095	0.22	89.3
1 - 2	0.000	0.02	100.0	0.091	0.05	90.1	0.092	0.07	90.0	0.097	0.20	89.5
1 - 3	0.000	0.02	100.0	0.093	0.06	90.0	0.095	0.08	89.8	0.098	0.23	89.5
1 - 4	0.000	0.02	100.0	0.094	0.05	90.0	0.097	0.22	89.7	0.100	0.24	89.4
1 - 5	0.000	0.02	100.0	0.098	0.06	89.9	0.102	0.09	89.5	0.104	0.20	89.3
Average		0.02	100.0		0.06	90.0		0.11	89.8		0.22	89.4
1 - 6	0.000	0.02	100.0	0.089	0.08	89.9	0.091	0.17	89.7	0.095	0.23	89.3
1 - 7	0.000	0.02	100.0	0.091	0.06	90.1	0.096	0.09	89.5	0.097	0.21	89.5
1 - 8	0.000	0.02	100.0	0.093	0.06	90.0	0.099	0.11	89.4	0.098	0.22	89.5
1 - 9	0.000	0.02	100.0	0.094	0.08	90.0	0.101	0.10	89.3	0.100	0.21	89.4
1 - 10	0.000	0.02	100.0	0.098	0.06	90.0	0.107	0.08	89.1	0.104	0.21	89.4
Average		0.02	100.0		0.07	90.0		0.11	89.4		0.22	89.4
1 - 11	0.000	0.02	100.0	0.089	0.06	89.9	0.091	0.07	89.7	0.095	0.21	89.3
1 - 12	0.000	0.02	100.0	0.091	0.08	90.1	0.096	0.08	89.5	0.097	0.19	89.5
1 - 13	0.000	0.02	100.0	0.093	0.07	90.0	0.099	0.08	89.4	0.098	0.25	89.5
1 - 14	0.000	0.02	100.0	0.094	0.07	90.0	0.101	0.07	89.3	0.100	0.27	89.4
1 - 15	0.000	0.02	100.0	0.098	0.06	90.2	0.108	0.08	89.2	0.104	0.22	89.6
Average		0.02	100.0		0.07	90.0		0.08	89.4		0.23	89.5
1 - 16	0.000	0.02	100.0	0.044	0.09	92.3	0.040	0.12	92.9	0.049	0.15	91.4
1 - 17	0.000	0.02	100.0	0.045	0.09	92.4	0.043	0.09	92.8	0.050	0.17	91.5
1 - 18	0.000	0.02	100.0	0.046	0.08	92.4	0.044	0.16	92.7	0.051	0.24	91.4
1 - 19	0.000	0.02	100.0	0.047	0.08	92.3	0.045	0.08	92.7	0.052	0.20	91.4
1 - 20	0.000	0.02	100.0	0.048	0.08	92.3	0.048	0.07	92.4	0.054	0.21	91.4
Average		0.02	100.0		0.08	92.4		0.11	92.7		0.19	91.4
1 - 21	0.000	0.02	100.0	0.023	0.06	92.1	0.011	0.10	96.2	0.025	0.19	91.1
1 - 22	0.000	0.02	100.0	0.023	0.06	92.3	0.011	0.12	96.3	0.026	0.20	91.3
1 - 23	0.000	0.02	100.0	0.023	0.06	92.2	0.011	0.10	96.2	0.026	0.17	91.2
1 - 24	0.000	0.03	100.0	0.024	0.07	92.2	0.012	0.09	96.2	0.027	0.25	91.2
1 - 25	0.000	0.02	100.0	0.025	0.06	92.1	0.012	0.09	96.2	0.028	0.21	91.2
Average		0.02	100.0		0.06	92.2		0.10	96.2		0.20	91.2
2 - 26	0.000	0.03	100.0	0.031	0.13	92.1	0.015	0.12	96.3	0.038	0.22	90.2
2 - 27	0.000	0.03	100.0	0.031	0.12	92.2	0.015	0.12	96.2	0.039	0.35	90.4
2 - 28	0.000	0.03	100.0	0.032	0.13	92.1	0.016	0.12	96.1	0.039	0.24	90.3
2 - 29	0.000	0.03	100.0	0.033	0.12	92.0	0.016	0.11	96.1	0.040	0.24	90.2
2 - 30	0.000	0.03	100.0	0.034	0.11	92.1	0.017	0.13	96.0	0.042	0.25	90.2
Average		0.03	100.0		0.12	92.1		0.12	96.1		0.26	90.3
2 - 31	0.000	0.03	100.0	0.031	0.13	92.1	0.015	0.11	96.3	0.038	0.22	90.2
2 - 32	0.000	0.02	100.0	0.031	0.12	92.2	0.015	0.12	96.2	0.039	0.35	90.4
2 - 33	0.000	0.02	100.0	0.032	0.12	92.1	0.016	0.11	96.1	0.039	0.47	90.3
2 - 34	0.000	0.02	100.0	0.033	0.13	92.0	0.016	0.10	96.1	0.040	0.27	90.2
2 - 35	0.000	0.02	100.0	0.034	0.12	92.1	0.017	0.13	96.0	0.042	0.25	90.2
Average		0.02	100.0		0.12	92.1		0.12	96.1		0.31	90.3

We then compare the scenario decomposition Algorithm 1 based on four different MILP for-

mulations (i.e., MILP.B, MILP.VI, MILP.CONV, MILP.VI.CONV) as well as two approximation algorithms (i.e., Algorithm 3, Algorithm 4), and results are reported in Table 3.3. Compared to directly solving MILP formulations using a solver, as shown in Table 3.1, we see that for each MILP method, their corresponding scenario decomposition counterpart is more effective and has a much shorter solution time. More precisely, except for the MILP.B model, employing scenario decomposition Algorithm 1 reduces the solution time by about 60% compared to solving its corresponding MILP formulation. This demonstrates the effectiveness of scenario decomposition Algorithm 1. As scenario decomposition based on MILP.VI method took the least time for nearly all the instances, we also used MILP.VI method when implementing the accelerated scenario decomposition Algorithm 3.

We see that if the Wasserstein radius θ increases, the solution time does not change too much for all the scenario decomposition methods. As the pandemic factor δ or the number of buses $\boldsymbol{\eta}$ increases, the solution time decreases. As the weight ω increases, the solution time of Algorithm 1 based on MILP.B, MILP.CONV, MILP.VI.CONV decreases, while the solution time of Algorithm 1 based on MILP.VI increases. As the number of routes I increases, the solution time increases for all the scenario decomposition methods.

When implementing the accelerated scenario decomposition Algorithm 3, we forced the lower bound to increase by 1% at each iteration. Therefore, compared to scenario decomposition Algorithm 1 based on MILP.VI, the accelerated scenario decomposition Algorithm 3 significantly reduces the running time by around 80%. Although the accelerated scenario decomposition Algorithm 3 may miss the optimal solution by cutting off plausible solutions, we see from Table 3.3 that it consistently finds optimal solutions for all the testing cases. We also applied the approximation Algorithm 4 by setting the maximum iteration to 1000. We notice from Table 3.3 that for all the testing cases, the approximation Algorithm 4 can obtain an optimal solution and takes less than a second to solve. This suggests that the

approximation Algorithm 4 can be a strong alternative when the exact methods might not work well. We also see that no matter how the parameters change, the solution time does not change too much for Algorithm 3 and Algorithm 4.

Table 3.3: Results of Four Scenario Decomposition Algorithm 1 Based on Four Different MILP Formulations and Two Approximate Methods (i.e., Algorithm 3, Algorithm 4)

Case	Scenario Decomposition								Approximate Methods			
	MILP.B		MILP.VI		MILP.CONV		MILP.VI.CONV		Algorithm 3		Algorithm 4	
	Time	Gap(%)	Time	Gap(%)	Time	Gap(%)	Time	Gap(%)	Time	Gap(%)	Time	Gap(%)
1 - 1	22	0.0	8	0.0	37	0.0	21	0.0	7	0.0	0.06	0.0
1 - 2	14	0.0	6	0.0	28	0.0	16	0.0	8	0.0	0.03	0.0
1 - 3	27	0.0	9	0.0	36	0.0	20	0.0	12	0.0	0.05	0.0
1 - 4	40	0.0	8	0.0	128	0.0	27	0.0	10	0.0	0.04	0.0
1 - 5	72	0.0	8	0.0	83	0.0	71	0.0	11	0.0	0.05	0.0
Average	35	0.0	8	0.0	62	0.0	31	0.0	10	0.0	0.05	0.0
1 - 6	33	0.0	9	0.0	39	0.0	32	0.0	9	0.0	0.04	0.0
1 - 7	19	0.0	7	0.0	35	0.0	21	0.0	7	0.0	0.03	0.0
1 - 8	50	0.0	6	0.0	34	0.0	20	0.0	6	0.0	0.05	0.0
1 - 9	23	0.0	13	0.0	49	0.0	18	0.0	15	0.0	0.04	0.0
1 - 10	22	0.0	17	0.0	69	0.0	38	0.0	10	0.0	0.06	0.0
Average	29	0.0	10	0.0	45	0.0	26	0.0	9	0.0	0.04	0.0
1 - 11	21	0.0	14	0.0	45	0.0	28	0.0	8	0.0	0.04	0.0
1 - 12	17	0.0	11	0.0	38	0.0	18	0.0	7	0.0	0.03	0.0
1 - 13	15	0.0	13	0.0	38	0.0	17	0.0	11	0.0	0.04	0.0
1 - 14	19	0.0	14	0.0	55	0.0	25	0.0	13	0.0	0.04	0.0
1 - 15	49	0.0	13	0.0	60	0.0	49	0.0	11	0.0	0.06	0.0
Average	24	0.0	13	0.0	47	0.0	27	0.0	10	0.0	0.04	0.0
1 - 16	39	0.0	13	0.0	65	0.0	36	0.0	5	0.0	0.03	0.0
1 - 17	25	0.0	11	0.0	52	0.0	33	0.0	5	0.0	0.02	0.0
1 - 18	27	0.0	10	0.0	45	0.0	35	0.0	5	0.0	0.03	0.0
1 - 19	33	0.0	9	0.0	76	0.0	33	0.0	5	0.0	0.02	0.0
1 - 20	33	0.0	9	0.0	54	0.0	31	0.0	3	0.0	0.03	0.0
Average	31	0.0	10	0.0	58	0.0	34	0.0	5	0.0	0.03	0.0
1 - 21	20	0.0	6	0.0	28	0.0	25	0.0	2	0.0	0.03	0.0
1 - 22	14	0.0	6	0.0	26	0.0	18	0.0	4	0.0	0.03	0.0
1 - 23	12	0.0	5	0.0	20	0.0	17	0.0	3	0.0	0.03	0.0
1 - 24	15	0.0	6	0.0	24	0.0	19	0.0	2	0.0	0.03	0.0
1 - 25	13	0.0	7	0.0	26	0.0	17	0.0	2	0.0	0.03	0.0
Average	15	0.0	6	0.0	25	0.0	19	0.0	3	0.0	0.03	0.0
2 - 26	38	0.0	7	0.0	83	0.0	47	0.0	7	0.0	0.04	0.0
2 - 27	44	0.0	7	0.0	51	0.0	29	0.0	9	0.0	0.04	0.0
2 - 28	41	0.0	8	0.0	57	0.0	29	0.0	8	0.0	0.05	0.0
2 - 29	35	0.0	5	0.0	66	0.0	20	0.0	9	0.0	0.03	0.0
2 - 30	25	0.0	12	0.0	53	0.0	24	0.0	9	0.0	0.04	0.0
Average	37	0.0	8	0.0	62	0.0	30	0.0	8	0.0	0.04	0.0
2 - 31	35	0.0	10	0.0	80	0.0	39	0.0	10	0.0	0.04	0.0
2 - 32	34	0.0	7	0.0	49	0.0	24	0.0	6	0.0	0.05	0.0
2 - 33	30	0.0	6	0.0	50	0.0	21	0.0	9	0.0	0.03	0.0
2 - 34	27	0.0	6	0.0	43	0.0	19	0.0	9	0.0	0.05	0.0
2 - 35	21	0.0	9	0.0	53	0.0	22	0.0	6	0.0	0.03	0.0
Average	29	0.0	8	0.0	55	0.0	25	0.0	8	0.0	0.04	0.0

According to the results in Table 3.1, Table 3.2, and Table 3.3, we see that MILP.VI is the most efficient one among four MILP formulations, scenario decomposition Algorithm 1 based on MILP.VI denoted by "Algorithm 1.VI" is the most efficient one among four different scenario decomposition methods using different MILP formulations, and both approximation methods are quite good. To further compare those methods, we applied MILP.B, MILP.VI,

SceDecomp.VI, Algorithm 3, and Algorithm 4 to harder instances with a larger objective value. For Algorithm 4, we let the maximum number of iterations equal to 5 and 100 to see the influence of the maximum number of iterations on the solution quality. These two different configurations are denoted by Algorithm 4(max iter 5) and Algorithm 4(max iter 100). Results are displayed in Table 3.4.

From Table 3.4, similar to previous results, we see that MILP.VI reduces the solution time compared to MILP.B. Although Algorithm 1.VI outperforms MILP.VI, Algorithm 3 is the best among these three. We also see that Algorithm 4 (max iter 5) has the shortest solution time but misses the optimal solution, while Algorithm 4(max iter 100) takes a longer average solution time. However, its solution quality is better, and its average solution time is overall shorter than that of accelerated scenario decomposition Algorithm 1. Therefore, in practice, we suggest using approximation Algorithm 4 with a properly chosen maximum number of iterations to solve hard instances.

Table 3.4: Results of Instances with a Larger Objective Value

Case	ω	θ	OPT	MILP.B	MILP.VI		Algorithm 1.VI		Algorithm 3		Algorithm 4 (max itr 5)			Algorithm 4(max itr 100)		
				Time	Time	Gap(%)	Time	Gap(%)	Time	Gap(%)	Obj.Val	Time	Gap(%)	Obj.Val	Time	Gap(%)
3 - 36	0.25	0	1.006	56	25	0.0	11	0.0	12	0.0	1.038	1	3.2	1.006	40	0.0
3 - 37		0.25	1.053	33	46	0.0	15	0.0	16	0.0	1.063	3	1.0	1.053	3	0.0
3 - 38		0.5	1.053	19	54	0.0	24	0.0	19	0.0	1.063	3	1.0	1.053	3	0.0
3 - 39		1	1.053	35	31	0.0	39	0.0	23	0.0	1.063	4	1.0	1.053	3	0.0
3 - 40		1.5	1.076	33	12	0.0	23	0.0	41	0.0	1.076	10	0.0	1.076	8	0.0
Average				35	34	0.0	22	0.0	22	0.0		4	1.2		11	0.0
4 - 41	0.5	0	1.032	24	41	0.0	15	0.0	22	0.0	1.056	2	2.3	1.032	56	0.0
4 - 42		0.25	1.105	48	24	0.0	33	0.0	24	0.0	1.135	3	2.7	1.105	5	0.0
4 - 43		0.5	1.105	40	19	0.0	26	0.0	17	0.0	1.135	3	2.7	1.105	5	0.0
4 - 44		1	1.105	23	25	0.0	21	0.0	20	0.0	1.135	4	2.7	1.105	6	0.0
4 - 45		1.5	1.152	35	11	0.0	24	0.0	23	0.0	1.152	10	0.0	1.152	16	0.0
Average				34	24	0.0	24	0.0	21	0.0		4	2.1		18	0.0
5 - 46	1	0	1.085	33	15	0.0	15	0.0	11	0.0	1.093	2	0.8	1.085	65	0.0
5 - 47		0.25	1.210	29	13	0.0	19	0.0	14	0.0	1.231	4	1.7	1.210	3	0.0
5 - 48		0.5	1.210	36	34	0.0	17	0.0	11	0.0	1.231	4	1.7	1.210	3	0.0
5 - 49		1	1.210	25	14	0.0	17	0.0	18	0.0	1.231	4	1.7	1.210	4	0.0
5 - 50		1.5	1.303	36	36	0.0	21	0.0	15	0.0	1.333	19	2.3	1.303	11	0.0
Average				32	22	0.0	18	0.0	14	0.0		7	1.6		17	0.0

3.7.2 Results of Larger Instances

This subsection focuses on larger instances. We generated 3 larger instances where the number of bus routes $I \in \{10, 20\}$ and the number of scenarios $N \in \{10, 20\}$. There are $K = 3$ types of buses with nominal capacities $c_1 = 60, c_2 = 80, c_3 = 120$ and each route has 10 to 40 stops. The pandemic factor δ is 0.25. We tested 20 cases based on these instances using different parameter configurations (i.e., different values of $N, I, \boldsymbol{\eta}, \omega, \theta$). Particularly, cases 51-60, 61-65, 66-70 correspond to instances 6, 7, 8, respectively.

Results of different MILP formulations are reported in Table 3.5 and Table 3.6, where "Obj.Val" denotes the best upper bound, "LB" denotes the best lower bound, "Opt.Gap" represents the optimality gap computed as the percentage of the difference between Obj.Val and LB divided by Obj.Val, and "/" denotes the cases in that no solution was found within the time limit (i.e., 3600 seconds). Unfortunately, no case can be solved to optimality within the time limit. For cases 64,65,69,70, MILP.VI.CONV cannot even find a feasible solution within the time limit. We notice that MILP.VI consistently obtains the best lower bound among the four MILP formulations almost for each case. However, albeit promising, MILP.VI may not be ideal for solving extremely large instances since the optimality gap is quite large within the time limit.

Results of continuous relaxations of MILP formulations are displayed in Table 3.7. Similarly, we see the continuous relaxation of MILP.VI.CONV is the best compared to other formulations; however, it takes the longest time to compute. On the other hand, the continuous relaxation values of MILP.VI are comparable to those of MILP.VI.CONV, but takes a much shorter time. This somehow explains why MILP.VI works the best among all the MILP formulations. Results of cases 61-70 show that for very large-scale cases, even solving a continuous relaxation takes a relatively long time to solve to optimality, indicating that

Table 3.5: Results of MILP.B and MILP.VI for Solving Larger Instances

Case	N	I	η	ω	θ	MILP.B					MILP.VI				
						Obj.Val	Time	Opt.Gap(%)	LB	Nodes	Obj.Val	Time	Opt.Gap(%)	LB	Nodes
6 - 51					0	0.743	3600	39.8	0.447	16791	0.743	3600	34.8	0.484	121062
6 - 52					0.25	0.763	3600	48.0	0.397	10684	0.763	3600	37.6	0.476	20532
6 - 53	10	10	(10,15,5)	0.5	0.5	0.775	3600	39.8	0.466	20265	0.775	3600	32.1	0.526	21055
6 - 54					1	0.778	3600	35.1	0.505	14401	0.778	3600	34.3	0.511	143685
6 - 55					1.5	0.817	3600	32.9	0.549	21088	0.817	3600	41.1	0.482	20586
Average							3600	34.0		16646		3600	37.7		65384
6 - 56					0	0.743	3600	24.3	0.563	27659	0.743	3600	34.5	0.487	164536
6 - 57					0.25	0.763	3600	30.5	0.530	25626	0.763	3600	40.8	0.452	20589
6 - 58	10	10	(10,15,5)	1	0.5	0.775	3600	39.4	0.469	18724	0.775	3600	44.7	0.428	20616
6 - 59					1	0.778	3600	35.3	0.503	12208	0.778	3600	35.1	0.505	22077
6 - 60					1.5	0.817	3600	27.5	0.593	34584	0.829	3600	46.9	0.440	20639
Average							3600	31.4		23760		3600	41.0		49691
7 - 61					0	1.309	3600	78.5	0.282	673	1.249	3600	62.4	0.470	13611
7 - 62					0.25	1.311	3600	77.4	0.296	869	1.300	3600	57.8	0.549	1111
7 - 63	10	20	(8,20,8)	0.5	0.5	1.341	3600	78.8	0.285	1040	1.272	3600	56.4	0.555	1116
7 - 64					1	1.316	3600	77.4	0.297	1035	1.340	3600	56.9	0.577	1071
7 - 65					1.5	1.335	3600	76.6	0.313	1058	1.299	3600	51.8	0.626	1085
Average							3600	77.0		935		3600	54.4		3599
8 - 66					0	1.378	3600	81.0	0.261	1	0.798	3600	61.1	0.311	1195
8 - 67					0.25	1.112	3600	80.6	0.215	20691	0.923	3600	64.2	0.331	1052
8 - 68	20	20	(20, 30, 15)	0.5	0.5	1.396	3600	80.5	0.272	1	1.349	3600	75.6	0.329	2958
8 - 69					1	1.332	3600	81.1	0.252	1	1.294	3600	72.9	0.351	1058
8 - 70					1.5	1.353	3600	80.3	0.267	1	0.867	3600	58.7	0.358	1088
Average							3600	80.7		4139		3600	65.8		1470

exact methods may also have trouble solving these cases to optimality within an hour.

Results of scenario decomposition Algorithm 1 based on four different MILP formulations, scenario decomposition with grouping Algorithm 2 based on MILP.VI, accelerated scenario decomposition Algorithm 3 based on MILP.VI and approximation algorithm Algorithm 4 (with maximum iteration equal to 5) are shown in Table 3.8 and Table 3.9, where "Best.Obj" represents the best objective value obtained by four MILP formulations and Algorithm 1 based on four MILP formulations for each case. In scenario bundling, we used K-means clustering algorithm to group the scenarios into 5 groups for instance 6 and 7, 10 groups for instance 8. It is seen that Algorithm 4 is the only method that can find feasible solutions to cases 61-65. For cases 66-70, only Algorithm 1 based on the MILP.VI formulation, Algorithm 3, and Algorithm 4 can obtain feasible solutions within the time limit. For the hard cases 61-70, Algorithm 4 finds better solutions than the best ones output by the exact methods. We notice that, in Table 3.9, based on the MILP.VI formulation, compared with Algorithm 1, Algorithm 2 using scenario group improves the optimality gap for instance 6, which shows

Table 3.6: Results of MILP.CONV and MILP.VI.CONV for Solving Larger Instances

Case	MILP.CONV					MILP.VI.CONV				
	Obj.Val	Time	Opt.Gap(%)	LB	Nodes	Obj.Val	Time	Opt.Gap(%)	LB	Nodes
6 - 51	0.755	3600	49.5	0.381	2487	0.755	3600	50.1	0.377	21512
6 - 52	0.773	3600	48.2	0.400	1352	0.773	3600	48.1	0.401	21526
6 - 53	0.787	3600	42.9	0.449	21090	0.775	3600	54.6	0.352	21166
6 - 54	0.788	3600	55.4	0.352	5154	0.778	3600	47.6	0.408	15570
6 - 55	0.861	3600	54.1	0.395	2274	0.829	3600	54.6	0.376	15002
Average		3600	54.8		3714		3600	51.1		15286
6 - 56	0.767	3600	45.4	0.419	20850	0.743	3600	48.6	0.382	21441
6 - 57	0.773	3600	40.5	0.460	1075	0.773	3600	53.5	0.360	15879
6 - 58	0.782	3600	44.9	0.431	1039	0.782	3600	48.5	0.403	20659
6 - 59	0.847	3600	51.3	0.413	1568	0.792	3600	51.2	0.386	18457
6 - 60	0.864	3600	47.8	0.451	21036	0.817	3600	48.8	0.418	12172
Average		3600	49.5		11302		3600	50.0		15315
7 - 61	1.392	3600	65.1	0.485	1	1.443	3600	73.7	0.380	1
7 - 62	1.393	3600	63.6	0.507	1	1.445	3600	69.1	0.446	11
7 - 63	1.385	3600	62.8	0.515	1	1.445	3600	69.0	0.448	7
7 - 64	1.405	3600	65.7	0.482	1	/	3600	/	/	/
7 - 65	1.411	3600	63.1	0.521	2903	/	3600	/	/	/
Average		3600	64.4		1452		3600	70.6		6
8 - 66	1.447	3600	79.1	0.302	1	1.447	3600	96.7	0.048	1
8 - 67	1.446	3600	80.7	0.279	18	1.446	3600	97.3	0.039	1
8 - 68	1.447	3600	75.3	0.357	1	1.447	3600	95.7	0.063	1
8 - 69	1.449	3600	80.3	0.286	1	/	3600	/	/	/
8 - 70	1.412	3600	76.4	0.334	1	/	3600	/	/	/
Average		3600	78.3		1		3600	96.5		1

that grouping can help solve medium-size instances. However, Algorithm 2 cannot obtain any feasible solution for instance 8 within the time limit, while Algorithm 1 can find at least one solution. This may be because scenario-grouping subproblems are more challenging to solve than those without grouping. Thus, for the large-scale instances, we suggest using the naive scenario decomposition method (i.e., Algorithm 1). For easy cases 51-60, both Algorithm 3 and Algorithm 4 find exactly the same solutions as the best ones output by the exact methods. Overall, we conclude that among all the exact methods, when solving moderate-sized cases, Algorithm 1 based on MILP.VI outperforms other methods by providing the smallest optimality gaps; on the other hand, for the hard cases, none of the exact methods works well, MILP.VI and Algorithm 1 based on MILP.VI are slightly better than others since they can consistently find a better solution. We also see that Algorithm 4 consistently finds either a better solution or the same quality solution. Therefore, in practice, when facing very large-scale cases or involving multiple-round cross-validations, we suggest using Algorithm 4.

Table 3.7: Results of Continuous Relaxations of Four Different MILP Formulations for Solving Larger Instances

Case	C.MILP.B		C.MILP.VI		C.MILP.CONV		C.MILP.VI.CONV	
	Obj.Val	Time	Obj.Val	Time	Obj.Val	Time	Obj.Val	Time
6 - 51	0.000	0.16	0.044	0.83	0.030	0.45	0.054	3.53
6 - 52	0.000	0.15	0.045	0.96	0.032	0.44	0.056	2.68
6 - 53	0.000	0.16	0.046	0.58	0.032	0.37	0.056	2.65
6 - 54	0.000	0.34	0.046	1.09	0.033	0.39	0.057	2.72
6 - 55	0.000	0.19	0.048	0.67	0.035	0.40	0.059	3.21
Average		0.20		0.83		0.41		2.96
6 - 56	0.000	0.16	0.044	0.98	0.030	0.36	0.054	2.38
6 - 57	0.000	0.15	0.045	0.74	0.032	0.53	0.056	2.52
6 - 58	0.000	0.14	0.046	0.62	0.032	0.46	0.056	2.53
6 - 59	0.000	0.14	0.046	0.85	0.033	0.62	0.057	3.48
6 - 60	0.000	0.14	0.048	0.79	0.035	0.37	0.059	2.95
Average		0.15		0.80		0.47		2.77
7 - 61	0.000	0.22	0.307	2.45	0.020	1.12	0.307	12.28
7 - 62	0.000	0.24	0.342	1.59	0.021	1.56	0.342	8.82
7 - 63	0.000	0.23	0.352	2.18	0.022	1.58	0.352	8.47
7 - 64	0.000	0.23	0.367	2.35	0.022	1.60	0.367	8.17
7 - 65	0.000	0.22	0.415	2.33	0.023	1.12	0.415	6.76
Average		0.23		2.18		1.40		8.90
8 - 66	0.000	0.52	0.023	5.01	0.003	4.61	0.027	22.80
8 - 67	0.000	0.64	0.024	4.50	0.003	3.69	0.028	25.73
8 - 68	0.000	0.50	0.024	6.05	0.003	3.49	0.028	40.80
8 - 69	0.000	0.56	0.024	5.01	0.003	3.75	0.028	29.88
8 - 70	0.000	0.53	0.025	4.21	0.009	3.12	0.030	29.71
Average		0.55		4.96		3.73		29.79

3.7.3 Out-of-sample Performance

In this section, we tested the out-of-sample performance of the proposed DrFRAM model. All the instances in this subsection are relatively small and were solved to optimality by MILP.VI. Let $\mathbb{P}^{\infty}$ denote the sample probability distribution, and $\mathbb{P}^{*}$ be the true distribution of random parameters $\tilde{\boldsymbol{\xi}}$. Motivated by Esfahani and Kuhn [96], we define the out-of-sample probability as

$$\mathbb{P}^{\infty}\left\{\tilde{\boldsymbol{\xi}} : v^{*} < \mathbb{E}_{\mathbb{P}^{*}}\left[\mathcal{Q}\left(\boldsymbol{n}^{D}, \boldsymbol{x}^{D}, \tilde{\boldsymbol{\xi}}\right)\right] + \rho \mathrm{CVaR}_{1-\varepsilon}\left(\boldsymbol{n}^{D}, \boldsymbol{x}^{D}, \tilde{\boldsymbol{\xi}}\right)\right\},$$

where $(\boldsymbol{n}^{D}, \boldsymbol{x}^{D})$ denotes the optimal solution of the DrFRAM model and $\mathcal{Q}(\cdot,\cdot,\cdot)$ represents the recourse function. That is, we would like to ensure that the probability that the DrFRAM optimal value is smaller than the mean-risk objective is small, e.g., no larger than 2α; in our numerical study, we let $\alpha = 5\%$, $\rho = 0.1$ and $\varepsilon = 0.1$. To measure this out-of-sample probability, for any given θ, we first solved the DrFRAM model using generated data and then generated new samples with the same sample size and obtained $(1-\alpha)$ confidence

Table 3.8: Results of Three Scenario Decomposition Algorithm 1 Based on Three Different MILP Formulations (i.e., MILP.B, MILP.CONV, MILP.CONV.VI) for Solving Larger Instances

Case	Scenario Decomposition											
	MILP.B				MILP.CONV				MILP.VI.CONV			
	Obj.Val	LB	Time	Opt.Gap(%)	Obj.Val	LB	Time	Opt.Gap(%)	Obj.Val	LB	Time	Opt.Gap(%)
6 - 51	0.743	0.708	3600	4.7	0.743	0.701	3600	5.7	0.743	0.717	3600	3.6
6 - 52	0.763	0.734	3600	3.8	0.763	0.731	3600	4.3	0.763	0.743	3600	2.7
6 - 53	0.775	0.745	3600	3.9	0.775	0.738	3600	4.7	0.775	0.740	3600	4.4
6 - 54	0.778	0.748	3600	3.8	0.778	0.741	3600	4.7	0.778	0.756	3600	2.8
6 - 55	0.817	0.785	3600	3.9	0.817	0.783	3600	4.2	0.817	0.795	3600	2.8
Average			3600	4.0			3600	4.7			3600	3.3
6 - 56	0.743	0.717	3600	3.6	0.743	0.702	3600	5.6	0.743	0.717	3600	3.6
6 - 57	0.763	0.737	3600	3.4	0.763	0.732	3600	4.1	0.763	0.743	3600	2.7
6 - 58	0.775	0.745	3600	3.9	0.775	0.738	3600	4.7	0.775	0.740	3600	4.4
6 - 59	0.778	0.748	3600	3.8	0.778	0.741	3600	4.7	0.778	0.748	3600	3.8
6 - 60	0.817	0.785	3600	3.9	0.817	0.783	3600	4.2	0.817	0.795	3600	2.8
Average			3600	3.7			3600	4.7			3600	3.5
7 - 61	/	/	3600	/	/	/	3600	/	/	/	3600	/
7 - 62	/	/	3600	/	/	/	3600	/	/	/	3600	/
7 - 63	/	/	3600	/	/	/	3600	/	/	/	3600	/
7 - 64	/	/	3600	/	/	/	3600	/	/	/	3600	/
7 - 65	/	/	3600	/	/	/	3600	/	/	/	3600	/
Average			3600	/			3600	/			3600	/
8 - 66	/	/	3600	/	/	/	3600	/	/	/	3600	/
8 - 67	/	/	3600	/	/	/	3600	/	/	/	3600	/
8 - 68	/	/	3600	/	/	/	3600	/	/	/	3600	/
8 - 69	/	/	3600	/	/	/	3600	/	/	/	3600	/
8 - 70	/	/	3600	/	/	/	3600	/	/	/	3600	/
Average			3600	/			3600	/			3600	/

intervals of the objective value by plugging in the solution to the DrFRAM and the mean-risk models. We repeated the same procedure for a list of θ values and selected the smallest θ that the confidence interval for the DrFRAM objective value is beyond that of the mean-risk objective value, i.e., to guarantee out-of-sample probability to be at most 2α. The probabilities used for out-of-sample or in-sample performances are all asymptotic.

In our numerical study, we supposed that the number of bus routes I is 5, each route has 10 to 40 stops, there are $K = 3$ types of buses with nominal capacities $c_1 = 60, c_2 = 80, c_3 = 120$, the number of buses is $\boldsymbol{\eta} = (6, 9, 3)$, the pandemic factor δ is 0.25, the weight ω is 0.5, and the number of scenarios $N = 10$. We also assumed that the passenger arrival rates follow discrete uniform distributions between 0 and 25. The percentage of passengers alighting from the bus follows a triangular distribution with a lower limit of 0.2, an upper limit of 0.9, and a mode of 0.4. To select the smallest θ that guaranteed a 90% asymptotic in-sample performance, we adopted the following procedure: (i) for each $\theta \in \{0, 0.2, \ldots, 4\}$, generate 10 scenarios for the DrFRAM model; (ii) generate 10 scenarios by plugging the solution

Table 3.9: Results of the Scenario Decomposition Algorithm 1 Based on MILP.VI, Denoted by Algorithm 1.VI, Scenario Decomposition with Grouping Algorithm 2 Based on MILP.VI, Denoted by Algorithm 2.VI, and Two Approximate Methods (i.e., Algorithm 3, Algorithm 4) for Solving Larger Instances

Case	Algorithm 1.VI				Algorithm 2.VI				Best.Obj	Algorithm 3		Algorithm 4	
	Obj.Val	LB	Time	Opt.Gap(%)	Obj.Val	LB	Time	Opt.Gap(%)		Obj.Val	Time	Obj.Val	Time
6 - 51	0.743	0.719	3600	3.3	0.743	0.719	3600	3.3	0.743	0.743	119	0.743	0.01
6 - 52	0.763	0.748	3600	2.0	0.763	0.750	3600	1.8	0.763	0.763	102	0.763	0.02
6 - 53	0.775	0.757	3600	2.2	0.775	0.759	3600	2.1	0.775	0.775	152	0.775	1.00
6 - 54	0.778	0.762	3600	2.0	0.778	0.765	3600	1.7	0.778	0.778	123	0.778	0.01
6 - 55	0.817	0.797	3600	2.5	0.817	0.798	3600	2.5	0.817	0.817	171	0.817	0.02
Average			3600	2.4			3600	2.3			133		0.21
6 - 56	0.743	0.719	3600	3.3	0.743	0.719	3600	3.3	0.743	0.743	159	0.743	0.01
6 - 57	0.763	0.748	3600	2.0	0.763	0.750	3600	1.8	0.763	0.763	139	0.763	0.02
6 - 58	0.775	0.754	3600	2.7	0.775	0.759	3600	2.1	0.775	0.775	233	0.775	1.00
6 - 59	0.778	0.766	3600	1.5	0.778	0.765	3600	1.7	0.778	0.778	234	0.778	0.01
6 - 60	0.817	0.800	3600	2.1	0.817	0.800	3600	2.1	0.817	0.817	212	0.817	0.02
Average			3600	2.3			3600	2.2			195		0.21
7 - 61	/	/	3600	/	/	/	3600	/	1.249	/	3600	1.124	3600
7 - 62	/	/	3600	/	/	/	3600	/	1.300	/	3600	1.139	3600
7 - 63	/	/	3600	/	/	/	3600	/	1.272	/	3600	1.140	3600
7 - 64	/	/	3600	/	/	/	3600	/	1.316	/	3600	1.148	3600
7 - 65	/	/	3600	/	/	/	3600	/	1.299	/	3600	1.163	3600
Average			3600	/			3600	/			3600		3600
8 - 66	0.768	0.695	3600	9.4	/	/	3600	/	0.798	0.767	3600	0.764	776
8 - 67	0.789	0.718	3600	9.0	/	/	3600	/	0.923	0.789	3600	0.780	270
8 - 68	0.800	0.723	3600	9.7	/	/	3600	/	1.349	0.800	3600	0.789	390
8 - 69	0.819	0.735	3600	10.3	/	/	3600	/	1.294	0.808	3600	0.800	349
8 - 70	0.849	0.769	3600	9.4	/	/	3600	/	0.867	0.848	3600	0.839	986
Average			3600	9.6			3600	/			3600		554

from part (i) into the DrFRAM and mean-risk models; (iii) repeat part (i) and (ii) 15 times and derive the asymptotic 95% confidence intervals of both models; and (iv) Choose the smallest θ such that the confidence interval of the DrFRAM model is completely above the confidence interval of the mean-risk model. We also compared the performances of the SAA model (i.e., in DrFRAM (3.5) with $\theta = 0$), RObust model (RO) with the box uncertainty set (i.e., for each parameter, we choose its lower and upper bounds to be equal to its mean value minus and plus 1.96 times the standard deviation, respectively) and the DrFRAM model. Specifically, we adopt the following procedure for the numerical comparison: (i) generate 10 scenarios to solve the DrFRAM model with the best-tuned Wasserstein radius, RO, and the SAA model separately; (ii) generate 10 scenarios with the same parameters and evaluate DrFRAM, RO and SAA solutions using the SAA model; (iii) repeat part (ii) 1000 times and compute the asymptotic 95% confidence interval for the mean of the objective value.

The result is displayed in Figure 3.1, and the best Wasserstein radius is $\theta = 1.6$. We compare the results of the SAA model, the RO model, and the DrFRAM with $\theta = 1.6$,

we see that both the SAA and the RO solutions yield higher objective values than that of the DrFRAM solution. This demonstrates that the DrFRAM model with the best-tuned Wasserstein radius can outperform the RO model and SAA model.

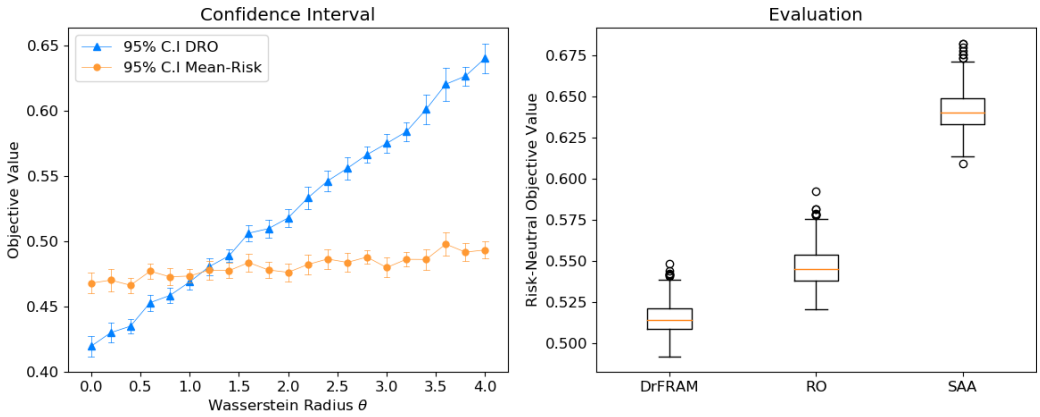

Figure 3.1: Tuning the Wasserstein Radius and Comparing the DrFRAM, RO and SAA Solutions.

3.7.4 Blacksburg Transit Case Study

In this section, we applied approximation Algorithm 4 to solve the real-world Blacksburg Transit allocation problem since the dataset provided by Blacksburg Transit is of a similar scale as the largest cases studied in the previous section. The operation data was provided by Blacksburg Transit, and passenger arrival and alighting data were collected in September 2020, amid the COVID-19 pandemic. Blacksburg Transit has 17 routes, three types of buses with different capacities, where the number of buses with the nominal capacity equal to 60, 80, 120 are $8, 20, 8$, respectively, and each route has 10 to 40 stops. As public policies and government regulations change as the pandemic evolves, we study the pandemic factor δ varying from 0.25 (social distancing required by CDC) to 1 (fully operated). We set the weight $\omega = 0.5$ in this numerical study since the priority during a pandemic is to enforce social distancing. We adopted the following cross-validation procedure to choose the best

Wasserstein radius θ for a given δ using 22 scenarios as training data: (i) randomly select 16 scenarios for solving the model; (ii) for each $\theta \in \{0, 0.2, \ldots, 3\}$, solve the DrFRAM model using the 16 selected scenarios and evaluate the solution using the remaining 6 scenarios; (iii) repeat (i) and (ii) for 15 times and derive the asymptotic 95% confidence interval of the objective values. We followed the same procedure in the previous subsection to select the smallest θ such that the confidence interval for the DrFRAM objective value is beyond that of the mean-risk objective value. We let $\rho = 0.5$ and $\varepsilon = 0.1$. A time limit of 3600 seconds was set for a single run. Note that when all the DrFRAM objective values corresponding to different Wasserstein radii θ are much less than 1, then the cross-validation takes about 1000 seconds; otherwise, if for some Wasserstein radii, their corresponding DrFRAM objective values are around or exceeding 1, then the cross-validation can take up to 15 hours.

We see that for any $\delta \in \{0.5, 0.75, 1\}$ and for any $\theta \in \{0, 0.2, \ldots, 3\}$, since objective values for all the scenarios are observed to be less than 1, according to Proposition 3.11 and its remark, the solution obtained by approximation Algorithm 4 can be very close to the optimality. Besides, since we obtain the same solution when $\delta \geq 0.5$, we only consider $\delta \in \{0.25, 0.5\}$. Thus, according to our cross-validation results in Table 3.10 and Figure 3.2, we chose $\theta = 1.8$ as the best Wasserstein radius when $\delta = 0.25$ and $\theta = 2.6$ for $\delta = 0.5$.

We evaluated the current bus assignment from Blacksburg Transit and compared the results of SAA model, RO model and DrFRAM model with the best-tuned Wasserstein radius θ with unused 6 scenarios as testing data. To simulate the possible changes in data, we applied a truncated Gaussian noise to each testing sample. The noise for the proportion of passengers alighting from the bus follows $\mathcal{N}(0, 0.001t)$ truncated to be nonnegative, while the noise for the passenger arrival rate follows $\mathcal{N}(0, 0.1t)$ rounded to the nearest nonnegative integer, where the parameter $t \in \{0, \ldots, 50\}$. We repeated the sampling process 100 times to derive the asymptotic 95% confidence interval.

Table 3.10: Cross Validation Results of Blacksburg Transit Data

$\delta = 0.25$			$\delta = 0.5$		
θ	95% C.I. of DrFRAM	95% C.I. of Mean-Risk	θ	95% C.I. of DrFRAM	95% C.I. of Mean-Risk
0.0	[0.122 , 0.135]	[0.219 , 0.254]	0.0	[0.056 , 0.059]	[0.104 , 0.110]
0.2	[0.559 , 0.580]	[0.555 , 0.590]	0.2	[0.290 , 0.296]	[0.283 , 0.300]
0.4	[0.565 , 0.586]	[0.559 , 0.594]	0.4	[0.292 , 0.298]	[0.283 , 0.300]
0.6	[0.571 , 0.593]	[0.563 , 0.598]	0.6	[0.295 , 0.302]	[0.285 , 0.302]
0.8	[0.578 , 0.600]	[0.569 , 0.603]	0.8	[0.299 , 0.306]	[0.287 , 0.304]
1.0	[0.588 , 0.612]	[0.578 , 0.616]	1.0	[0.304 , 0.311]	[0.291 , 0.310]
1.2	[1.051 , 1.131]	[0.845 , 1.001]	1.2	[0.651 , 0.741]	[0.535 , 0.712]
1.4	[1.130 , 1.217]	[1.005 , 1.129]	1.4	[0.797 , 0.952]	[0.747 , 0.996]
1.6	[1.134 , 1.224]	[1.001 , 1.163]	1.6	[0.686 , 0.774]	[0.544 , 0.656]
1.8	[1.073 , 1.154]	[0.865 , 0.984]	1.8	[0.690 , 0.781]	[0.550 , 0.670]
2.0	[1.016 , 1.075]	[0.784 , 0.873]	2.0	[0.793 , 0.929]	[0.663 , 0.820]
2.2	[1.412 , 1.452]	[1.081 , 1.090]	2.2	[0.996 , 1.090]	[0.820 , 1.023]
2.4	[1.418 , 1.451]	[1.070 , 1.082]	2.4	[1.032 , 1.136]	[0.847 , 1.027]
2.6	[1.377 , 1.418]	[1.099 , 1.149]	2.6	[1.038 , 1.130]	[0.824 , 0.956]
2.8	[1.427 , 1.454]	[1.083 , 1.089]	2.8	[1.044 , 1.145]	[0.831 , 0.989]
3.0	[1.430 , 1.462]	[1.084 , 1.098]	3.0	[1.151 , 1.264]	[0.968 , 1.138]

The result is illustrated in Figure 3.3. It is seen that our solutions can significantly reduce the highest bus utilization rate and passenger abandon rate compared to the current assignment from Blacksburg Transit. We also see that our DrFRAM solution outperforms RO and SAA ones across all the noise levels. This indicates that our proposed approach can consistently provide a better solution than RO and SAA even when the underlying distribution of uncertain parameters is unknown or varies over time.

We analyzed the impact of model parameters, i.e., pandemic factor δ and weight ω by varying δ from 0.25 to 1 and ω from 0.25 to 2. While varying δ, we let $\omega = 0.5$; while varying ω, we let $\delta = 0.25$. We tuned θ following the same procedure as introduced at the beginning of this subsection for the different parameter combinations and did the evaluation with the best-tuned θ to derive the asymptotic 95% confidence intervals. The results are illustrated in Figure 3.4. It is seen that the objective value gets smaller when the pandemic factor δ increases, which indicates that the weighted sum of bus utilization and passenger abandon

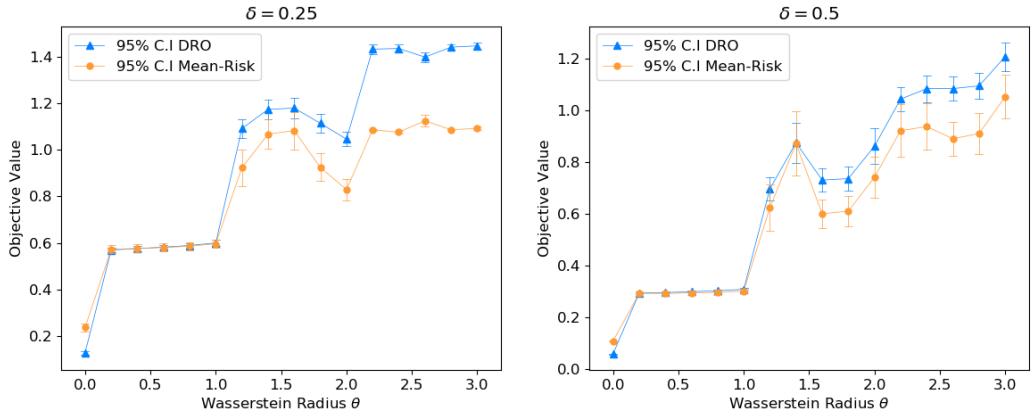

Figure 3.2: Confidence Intervals of DrFRAM Objective Values and Mean-Risk Objective Values

rates decreases when more passengers are allowed to get on board. The objective value increases when the weight ω increases since a higher weight ω leads to a larger objective value.

We also compared the weighted sum of bus utilization rate and passenger abandon rate among all the routes, as illustrated in Figure 3.5. It is seen that our solution yields much stable route-based objectives than the current one from Blacksburg Transit, RO, or SAA one. This implies that our DrFRAM solution can be indeed fairer and significantly reduce the transit resource inequity among different routes. We also compared our proposed assignment solution with the current one in average total bus capacity for each route, as illustrated in Figure 3.6. It is seen that our proposed solution assigns more buses to several routes but fewer buses to others than the current assignment. For example, our solution assigns more buses to route MSA (see Figure 3.7), connecting downtown Blacksburg to the campus. Although passenger demand decreased due to the COVID-19 pandemic, residents still commuted to downtown for daily essential products. On the other hand, our solution assigns fewer buses to route HWA and HWB, which connect the largest residential communities to the campus, since most residents were taking virtual classes and working from home. By exploring the

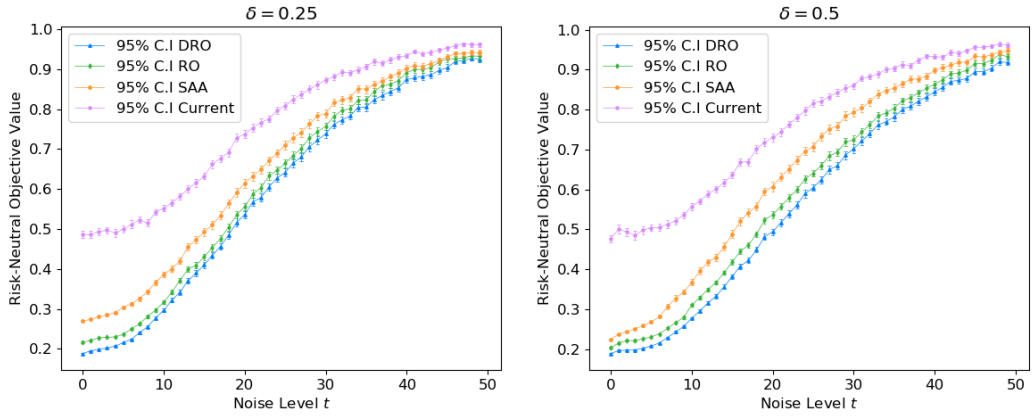

Figure 3.3: A Comparison of Risk-Neutral Objective Values for Four Different Methods with Different Noise Levels

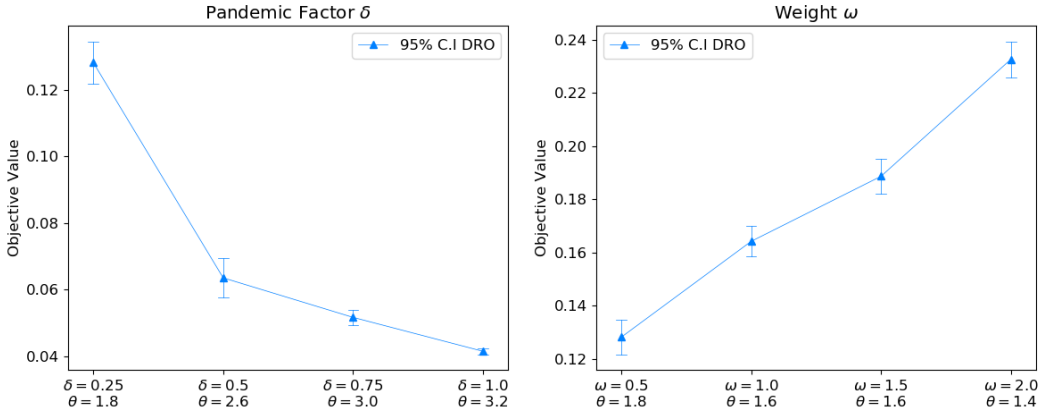

Figure 3.4: Sensitivity Analysis on Model Parameters

outdoor activities, we see that passengers reduced their daily commute to school or work but kept the necessary short trips for daily essentials during the pandemic, which could result in more imbalance in passenger demand among different routes. Our data-driven model can help enhance the policy-making for Blacksburg Transit by handling the shifts in passenger demand among bus routes and stops during a pandemic.

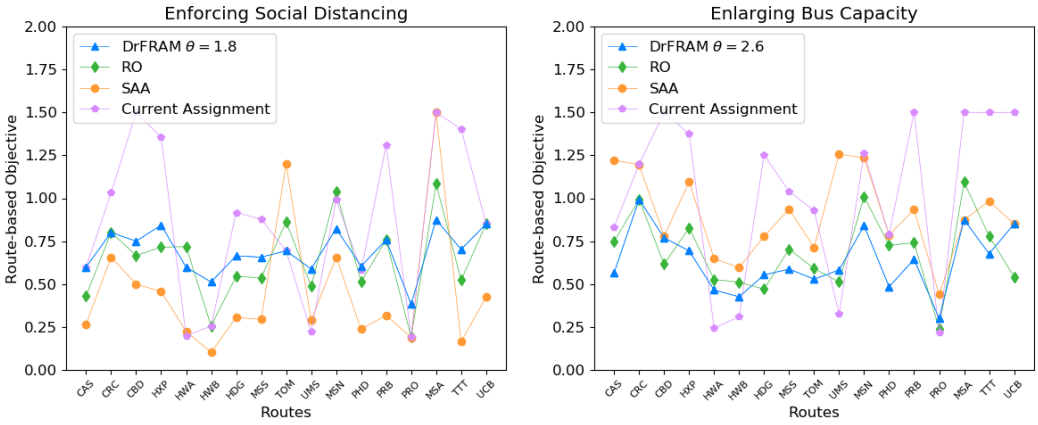

Figure 3.5: A Comparison of Route-based Weighted Sum of Bus Utilization Rate and Passenger Abandon Rate Among Four Different Results. Here, xticks are route names of Blacksburg Transit and route-based objective represents the weighted sum of bus utilization rate and passenger abandon rate for each route.

3.8 Conclusion

In this chapter, we study the transit resource allocation problem to minimize the highest utilization rate and the largest passenger abandon rate under stochastic passenger arrival and alighting rates. We propose a DrFRAM under type-∞ Wasserstein ambiguity set, which is proven to be NP-hard. To simplify the DrFRAM, we derive the monotonicity properties of the DrFRAM and use McCormick inequalities to linearize the nonlinear components, which allows us to derive an MILP formulation. To further improve the MILP formulation, valid inequalities and stronger formulations are derived. We also develop scenario decomposition methods and No-one-left based approximation algorithm to solve DrFRAM. Finally, we numerically demonstrate the effectiveness of the proposed approaches in both small and large instances and apply them to solve the real-world instance using the data provided by Blacksburg Transit. Compared to the current allocation plan, our result is demonstrated to be more robust and fairer. More importantly, Blacksburg Transit is using our model to help measure the unbalance of their transit resource assignment. Blacksburg Transit is now

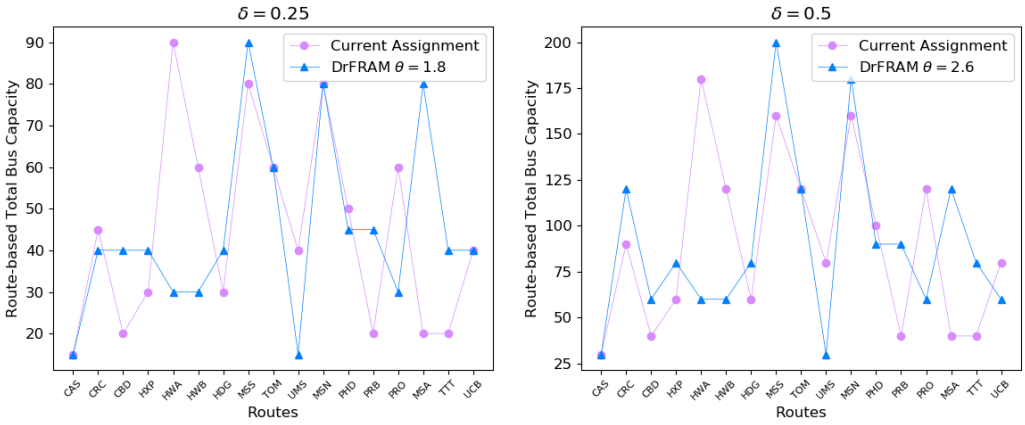

Figure 3.6: A Comparison of Routed-based Total Bus Capacity Between the Current Assignment and DrFRAM Result

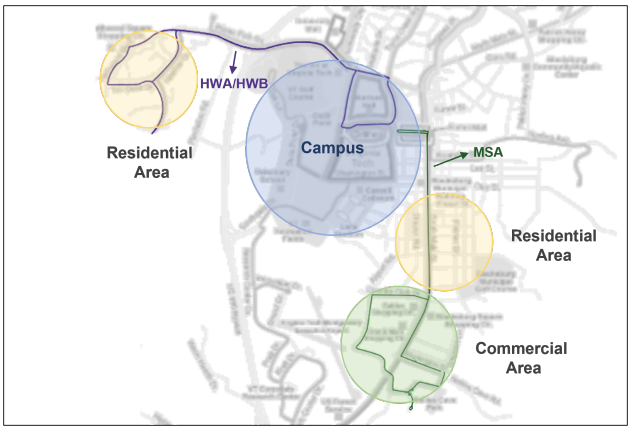

Figure 3.7: Illustration of Route HWA/HWB and Route MSA

following our recommendations in the internal system to make better decisions during the COVID-19 crisis. The proposed DrFRAM framework can be generalized to other problems with uncertain demand and fair resource allocation issues. For instance, we can extend our framework to the truck platooning problems with fair truck resource allocation and passenger demand uncertainty. We can also generalize the model to the call center problems, aiming to minimize the waiting time and maximize fairness and customer satisfaction.

Chapter 4

On a Fair and Risk-averse Urban Air Mobility Resource Allocation Problem Under Demand and Capacity Uncertainties

4.1 Introduction

The urban population in the U.S. is expected to increase from 83% in 2020 to 89% in 2050 (United Nations [114]). Albeit benefiting people with better opportunities, urbanization leads to more severe traffic congestion problems with higher traffic volume, larger travel delays, and more energy consumption and air pollution (Schrank et al. [115]), which calls for efficient alternative transportation modes (Speranza [116]). One promising way is the on-demand point-to-point Urban Air Mobility (UAM) service, which relies on automated electric Vertical Take-Off and Landing vehicles (eVTOLs) to transport passengers at lower altitudes in and around metropolitan areas. It has been recognized recently that the UAM has the potential to improve personal mobility by reducing travel time and cost, reduce energy consumption and air pollution by using eVTOL with zero direct emission, as well as enhance economic vitality (Price et al. [117]). In the meantime, thanks to the emerging

aircraft technologies in increasing reliability, aviation companies, including Joby, Archer, Eve, etc., can launch their products and prototypes to make UAM possible in the near future. Due to the potential economic scaling effects, the UAM traffic flow is expected to increase dramatically once implemented, and its market can be substantially large (Lineberger et al. [118]). To be prepared for the era of UAM, NASA recently established a UAM framework from different aspects (Price et al. [117]). One important aspect lies in UAM operations management, namely,

> *"Provide airspace operations management services as well as fleet operations management services that ensure safe, efficient, scalable, and resilient UAM operations in and around metropolitan areas."*

This high-level view echoes that a reliable and robust UAM traffic management system is required to guarantee safety and efficiency for high-density UAM traffic. Different from conventional air traffic management, UAM traffic manager and service providers are facing new challenges in cost reduction and safety promise due to higher operation density and frequency, new operating environment design, and electric propulsion system limitations. One possible solution is to design a sophisticated centralized traffic management system to guarantee a safe and efficient operation environment within a complex UAM network to coordinate among stakeholders, including aircraft operators, airspace managers, data providers, etc., especially when facing large-scale aircraft operations.

Within a centralized UAM traffic management system, the UAM traffic manager has all the shared information from the UAM service providers and airspace data support from the third party, including weather and hazard forecasts *a priori* or during the flight. The UAM traffic manager is responsible for allocating aircraft to different flight paths, balancing the UAM traffic flow and airspace capacity, and taking the uncertainties into consideration. The

first type of uncertainty comes from fluctuations in passenger demand, while the second one is the airspace capacity uncertainty that arises from stochastic weather events. Specifically, when the passenger demand exceeds the airspace capacity, air traffic congestion occurs at some bottleneck points, i.e., busy areas in the airspace which causes airborne delay. Since the aircraft cannot afford too much energy for a large airborne delay due to limited battery life and aircraft payload, an unpredictable airborne delay should be avoided as much as we can. In the UAM network, balancing the UAM traffic flow and airspace capacity in the UAM network with a proper traffic management system is of great importance to hedge against potential risks as well as to enforce safety. In this chapter, we focus on allocating the aircraft in a risk-averse way under passenger demand and airspace capacity uncertainties to minimize the total aircraft operation cost. In addition, sorely minimizing the total cost may cause some UAM service providers to bear the most delays (citetlulli2007european). To achieve company-level fairness, we also would like to assign the airborne delay fairly among different aircraft. Therefore, this work aims to seek an appropriate trade-off between system-level efficiency (i.e., simultaneously minimizing the total operation cost) and achieving company-level fairness.

4.1.1 Summary of Main Contribution

This chapter studies the Fair and Risk-averse Urban Air Mobility resource allocation model (FairUAM) to coordinate multiple UAM service providers. The goal of FairUAM is to determine the optimal UAM aircraft resource allocation and delay assignment under passenger demand and airspace uncertainties to minimize the weighted sum of total cost and highest average company cost to achieve both system-level efficiency (i.e., total operation cost) and company-level fairness. The main contributions of FairUAM are summarized below.

i. We develop a novel formulation for FairUAM to allocate aircraft from multiple UAM service providers under passenger demand and airspace capacity uncertainties. The proposed FairUAM is versatile and can handle the unsatisfied demand (i.e., the UAM traffic flow needed exceeds the airspace capacity when passenger demand is very large) and can also address company-level fairness as well as achieve the overall airspace efficiency.

ii. Without considering delay assignment, we prove that FairUAM reduces to UAM aircraft resource allocation problem which is NP-hard even with one UAM service provider. Given aircraft allocation, FairUAM reduces to UAM delay assignment problem, which is also NP-hard. These complexity results motivate us to study an effective solution algorithm to solve FairUAM.

iii. We derive monotonicity properties such that an increase in passenger demand, a decrease in airspace capacity or an increase in unsatisfied passenger demand leads to a possible increase in objective value. While achieving the same optimality as the original model, these properties allow us to simplify the FairUAM model and further relax the integrality of some decision variables for computational advantages.

iv. To strengthen the formulation, we develop several families of valid inequalities by exploring the model structures and discovering the hidden relationship between different decision variables. Specifically, we derive airspace guarantee inequalities, symmetry-breaking inequalities, data pre-processing inequalities, bottleneck point arrival time inequalities, total arrival time inequalities, and accumulated delay inequalities. These valid inequalities allow us to design and strengthen the decomposition-based algorithm, which can solve larger-scale instances with 5 times more binary variables compared to solving the vanilla model directly via the off-the-shelf solvers.

v. We numerically demonstrate the effectiveness of the proposed method using generated

instances and apply it to a case study of a real-world network. We find that with only a 20% increase in the total operation cost, we can reduce the unfairness by 68%. We also observe that the risk-averse solution is more robust compared to the risk-neutral one, when accurate estimation of the uncertainties is not practical. We show that our framework can be useful in identifying the network hotspots and supporting UAM service providers with better path-planning insights.

Notation For readers' convenience, we list the notation used throughout the chapter. Bold letters (e.g., $\boldsymbol{y}$) are used to represent vectors and matrices, and the corresponding non-bold letters denote their components. We let bold script letters (e.g., $\mathcal{R}$) denote sets and $|\mathcal{R}|$ denote their cardinality. We use $\widetilde{\boldsymbol{\xi}}$ to represent a random vector and let $\boldsymbol{\xi}$ be its realizations. Additional notations related to our model will be introduced in the next section.

Organization The remainder of the chapter is organized as follows. In Section 4.2, we introduce the problem setting and model formulation. Section 4.3 derives model properties. Section 4.4 proposes valid inequalities and develops a decomposition algorithm. Finally, Section 4.5 numerically demonstrates the performance of the proposed valid inequalities and algorithm, and Section 4.6 concludes this chapter.

4.2 Model Formulation

In this work, we consider a network, as shown in Figure 4.1, which consists of multiple UAM service providers each having their own aircraft, and multiple origin-destination (OD) pairs each having multiple candidate routes, under airspace capacity and passenger demand uncertainties. Typically, the intersections of routes are considered as bottleneck points where

congestion may occur. Besides, weather events at bottleneck points further influence their capability to accommodate air traffic flow, which leads to airspace capacity uncertainty at bottleneck points. As on-demand services, passengers are allowed to make the reservation including an origin and a destination a day or hours before the actual departure time, which in turn brings in passenger demand uncertainty. In our framework, the UAM traffic manager optimizes the operation plan for the whole planning horizon by assigning the aircraft to OD pairs and routes. After the UAM service providers submit their realized passenger demand, the UAM traffic manager assigns delays to aircraft to achieve efficiency and company-level fairness at the same time.

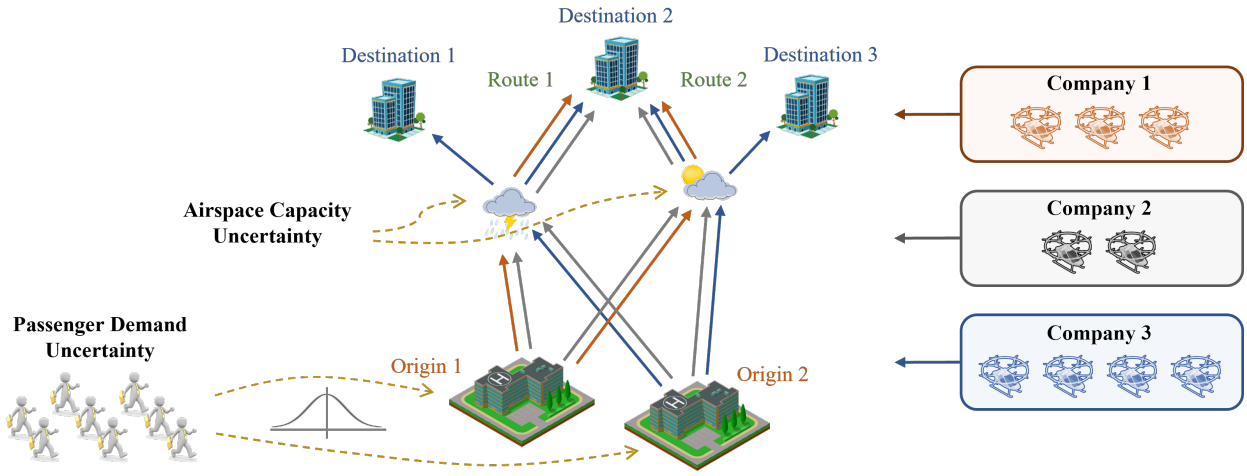

Figure 4.1: An illustration of the FairUAM network and its components

The FairUAM consists of a set of UAM service providers $\mathcal{L}$, where the service provider $\ell \in \mathcal{L}$ owns $|\mathcal{I}_\ell|$ aircraft. Each service provider (or company) would like to satisfy their own passenger demand to transport passengers from origin vertiports to destination vertiports in their favor. Each aircraft can transport a certain number of passengers with the same origin and destination. We let m_i be the passenger capacity for each aircraft $i \in \mathcal{I}_\ell$ for each $\ell \in \mathcal{L}$ and $\mathcal{R}$ represent the set of OD pairs. While multiple aircraft are operated on different OD pairs, intersections between OD pairs may exist and congestion may happen.

To circumvent aircraft conflict on such intersected OD pairs, we suppose that the airspace network consists of a set of bottleneck points $\mathcal{K}$ for flow management. There are multiple routes for each aircraft to choose from, where for a given OD pair, some aircraft need to reroute or detour such that the number of aircraft passing the same bottleneck within a time unit is restricted within its capacity. Particularly, we let $\mathcal{J}_r$ denote the sets of routes for each OD pair $r \in \mathcal{R}$. To generate a better operation plan for upcoming travel needs, we consider a planning horizon $\mathcal{T}$ which includes finite time units. The length of a time unit can be changed based on our needs, for example, according to aircraft density and different operation requirements.

Since UAM operations are quite sensitive to severe weather events, airspace capacity is random due to unexpected weather conditions and safety. Particularly, we let a random parameter $\widetilde{C}_t^k \in \mathbb{Z}_+$ denote the airspace capacity of each bottleneck point $k \in \mathcal{K}$ at a given time unit $t \in \mathcal{T}$. The objective of FairUAM is to dispatch aircraft to OD pairs and routes based on companies' needs, but it may delay some aircraft to achieve better utilization of the limited airspace capacities and minimize the operation cost. As an on-demand service, passenger demand is stochastic since passengers are allowed to book their seats just one day or even hours before their departure time. Considering the relocation of aircraft, passenger demand may be realized after the aircraft assignment. We let the random parameter $\widetilde{D}_\ell^r \in \mathbb{Z}_+$ denote the passenger demand of service provider $\ell \in \mathcal{L}$ on OD pair $r \in \mathcal{R}$. For notational convenience, we let random parameters $\widetilde{\boldsymbol{\xi}} = (\widetilde{\boldsymbol{C}}, \widetilde{\boldsymbol{D}})$. Note that the UAM traffic manager and service providers make decisions independently, following all the regulations in an information-sharing environment, which may not necessarily lead to efficient aircraft operations and airspace utilization. In this context, the decisions in FairUAM are made by a central authority on proposing a collaborative UAM air traffic management system.

In our model, the operation cost for each service provider $\ell \in \mathcal{L}$ includes assignment cost, relocation cost, delay cost, and penalty cost. The assignment cost is the fixed travel cost for an aircraft assigned to a route, including the cost needed in the free-condition airspace, denoted by c_{ij}^r for aircraft $i \in \mathcal{I}_\ell$ assigned to OD pair $r \in \mathcal{R}$ and route $j \in \mathcal{J}_r$. The relocation cost is the fixed cost for an aircraft assigned to an OD pair, denoted by q_i^r for aircraft $i \in \mathcal{I}_\ell$ relocated to OD pair $r \in \mathcal{R}$. The delay cost includes ground delay cost α_{ij}^r at the origin vertiport and airborne delay cost β_{ij}^r at each bottleneck point for aircraft $i \in \mathcal{I}_\ell$ assigned to OD pair $r \in \mathcal{R}$ and route $j \in \mathcal{J}_r$. An UAM service provider ℓ bears a penalty cost p_ℓ^r for the business loss when they are not able to satisfy its passenger demand on OD pair $r \in \mathcal{R}$. Besides minimizing the total operation cost, we also consider inter-airline fairness, i.e., the average operation cost per aircraft for each airline. In this case, we also include the fairness term into our objective so that the largest average airline operation cost is also minimized. To better balance the two goals, we introduce a weighted scalar λ to balance efficiency and fairness. Therefore, the objective of FairUAM is to minimize the weighted sum of the total operation costs and the largest average airline operation cost.

The traffic manager in FairUAM needs to decide OD pair and route assignment for each aircraft upfront and determine the aircraft's delays after random parameters such as passenger demand and airspace capacity are realized. We let $y_i^r \in \{0, 1\}$ denote whether aircraft $i \in \mathcal{I}_\ell$ of service provider $\ell \in \mathcal{L}$ is assigned to OD pair $r \in \mathcal{R}$ and let $\delta_{ij}^r \in \{0, 1\}$ denote whether it is assigned to route $j \in \mathcal{J}_r$ on OD pair $r \in \mathcal{R}$ or not. In FairUAM, given a realization $\boldsymbol{\xi}$ of the random parameters $\widetilde{\boldsymbol{\xi}}$, we let $g_{ij}^r(\boldsymbol{\xi})$ denote the ground delay of aircraft $i \in \mathcal{I}_\ell$ of service provider $\ell \in \mathcal{L}$ on route $j \in \mathcal{J}_r$ and OD pair $r \in \mathcal{R}$ and let the corresponding airborne delay at bottleneck point $k \in \mathcal{K}$ be $a_{ijk}^r(\boldsymbol{\xi})$. When the number of aircraft required to satisfy the passenger demand exceeds the available airspace capacity or the number of available aircraft, some passengers may be turned down, and the service provider will incur a

penalty cost for the loss of business. To model this effect, we let $s_\ell^r(\boldsymbol{\xi})$ denote the unsatisfied passenger demand of service provider $\ell \in \mathcal{L}$ on OD pair $r \in \mathcal{R}$.

To better ensure safety, it is important to hedge against the risk of passenger demand and airspace capacity uncertainties in the UAM operating environment. For FairUAM, we consider the Conditional Value-at-Risk (CVaR) (Rockafellar et al. [119]),

$$\rho(Z) = \text{CVaR}_{1-\varepsilon}(Z) := \inf_{v \in \mathbb{R}} \left\{ v + \frac{1}{\varepsilon}\mathbb{E}[Z - v]_+ \right\}$$

where $[n]_+ := \max\{n, 0\}$ and $v = \text{VaR}_{1-\varepsilon}(Z) := \inf\{v : \mathbb{P}(Z \leq v) \geq 1 - \varepsilon\}$. We can simply extend our model to other coherent risk measures. For simplicity and generality, we mainly focus on the most representative one- CVaR. Under this setting, FairUAM is given by:

$$\min_{\boldsymbol{\delta}, \boldsymbol{y}} \quad \rho\left[\mathcal{Q}\left(\boldsymbol{y}, \boldsymbol{\delta}, \widetilde{\boldsymbol{\xi}}\right)\right], \tag{4.1a}$$

$$\text{s.t.} \quad \sum_{r \in \mathcal{R}} y_i^r \leq 1, \quad \forall i \in \mathcal{I}_\ell, \ell \in \mathcal{L}, \tag{4.1b}$$

$$\sum_{j \in \mathcal{J}_r} \delta_{ij}^r = y_i^r, \quad \forall r \in \mathcal{R}, i \in \mathcal{I}_\ell, \ell \in \mathcal{L}, \tag{4.1c}$$

$$y_i^r, \delta_{ij}^r \in \{0, 1\}, \quad \forall j \in \mathcal{J}_r, r \in \mathcal{R}, i \in \mathcal{I}_\ell, \ell \in \mathcal{L}. \tag{4.1d}$$

In FairUAM (4.1), the objective is to minimize the risk of the planning outcome and $\mathcal{Q}(\boldsymbol{y}, \boldsymbol{\delta}, \widetilde{\boldsymbol{\xi}})$ denotes the random recourse function, which is specified in the next paragraph. Constraints (4.1b) guarantee that each aircraft can only be assigned to at most one OD pair. Constraints (4.1c) ensure that if an aircraft is assigned to an OD pair, it can be assigned to only one route. Otherwise, it will not be assigned to any route. Constraints (4.1d) specify the boundaries of the decision variables.

Given a realization $\boldsymbol{\xi}$ of random parameters $\widetilde{\boldsymbol{\xi}}$ and the values of first-stage decisions $(\boldsymbol{y}, \boldsymbol{\delta})$,

we can formulate the recourse function as follows:

$$\mathcal{Q}(\boldsymbol{y}, \boldsymbol{\delta}, \boldsymbol{\xi}) =$$

$$\min_{\boldsymbol{g}(\boldsymbol{\xi}), \boldsymbol{a}(\boldsymbol{\xi}), \boldsymbol{s}(\boldsymbol{\xi}), \boldsymbol{B}(\boldsymbol{\xi})} Q(\boldsymbol{y}, \boldsymbol{\delta}, \boldsymbol{\xi}, \boldsymbol{g}(\boldsymbol{\xi}), \boldsymbol{a}(\boldsymbol{\xi}), \boldsymbol{s}(\boldsymbol{\xi}), \boldsymbol{B}(\boldsymbol{\xi})) := \left\{ \lambda \sum_{\ell \in \mathcal{L}} \frac{\phi_\ell(\boldsymbol{\xi})}{|\mathcal{I}_\ell|} + (1-\lambda) \max_{\ell \in \mathcal{L}} \frac{\phi_\ell(\boldsymbol{\xi})}{|\mathcal{I}_\ell|} \right\}, \tag{4.2a}$$

$$\text{s.t.} \quad \phi_\ell(\boldsymbol{\xi}) = \sum_{r \in \mathcal{R}} \left\{ p_\ell^r s_\ell^r(\boldsymbol{\xi}) + \sum_{i \in \mathcal{I}_\ell} \left[q_i^r y_i^r + \sum_{j \in \mathcal{J}_r} \left(c_{ij}^r \delta_{ij}^r + \alpha_{ij}^r g_{ij}^r(\boldsymbol{\xi}) + \beta_{ij}^r \sum_{k \in \mathcal{K}} a_{ijk}^r(\boldsymbol{\xi}) \right) \right] \right\}, \forall \ell \in \mathcal{L}, \tag{4.2b}$$

$$s_\ell^r(\boldsymbol{\xi}) + \sum_{i \in \mathcal{I}_\ell} m_i y_i^r \geq D_\ell^r, \quad \forall r \in \mathcal{R}, \ell \in \mathcal{L}, \tag{4.2c}$$

$$g_{ij}^r(\boldsymbol{\xi}) + \sum_{k \in \mathcal{K}} a_{ijk}^r(\boldsymbol{\xi}) \leq \delta_{ij}^r \bar{L}, \quad \forall j \in \mathcal{J}_r, r \in \mathcal{R}, i \in \mathcal{I}_\ell, \ell \in \mathcal{L}, \tag{4.2d}$$

$$\sum_{k \in \mathcal{K}} a_{ijk}^r(\boldsymbol{\xi}) \leq \delta_{ij}^r \bar{R}_{ij}^r, \quad \forall j \in \mathcal{J}_r, r \in \mathcal{R}, i \in \mathcal{I}_\ell, \ell \in \mathcal{L}, \tag{4.2e}$$

$$\sum_{t \in \mathcal{T}} B_{it}^k(\boldsymbol{\xi}) \leq 1, \quad \forall i \in \mathcal{I}_\ell, \ell \in \mathcal{L}, k \in \mathcal{K}, \tag{4.2f}$$

$$\sum_{t \in \mathcal{T}} t B_{it}^k(\boldsymbol{\xi}) = \sum_{r \in \mathcal{R}} \left(\sum_{j \in \mathcal{J}_r} \left(\tau_{ijk}^r \delta_{ij}^r + g_{ij}^r(\boldsymbol{\xi}) + \sum_{\substack{id_j(k) \geq id_j(k') \\ k' \in \mathcal{K}}} a_{ijk'}^r(\boldsymbol{\xi}) \right) \right), \forall i \in \mathcal{I}_\ell, \ell \in \mathcal{L}, k \in \mathcal{K}, \tag{4.2g}$$

$$\sum_{\ell \in \mathcal{L}} \sum_{i \in \mathcal{I}_\ell} B_{it}^k(\boldsymbol{\xi}) \leq C_t^k, \quad \forall k \in \mathcal{K}, t \in \mathcal{T} \setminus \{0\}, \tag{4.2h}$$

$$B_{it}^k(\boldsymbol{\xi}) \in \{0,1\}, \quad \forall i \in \mathcal{I}_\ell, \ell \in \mathcal{L}, k \in \mathcal{K}, t \in \mathcal{T}, \tag{4.2i}$$

$$g_{ij}^r(\boldsymbol{\xi}), a_{ijk}^r(\boldsymbol{\xi}), s_\ell^r(\boldsymbol{\xi}) \in \mathbb{Z}_+, \quad \forall j \in \mathcal{J}_r, r \in \mathcal{R}, i \in \mathcal{I}_\ell, \ell \in \mathcal{L}, k \in \mathcal{K}, \tag{4.2j}$$

$$\phi_\ell(\boldsymbol{\xi}) \geq 0, \quad \forall \ell \in \mathcal{L}. \tag{4.2k}$$

Here, $\boldsymbol{B}(\boldsymbol{\xi})$ are auxiliary variables enforcing the connection between time and location for

each aircraft. Specifically, we let $B_{it}^{k}(\boldsymbol{\xi})$ denote whether aircraft $i \in \mathcal{I}_\ell$ for service provider $\ell \in \mathcal{L}$ arrives at a bottleneck point $k \in \mathcal{K}$ at time $t \in \mathcal{T}$. Objective (4.2a) is to minimize the weighted sum of the efficiency term (i.e., total operation cost), and the fairness term (i.e., the largest average company operation cost). To make sure the efficiency term is of the same magnitude as the fairness term, instead of taking the summation of the company operation costs, we use the summation of the average company operation cost. Inspired by Rodionova et al. [84], we use the widely used min-max fairness for the fairness term (Radunovic and Le Boudec [92], Du et al. [93]). Constraints (4.2b) compute the total operation cost for each service provider. Constraints (4.2c) ensure that the satisfied and unsatisfied passenger demand should meet the requirement. Constraints (4.2d) and (4.2e) specify the total delay and airborne delay limit and postulate the number of passengers on board at each stop, respectively. Constraints (4.2f) and (4.2g) define the auxiliary variables $\boldsymbol{B}(\boldsymbol{\xi})$ such that each aircraft can only pass a specific bottleneck point once, and the time it arrives at the bottleneck should be equal to the sum of the travel time τ_{ijk}^{r} needed for aircraft $i \in \mathcal{I}_\ell$ from the service provider $\ell \in \mathcal{L}$ on the OD pair $r \in \mathcal{R}$ and the route $j \in \mathcal{J}_r$ in the free-condition airspace and the accumulated ground and airborne delay before visiting this bottleneck point. Note that we use $id_j(k)$ to denote the order of bottleneck point $k \in \mathcal{K}$ being visited on route $j \in \mathcal{J}_r$ of OD pair $r \in \mathcal{R}$ and let $\sum_{id_j(k) \geq id_j(k'), k' \in \mathcal{K}} a_{ijk'}^{r}(\boldsymbol{\xi})$ denote the total airborne delay before visiting bottleneck point k. Constraints (4.2h) guarantee that the total number of aircraft at the bottleneck point within a unit of time cannot exceed the airspace capacity. Constraints (4.2i) - (4.2k) specify the boundary conditions of the decision variables and the auxiliary variables.

4.3 Model Properties

In this section, we first prove the complexity of FairUAM (4.1) and then explore its properties for formulation simplification and managerial insights.

4.3.1 Computational Complexity of FairUAM (4.1)

We observe that FairUAM (4.1) is a mixed-integer nonlinear program which is expected to be a difficult problem. This motivates us to develop model properties and a customized algorithm to accelerate the solution procedure. In fact, we prove that solving FairUAM (4.1) is NP-hard with the reduction to the well-known NP-complete partition problem.

Proposition 4.1. *Solving FairUAM (4.1), in general, is NP-hard even when* $\lambda = 1, |\mathcal{L}| = 1, |\mathcal{R}| = 2, |\mathcal{J}_r| = 1$, *and the random variables* $\widetilde{\boldsymbol{\xi}}$ *have only one realization.*

Proof: Let us consider the following NP-complete problem.

> *Partition Problem: Consider* $|\mathcal{I}_1|$ *positive numbers* $\{m_i\}_{i\in\mathcal{I}_1} \subseteq \mathbb{Z}_{++}$ *having an even sum, is there a partition* S_1, S_2 *such that* $\sum_{i\in S_1} m_i = \sum_{i\in S_2} m_i = \bar{D}, S_1 \cap S_2 = \emptyset, S_1 \cup S_2 = \mathcal{I}_1$*?*

We show that finding a feasible solution for a special case of FairUAM (4.1) can be reduced to the partition problem. We first let $\boldsymbol{p} = \mathbf{1}, \boldsymbol{q} = \mathbf{0}, \boldsymbol{c} = \mathbf{0}, \bar{L} = 0, \bar{\boldsymbol{R}} = \mathbf{0}, \boldsymbol{C} = \mathcal{M}\mathbf{1}$ where $\mathcal{M} = |\mathcal{I}_1|$. Suppose that $\epsilon = 1$ in the risk measure, i.e., $\rho(\cdot) = \mathbb{E}[\cdot]$, and the passenger demand is $\bar{D} = 1/2 \sum_{i\in\mathcal{I}_1} m_i$ for both routes. Then FairUAM (4.1) reduces to

$$z_1^* = \min_{\boldsymbol{\delta},\boldsymbol{y},\boldsymbol{s}} \quad \frac{1}{|\mathcal{I}_1|} \sum_{r\in[2]} s^r, \tag{4.3a}$$

$$\text{s.t.} \quad \sum_{r\in[2]} y_i^r \le 1, \quad \forall i \in \mathcal{I}_1, \tag{4.3b}$$

$$s^r + \sum_{i\in\mathcal{I}_1} m_i y_i^r \ge \bar{D}, \quad \forall r \in [2], \tag{4.3c}$$

$$y_i^r \in \{0,1\}, s^r \ge 0, \forall r \in [2], \forall i \in \mathcal{I}_1, \tag{4.3d}$$

where $[n] := \{1, 2, \ldots, n\}$. Thus, we claim that the optimal value of formulation (4.3) $z_1^* \le 0$ if and only if there exists a feasible solution $(\boldsymbol{s}, \boldsymbol{y})$ satisfying $\sum_{i\in\mathcal{I}_1} m_i y_i^r \ge \bar{D}, \forall r \in [2]$. This is because when $2\bar{D} = \sum_{i\in\mathcal{I}_1} m_i$, we must have $\sum_{i\in\mathcal{I}_1} m_i y_i^r = \bar{D}, \forall r \in [2]$ and $\sum_{r\in[2]} y_i^r = 1, \forall i \in \mathcal{I}_1$. Thus, solving formulation (4.3) is equivalent to solve the following problem

$$\sum_{r\in[2]} y_i^r = 1, \sum_{i\in\mathcal{I}_1} m_i y_i^r = \bar{D}, y_i^r \in \{0,1\}, \forall i \in \mathcal{I}_1, r \in [2],$$

which is exactly equivalent to the partition problem. Thus, checking the special case (4.3) of FairUAM (4.1) having the optimal value being equal to 0 or not is equivalent to solving the partition problem. This proves the NP-hardness of FairUAM (4.1). □

The complexity of Proposition 4.1 is owing to the binary variables in the first-stage problem. In fact, we prove that even with a given first-stage solution, the resulting problem, due to the special network structure in FairUAM (4.1) (i.e., bottleneck points), is still NP-hard to solve. More specifically, assigning ground and airborne delays with a given OD pair and route assignment can be an NP-hard combinatorial optimization problem. The complexity result is summarized below.

Proposition 4.2. *Solving the second-stage problem (4.2) is NP-hard even when a first-stage decision is given, the random parameters have one realization, and $\lambda = 1, |\mathcal{L}| = 1, |\mathcal{J}_r| = 1$ for all OD pair $r \in \mathcal{R}$.*

Proof: Let us consider a special case of the second-stage problem (4.2). Suppose the given

first-stage decision $(\boldsymbol{y}, \boldsymbol{\delta})$ is feasible, and we let $\boldsymbol{p} = \boldsymbol{0}, \boldsymbol{q} = \boldsymbol{0}, \boldsymbol{c} = \boldsymbol{0}, \boldsymbol{\tau} = \boldsymbol{0}, \bar{L} = |\mathcal{T}|, \bar{\boldsymbol{R}} = |\mathcal{T}|$. Since the random parameters have one realization, and we let airspace capacity $\boldsymbol{C} = \boldsymbol{1}$, the second-stage problem (4.2) reduces to

$$\min_{\boldsymbol{g},\boldsymbol{a},\boldsymbol{s},\boldsymbol{B}} \frac{1}{|\mathcal{I}_1|} \sum_{r\in\mathcal{R}} \sum_{i\in\mathcal{I}_1} \left(\alpha_i^r g_i^r + \beta_i^r \sum_{k\in\mathcal{K}} a_{ik}^r \right), \tag{4.4a}$$

$$\text{s.t.} \quad \sum_{t\in\mathcal{T}} B_{it}^k \le 1, \quad \forall i \in \mathcal{I}_1, k \in \mathcal{K}, \tag{4.4b}$$

$$\sum_{t\in\mathcal{T}} t B_{it}^k = \sum_{r\in\mathcal{R}} \left(g_i^r + \sum_{\substack{id(k) \ge id(k') \\ k' \in \mathcal{K}}} a_{ik'}^r \right), \quad \forall i \in \mathcal{I}_1, k \in \mathcal{K} \tag{4.4c}$$

$$\sum_{i\in\mathcal{I}_1} B_{it}^k \le 1, \quad \forall k \in \mathcal{K}, t \in \mathcal{T} \tag{4.4d}$$

$$B_{it}^k \in \{0,1\}, \quad \forall i \in \mathcal{I}_1, k \in \mathcal{K}, t \in \mathcal{T}, \tag{4.4e}$$

$$g_i^r, a_{ik}^r \in \mathbb{Z}_+, \quad \forall r \in \mathcal{R}, i \in \mathcal{I}_1, k \in \mathcal{K}. \tag{4.4f}$$

We show that job-shop scheduling problem (JSP) (Graham [120]), which is NP-complete even with unit processing time (see, e.g., theorem 3.5 in Hoogeveen et al. [121]), reduces to formulation (4.4).

> *Job-shop scheduling problem (JSP): There are a set $\mathcal{K}$ of machines and a set $\mathcal{I}$ of jobs. Each job $i \in \mathcal{I}$ consists of an ordered collection of operations $\{k_1, \ldots, k_{n_i}\} \subseteq \mathcal{K}$, and each operation must be completed at a specific machine and requires a unit of processing time on that machine. Each machine can only process one operation at a time. The goal is to optimize the order of operations completed on each machine to minimize the overall delay.*

In formulation (4.4), we let each aircraft represent a job and each bottleneck point denote a machine. We also let the visiting sequence of bottleneck points of an aircraft represent

the ordered collection of operations of a job. Furthermore, the unit processing time of an operation associates with the time that an aircraft passes the bottleneck point. The requirement that no two operations can be performed simultaneously is equivalent to the unit bottleneck point capacity. Therefore, in this case, the job-shop problem with unit processing time reduces to formulation (4.4). This proves the NP-hardness of the second-stage problem (4.2). □

Proposition 4.1 and Proposition 4.2 show that even under simple settings, FairUAM (4.1) may not be polynomial-time solvable. This motivates us to strengthen the original formulation and develop an exact method to solve it in the next section.

4.3.2 Sensitivity Analyses

In this subsection, we analyze the properties of the recourse function $\mathcal{Q}(\boldsymbol{y}, \boldsymbol{\delta}, \boldsymbol{\xi})$ and the second-stage objective function $Q(\boldsymbol{y}, \boldsymbol{\delta}, \boldsymbol{\xi}, \boldsymbol{g}(\boldsymbol{\xi}), \boldsymbol{a}(\boldsymbol{\xi}), \boldsymbol{s}(\boldsymbol{\xi}), \boldsymbol{u}(\boldsymbol{\xi}), \boldsymbol{B}(\boldsymbol{\xi}))$. These properties allow us to further simplify FairUAM (4.1) in the following sections. We first introduce the results for the second-stage objective function $Q(\boldsymbol{y}, \boldsymbol{\delta}, \boldsymbol{\xi}, \boldsymbol{g}(\boldsymbol{\xi}), \boldsymbol{a}(\boldsymbol{\xi}), \boldsymbol{s}(\boldsymbol{\xi}), \boldsymbol{u}(\boldsymbol{\xi}), \boldsymbol{B}(\boldsymbol{\xi}))$.

Proposition 4.3. *For the second-stage objective function $Q(\boldsymbol{y}, \boldsymbol{\delta}, \boldsymbol{\xi}, \boldsymbol{g}(\boldsymbol{\xi}), \boldsymbol{a}(\boldsymbol{\xi}), \boldsymbol{s}(\boldsymbol{\xi}), \boldsymbol{u}(\boldsymbol{\xi}), \boldsymbol{B}(\boldsymbol{\xi}))$, we have the following results:*

- *Function $Q(\boldsymbol{y}, \boldsymbol{\delta}, \boldsymbol{\xi}, \boldsymbol{g}(\boldsymbol{\xi}), \boldsymbol{a}(\boldsymbol{\xi}), \boldsymbol{s}(\boldsymbol{\xi}), \boldsymbol{u}(\boldsymbol{\xi}), \boldsymbol{B}(\boldsymbol{\xi}))$ is monotone non-decreasing as the second-stage decision unsatisfied trafic demand $s_\ell^r(\boldsymbol{\xi})$ non-decreases for some $\ell \in \mathcal{L}, r \in \mathcal{R}$;*
- *Function $Q(\boldsymbol{y}, \boldsymbol{\delta}, \boldsymbol{\xi}, \boldsymbol{g}(\boldsymbol{\xi}), \boldsymbol{a}(\boldsymbol{\xi}), \boldsymbol{s}(\boldsymbol{\xi}), \boldsymbol{u}(\boldsymbol{\xi}), \boldsymbol{B}(\boldsymbol{\xi}))$ is monotone non-decreasing as the passenger demand D_ℓ^r increases for some $\ell \in \mathcal{L}, r \in \mathcal{R}$; and*
- *Function $Q(\boldsymbol{y}, \boldsymbol{\delta}, \boldsymbol{\xi}, \boldsymbol{g}(\boldsymbol{\xi}), \boldsymbol{a}(\boldsymbol{\xi}), \boldsymbol{s}(\boldsymbol{\xi}), \boldsymbol{u}(\boldsymbol{\xi}), \boldsymbol{B}(\boldsymbol{\xi}))$ is monotone non-increasing as the airspace*

capacity C_t^k *increases for some* $t \in \mathcal{T}, k \in \mathcal{K}$.

Proof: We prove the results according to their order.

- The first monotonicity result is because an increase in unsatisfied passenger demand leads to an increase in airline operation cost, i.e., both efficiency and fairness costs increase or stay the same.
- The second monotonicity result is because when the passenger demand increases, more aircraft are needed to satisfy the passenger demand which leads to an increase in airline operation cost. Thus, both efficiency and fairness costs in the objective decrease or stay the same.
- The third monotonicity result is because when the airspace capacity increases, more aircraft are allowed to pass the same bottleneck point at the same time instead of waiting before entering this bottleneck point. In addition, more aircraft if available can be used to satisfy the passenger demand which helps reduce the airline operation cost. Thus, both efficiency and fairness costs in the objective decrease or stay the same. □

As the minimization operator preserves the monotonicity of a function, the second and third results of Proposition 4.3 still hold for the recourse function $\mathcal{Q}(\boldsymbol{y}, \boldsymbol{\delta}, \boldsymbol{\xi})$.

Corollary 4.4. *The following hold for the recourse function* $\mathcal{Q}(\boldsymbol{y}, \boldsymbol{\delta}, \boldsymbol{\xi})$*:*

- *Recourse function* $\mathcal{Q}(\boldsymbol{y}, \boldsymbol{\delta}, \boldsymbol{\xi})$ *is monotone non-decreasing as the passenger demand* D_ℓ^r *increases for some* $\ell \in \mathcal{L}, r \in \mathcal{R}$*; and*
- *Recourse function* $Q(\boldsymbol{y}, \boldsymbol{\delta}, \boldsymbol{\xi})$ *is monotone non-increasing as the airspace capacity* C_t^k *increases for some* $t \in \mathcal{T}, k \in \mathcal{K}$.

Proposition 4.3 and Corollary 4.4 motivate us that FairUAM (4.1) can be further simplified based on the monotonicity. It also shows that when the airspace capacity is large enough, aircraft can be assigned to OD pairs and routes without any airspace capacity limitation such that the ground delay and airborne delay can be nearly zero. In this case, when all aircraft can travel in free-condition airspace, the original problem can be reduced to an aircraft allocation problem.

4.3.3 Model Simplification and Integrality of Decision Variables

In this subsection, we first simplify FairUAM (4.1) by linearizing the nonlinear terms, then prove that at optimality, several classes of second-stage integer decision variables can be relaxed to be continuous to relieve the computational effort.

Linearization As mentioned at the beginning of this section, one difficulty of FairUAM (4.1) resides in the nonlinear terms in the first-stage objective (4.1a) and second-stage objective (4.2a). By introducing one more variable and two extra constraints, we can equivalently represent FairUAM (4.1) as follows:

$$\min_{\boldsymbol{\delta},\boldsymbol{y},v} \quad v + \varepsilon^{-1}\mathbb{E}_{\mathbb{P}}\left[h(\widetilde{\boldsymbol{\xi}})\right], \tag{4.5a}$$

$$\text{s.t.} \quad h(\boldsymbol{\xi}) \geq \mathcal{Q}(\boldsymbol{\delta},\boldsymbol{y},\boldsymbol{\xi}) - v, \tag{4.5b}$$

$$h(\boldsymbol{\xi}), v \geq 0, \tag{4.5c}$$

$$(4.1b) - (4.1d).$$

For the second-stage problem (4.2), we let $\psi(\boldsymbol{\xi})$ denote the fairness term. Then the second-stage problem (4.2) is equivalent to

$$\min_{\boldsymbol{g}(\boldsymbol{\xi}),\boldsymbol{a}(\boldsymbol{\xi}),\boldsymbol{s}(\boldsymbol{\xi}),\boldsymbol{B}(\boldsymbol{\xi})} Q(\boldsymbol{y},\boldsymbol{\delta},\boldsymbol{\xi},\boldsymbol{g}(\boldsymbol{\xi}),\boldsymbol{a}(\boldsymbol{\xi}),\boldsymbol{s}(\boldsymbol{\xi}),\boldsymbol{B}(\boldsymbol{\xi})) = \lambda \sum_{\ell\in\mathcal{L}} \frac{\phi_\ell(\boldsymbol{\xi})}{|\mathcal{I}_\ell|} + (1-\lambda)\psi(\boldsymbol{\xi}), \tag{4.6a}$$

$$\text{s.t.} \quad \phi_\ell(\boldsymbol{\xi}) - \psi(\boldsymbol{\xi})|\mathcal{I}_\ell| \le 0, \quad \forall \ell \in \mathcal{L}, \tag{4.6b}$$

$$\psi(\boldsymbol{\xi}) \ge 0, \tag{4.6c}$$

$$(4.2b) - (4.2k).$$

Relaxing Integrality of Decision Variables Based on the monotonicity results and problem structure, we prove that at optimality, we can relax the integrality of variables, which can enhance the efficacy to solve FairUAM (4.1) more efficiently.

Proposition 4.5. *Relaxing the integrality of $\boldsymbol{s}(\boldsymbol{\xi}), \boldsymbol{g}(\boldsymbol{\xi})$ in FairUAM (4.1) preserves the same optimal value.*

Proof: Notice that in constraints (4.2c) and (4.2d), at optimality, we must have $s^r_\ell(\boldsymbol{\xi}) = \max\{0, D^r_\ell - \sum_{i\in\mathcal{I}_\ell} m_i y^r_i\}$ for all $r \in \mathcal{R}, \ell \in \mathcal{L}$. Thus, we can relax the integrality of variables $\boldsymbol{s}$.

We also observe that when fixing the other variables, the constraint matrix related to variables $\boldsymbol{g}(\boldsymbol{\xi})$ is an interval matrix $\boldsymbol{G}_i(\boldsymbol{\xi}) = [g^r_{ij}(\boldsymbol{\xi})]_{|\mathcal{J}_r|\times|\mathcal{R}|}$, which is totally unimodular. Thus, we can relax the integrality of $\boldsymbol{g}(\boldsymbol{\xi})$. □

We can also relax the airborne delay variables $\boldsymbol{a}(\boldsymbol{\xi})$ when the airborne delay cost is higher than the ground delay cost, i.e., $\beta^r_{ij} > \alpha^r_{ij}$ for any aircraft $i \in \mathcal{I}_\ell$ on route $j \in \mathcal{J}_r$ and OD pair $r \in \mathcal{R}$.

Proposition 4.6. *Relaxing the integrality of variables $\boldsymbol{g}(\boldsymbol{\xi}), \boldsymbol{a}(\boldsymbol{\xi})$ in FairUAM (4.1) achieves*

the same optimal value when $\beta_{ij}^r > \alpha_{ij}^r$.

Proof: In FairUAM (4.1), let the variables $\boldsymbol{g}(\boldsymbol{\xi}), \boldsymbol{a}(\boldsymbol{\xi})$ be continuous, and let $(\hat{\boldsymbol{y}}, \hat{\boldsymbol{\delta}}, \hat{\boldsymbol{B}}, \hat{\boldsymbol{g}}, \hat{\boldsymbol{a}}, \hat{\boldsymbol{s}}, \hat{\boldsymbol{u}})$ be an optimal solution of the relaxed problem. According to (4.1b), (4.1c) and (4.2d), for any aircraft $i \in \mathcal{I}_\ell$, we must have $\hat{\delta}_{i\bar{j}}^{\bar{r}} = 1$ if there exists $\hat{g}_{i\bar{j}}^{\bar{r}} > 0$ or $\hat{a}_{i\bar{j}k}^{\bar{r}} > 0$, and $\hat{g}_{i\bar{j}}^{\bar{r}} = \hat{a}_{i\bar{j}k}^{\bar{r}} = 0$ for any $j \neq \bar{j}, \forall r \neq \bar{r}$. Let $\{k_1, k_2, \ldots, k_n\}$ be the bottleneck points in the visiting order on route $\bar{j}$ of OD pair $\bar{r}$. According to (4.2g), we must have

$$
\begin{aligned}
\sum_{t\in\mathcal{T}} tB_{i,t}^{k_1}(\boldsymbol{\xi}) &= \tau_{i\bar{j}k_1}^{o\bar{d}}\delta_{i\bar{j}}^{\bar{r}} + g_{i\bar{j}}^{\bar{r}} + a_{i\bar{j}k_1}^{\bar{r}}, \\
\sum_{t\in\mathcal{T}} tB_{i,t}^{k_2}(\boldsymbol{\xi}) &= \tau_{i\bar{j}k_1}^{o\bar{d}}\delta_{i\bar{j}}^{\bar{r}} + g_{i\bar{j}}^{\bar{r}} + a_{i\bar{j}k_1}^{\bar{r}} + a_{i\bar{j}k_2}^{\bar{r}}, \\
&\vdots \\
\sum_{t\in\mathcal{T}} tB_{i,t}^{k_n}(\boldsymbol{\xi}) &= \tau_{i\bar{j}k_1}^{\bar{r}}\delta_{i\bar{j}}^{\bar{r}} + g_{i\bar{j}}^{\bar{r}} + \sum_{k\in\{k_1,\ldots,k_n\}} a_{i\bar{j}k}^{\bar{r}}.
\end{aligned}
$$

Since all the left-hand sides are integers, $g_{i\bar{j}}^{\bar{r}} + a_{i\bar{j}k_1}^{\bar{r}}, a_{i\bar{j}k_2}^{\bar{r}}, \ldots, a_{i\bar{j}k_n}^{\bar{r}}$ must be integers. Since the unit airborne delay cost $\beta_{ij}^r > \alpha_{ij}^r$, the ground delay $g_{i\bar{j}}^{\bar{r}}$ should be the largest integer allowed. Thus, both variables $\boldsymbol{g}(\boldsymbol{\xi}), \boldsymbol{a}(\boldsymbol{\xi})$ must be integral. □

Since in most practical situations, an airborne delay is much more expensive than a ground delay due to the limitation in aircraft and airspace, both Proposition 4.5 and Proposition 4.6 can improve the second-stage problem (4.2). We also demonstrate the effectiveness of Proposition 4.5 and Proposition 4.6 in Section 4.5.1.

We also notice that when the airborne delay is too expensive, in the optimal decision, we can either assign zero airborne delay to the aircraft or assign no task to the aircraft, which is summarized below.

Proposition 4.7. *When* $\beta_{ij}^r > m_i p_\ell^r, \forall i \in \mathcal{N}_\ell, \ell \in \mathcal{L}, j \in \mathcal{J}_r, od \in \mathcal{R}$, *we must have* $\boldsymbol{a} = 0$ *in*

an optimal solution.

Proof: Suppose that there exists an optimal solution $(\bar{\boldsymbol{y}}, \bar{\boldsymbol{\delta}}, \bar{\boldsymbol{B}}, \bar{\boldsymbol{g}}, \bar{\boldsymbol{a}}, \bar{\boldsymbol{s}}, \bar{\boldsymbol{u}})$ of FairUAM (4.1) such that $\bar{a}^r_{ijk} > 0$ for some bottleneck point $k \in \mathcal{K}$, aircraft $i \in \mathcal{N}_\ell$ from service provider $\ell \in \mathcal{L}$ on route $j \in \mathcal{J}_r$ and OD pair $r \in \mathcal{R}$ and the corresponding $\bar{s}^r_\ell \geq 0$. Let us construct a new solution such that $\bar{s}^r_\ell := \bar{s}^r_\ell + \sum_{i \in \mathcal{N}_\ell} m_i \sum_{j \in \mathcal{J}_r} \sum_{k \in \mathcal{K}} a^r_{ijk}(\boldsymbol{\xi}), \bar{a}^r_{ijk} = 0$ and other variables keep the same. The new solution satisfies all the constraints and leads to a lower objective, a contradiction. □

Proposition 4.7 indicates that, when the air delay is too expensive, we can force the air delay to be zero to save computational effort. It also indicates that during some severe weather events, the air delay is much more expensive than usual and the service operators may directly cancel the flight plan to enforce safety.

4.4 Valid Inequalities and A Solution Method

In this section, we explore the formulation structure and strengthen FairUAM (4.1) by developing different families of valid inequalities and based on these efforts, we develop an efficient decomposition algorithm.

4.4.1 Valid Inequalities

In this subsection, we develop different families of valid inequalities to strengthen FairUAM (4.1).

Airspace Guarantee Inequalities According to constraints (4.1c), if an aircraft is assigned to an OD pair, it must be assigned to a particular route corresponding to the OD

pair. Consequently, the aircraft must go through the bottleneck points on its assigned route at some time points during the planning horizon according to constraints (4.2f) and (4.2g). Otherwise, no bottleneck point will be visited when the aircraft is idling. This motivates us to derive the following valid inequalities:

$$\sum_{t\in\mathcal{T}} B^k_{it}(\boldsymbol{\xi}) \leq \sum_{r\in\mathcal{R}} y^r_i, \quad \forall i \in \mathcal{I}_\ell, \ell \in \mathcal{L}, k \in \mathcal{K}, \tag{4.7a}$$

$$\sum_{t\in\mathcal{T}} \sum_{k\in\mathcal{K}} B^k_{it}(\boldsymbol{\xi}) \geq \omega \sum_{r\in\mathcal{R}} y^r_i, \quad \forall i \in \mathcal{I}_\ell, \ell \in \mathcal{L}, \tag{4.7b}$$

where ω is the minimum number of bottleneck points that need to be visited among all the possible OD pairs.

Symmetry-Breaking Inequalities For multiple identical aircraft from the same service provider, their assignment decisions to OD pairs are interchangeable, which causes unnecessary larger decision space. To avoid redundant branch and bound time in exploring such equivalent solutions, this motivates the symmetry-breaking valid inequalities. For two identical aircraft $i, i' \in \mathcal{I}_\ell, i' \geq i+1, \ell \in \mathcal{L}$ with $m_i = m_{i'}, q^r_i = q^r_{i'}, c^r_{ij} = c^r_{i'j}, \alpha^r_{ij} = \alpha^r_{i'j}, \beta^r_{ij} = \beta^r_{i'j}$, we add the following inequalities to FairUAM (4.1):

$$\sum_{r\in\mathcal{R}} 2^r y^r_i \geq \sum_{r\in\mathcal{R}} 2^r y^r_{i'} \tag{4.8}$$

For two identical aircraft $i, i' \in \mathcal{I}_\ell, i' \geq i+1, \ell \in \mathcal{L}$ assigned to the same OD pairs, we can have the symmetry-breaking inequalities for different routes as follows:

$$\text{if } y^r_i = y^r_{i'}, \text{ then } \sum_{j\in\mathcal{J}_r} 2^j \delta^r_{ij} \geq \sum_{j\in\mathcal{J}_r} 2^j \delta^r_{i'j}, \quad \forall r \in \mathcal{R},$$

which can be equivalently represented as

$$\sum_{j\in\mathcal{J}_r} 2^j \delta^r_{i'j} - \sum_{j\in\mathcal{J}_r} 2^j \delta^r_{ij} \le |y^r_i - y^r_{i'}|\mathcal{M}_r, \quad \forall r \in \mathcal{R}.$$

Above, for each route $r \in \mathcal{R}$, we let $\mathcal{M}_r$ be the upper bound of the left-hand side, where the value $2^{|\mathcal{J}_r|}$ suffices. To linearize the absolute operator, we can replace it with a variable $\bar{y}^r_{ii'} = |y^r_i - y^r_{i'}|$. In this case, we have $\bar{y}^r_{ii'} \ge |y^r_i - y^r_{i'}|$ and $\bar{y}^r_{ii'} \le |y^r_i - y^r_{i'}|$. We can replace $\bar{y}^r_{ii'} \ge |y^r_i - y^r_{i'}|$ by introducing additional constraints:

$$\bar{y}^r_{ii'} \ge y^r_i - y^r_{i'}, \bar{y}^r_{ii'} \ge y^r_{i'} - y^r_i, \bar{y}^r_{ii'} \ge 0, \quad \forall r \in \mathcal{R}. \tag{4.9a}$$

Then, we introduce an additional binary variable $u^r_{ii'} \in \{0,1\}$ to linearize $\bar{y}^r_{ii'} \le |y^r_i - y^r_{i'}|$ with constraints:

$$\bar{y}^r_{ii'} \le y^r_i - y^r_{i'} + 2u^r_{ii'}, \bar{y}^r_{ii'} \le y^r_{i'} - y^r_i + 2(1 - u^r_{ii'}), \quad \forall r \in \mathcal{R}. \tag{4.9b}$$

Since both variables $y^r_i, y^r_{i'}$ are binary, we can further relax the binary variable $u^r_{ii'}$ to be continuous by adding the following constraints:

$$1 - u^r_{ii'} \ge y^r_i - y^r_{i'}, u^r_{ii'} \ge y^r_{i'} - y^r_i, u^r_{ii'} \in [0,1], \quad \forall r \in \mathcal{R}. \tag{4.9c}$$

Finally, we arrive at the following symmetry-breaking inequalities for route assignment. For any two identical aircraft $i, i' \in \mathcal{I}_\ell, i' \ge i+1, \ell \in \mathcal{L}$ such that $m_i = m_{i'}, q^r_i = q^r_{i'}, c^r_{ij} = c^r_{i'j}, \alpha^r_{ij} = \alpha^r_{i'j}, \beta^r_{ij} = \beta^r_{i'j}$, we have

$$\sum_{j\in\mathcal{J}_r} 2^j \delta^r_{i'j} - \sum_{j\in\mathcal{J}_r} 2^j \delta^r_{ij} \le \bar{y}^r_{ii'}\mathcal{M}_r, \quad \forall r \in \mathcal{R}, \tag{4.10}$$

(4.9a) – (4.9c).

Data Pre-processing Inequalities Since the auxiliary variables $\boldsymbol{B}(\boldsymbol{\xi})$ relate the aircraft location with bottleneck visiting time, their values can be one only between the earliest arrival time and latest arrival time for each bottleneck point, i.e., we have the following pre-processing inequalities

$$B_{it}^k(\boldsymbol{\xi}) = 0, \quad \forall t < \underline{\tau}_{ik}, t \in \mathcal{T}, i \in \mathcal{I}_\ell, \ell \in \mathcal{L}, k \in \mathcal{K}, \tag{4.11a}$$

$$B_{it}^k(\boldsymbol{\xi}) = 0, \quad \forall t > \bar{L} + \bar{\tau}_{ik}, t \in \mathcal{T}, \forall i \in \mathcal{I}_\ell, \ell \in \mathcal{L}, k \in \mathcal{K}, \tag{4.11b}$$

where $\underline{\tau}_{ik} := \min_{r \in \mathcal{R}, j \in \mathcal{J}_r} \tau_{ijk}^r$ denotes the minimum time needed for aircraft $i \in I_\ell$ from service provider $\ell \in \mathcal{L}$ to arrive at bottleneck point $k \in \mathcal{K}$ in the free-condition airspace while $\bar{\tau}_{ik} := \max_{r \in \mathcal{R}, j \in \mathcal{J}_r} \tau_{ijk}^r$ denotes the maximum arrival time allowed.

Bottleneck Point Arrival Time Inequalities Similarly, the bottleneck arrival time for an aircraft is also related to its assignment. Therefore, we can also bound the bottleneck arrival time based on OD pair assignment

$$\sum_{t \in \mathcal{T}} t B_{it}^k(\boldsymbol{\xi}) \leq \left(\bar{L} + \bar{\tau}_{ik}\right) \sum_{r \in \mathcal{R}} y_i^r, \quad \forall t \in \mathcal{T}, i \in \mathcal{I}_\ell, \ell \in \mathcal{L}, k \in \mathcal{K}, \tag{4.12a}$$

$$\sum_{t \in \mathcal{T}} t B_{it}^k(\boldsymbol{\xi}) \geq \underline{\tau}_{ik} \sum_{r \in \mathcal{R}} y_i^r, \quad \forall t \in \mathcal{T}, i \in \mathcal{I}_\ell, \ell \in \mathcal{L}, k \in \mathcal{K}. \tag{4.12b}$$

Total Arrival Time Inequalities We can upper bound the total arrival time of all aircraft at a specific bottleneck point based on its airspace capacity, which is

$$|\mathcal{T}| \max_{t\in\mathcal{T}} C_t^k \geq \sum_{\ell\in\mathcal{L}} \sum_{i\in\mathcal{N}_\ell} \sum_{r\in\mathcal{R}} \sum_{j\in\mathcal{J}_r} \left(\tau_{ijk}^r \delta_{ij}^r + g_{ij}^r(\boldsymbol{\xi}) + \sum_{\substack{id(k) \geq id(k') \\ k' \in \mathcal{K}}} a_{ijk'}^r(\boldsymbol{\xi}) \right), \quad \forall k \in \mathcal{K}. \tag{4.13}$$

Accumulated Delay Inequalities When OD pair and route assignments (i.e., the first-stage decision variables) are given, an aircraft travels according to the predetermined bottleneck sequence. In other words, the bottleneck sequence depends on the first-stage assignment. Figure 4.2 is a demonstration, where we consider one OD pair with two alternative routes. In the first route, an aircraft visits bottleneck point $k_1 \in \mathcal{K}$ before bottleneck point $k_2 \in \mathcal{K}$, while it visits bottleneck point k_2 before bottleneck point k_1 in the second route.

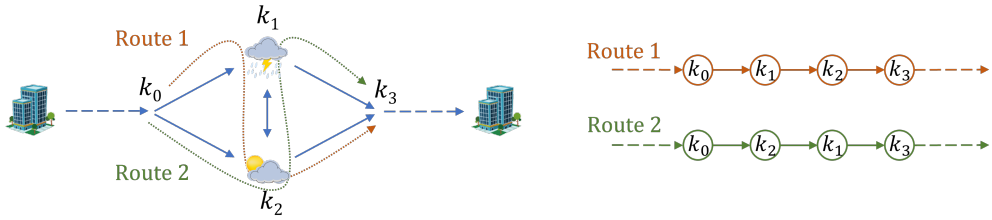

Figure 4.2: An illustration of one OD pair and two routes with different bottleneck visiting sequences

In this case, there is no clear delay arrival time relationship between these two bottleneck points. Instead, we derive the relationship between the accumulated delays before visiting two bottleneck points. According to constraints (4.2g), the accumulated delay before visiting bottleneck point $k \in \mathcal{K}$ can be represented by the difference between the bottleneck actual arrival time $\sum_{t\in\mathcal{T}} tB_{it}^k(\boldsymbol{\xi})$ and the travel time needed in the free-condition airspace $\tau_{ijk}^r \delta_{ij}^r$ for any aircraft $i \in \mathcal{I}_\ell$ from service provider $\ell \in \mathcal{L}$ on route $j \in \mathcal{J}_r$ and OD pair $r \in \mathcal{R}$. Therefore, for any given route assignment, when $id_j(k_1) < id_j(k_2)$ on route $j \in \mathcal{J}_r$ and OD

pair $r \in \mathcal{R}$, we have the following valid inequalities:

$$\sum_{t\in\mathcal{T}} tB_{it}^{k_1}(\boldsymbol{\xi}) - \tau_{ijk_1}^r \delta_{ij}^r \leq \sum_{t\in\mathcal{T}} tB_{i,t}^{k_2}(\boldsymbol{\xi}) - \tau_{ijk_2}^r \delta_{ij}^r + (1-\delta_{ij}^r)L, \quad \forall i \in \mathcal{I}_\ell, \ell \in \mathcal{L}. \tag{4.14}$$

We remark that inequalities (4.14) are very useful when we are given and want to evaluate a first-stage decision.

The effectiveness of inequalities (4.7) - (4.14) is demonstrated in Section 4.5.1 which further accelerates the algorithm proposed in the next section.

4.4.2 A Decomposition Algorithm

In this subsection, we present an exact decomposition algorithm to solve the FairUAM (4.1) together with valid inequalities. Our decomposition algorithm follows from Benders decomposition (Benders [122]). Note that in a conventional Benders decomposition, the original problem is partitioned into a master problem and a group of linear subproblems, which are much easier to solve for a given master solution. Following the same spirit, we partition FairUAM (4.1) into a master problem associated with OD pair and route assignment and a subproblem for ground and airborne delay assignment by relaxing the variables $\boldsymbol{B}(\boldsymbol{\xi})$ to be continuous. At each iteration, the upper bound can be obtained by plugging in the feasible delay assignment subproblem to the original formulation (4.1), and the lower bound can be computed by solving the master problem. It is known that the Benders cut is insufficient to recover the optimal value of FairUAM (4.1). To improve it, we adopt the L-shaped cut (Laporte and Louveaux [123]) which ensures the decomposition algorithm generates the exact optimal solution when terminated. Note that the L-shaped cut is generated by evaluating the subproblem with a given feasible first-stage solution.

Specifically, we let $\mathcal{X} = \{(\boldsymbol{\delta}, \boldsymbol{y}) : (4.1b) - (4.1d)\}$ denote the feasible region of first-stage decision variables. By introducing an additional variable θ for the overall operation cost, we can formulate the *OD pair/route assignment master problem (MP)* as follows:

$$z_{mp} = \min_{\theta, \boldsymbol{\delta}, \boldsymbol{y}} \left\{ v + \varepsilon^{-1} \mathbb{E}_{\mathbb{P}}[h(\widetilde{\boldsymbol{\xi}})] : h(\widetilde{\boldsymbol{\xi}}) \geq \theta(\boldsymbol{\xi}) - v, (\boldsymbol{y}, \boldsymbol{\delta}) \in \mathcal{X}, (4.5c), (4.8) - (4.10) \right\} \tag{4.15}$$

For any fixed $(\bar{\boldsymbol{y}}, \bar{\boldsymbol{\delta}}) \in \mathcal{X}$ and a realization of random parameter $\boldsymbol{\xi}$, the *delay assignment subproblem (SP)* is

$$z_{sp}(\boldsymbol{\xi}) = \min_{\boldsymbol{g}(\boldsymbol{\xi}), \boldsymbol{a}(\boldsymbol{\xi}), \boldsymbol{s}(\boldsymbol{\xi}), \boldsymbol{B}(\boldsymbol{\xi})} Q(\bar{\boldsymbol{y}}, \bar{\boldsymbol{\delta}}, \boldsymbol{\xi}, \boldsymbol{g}(\boldsymbol{\xi}), \boldsymbol{a}(\boldsymbol{\xi}), \boldsymbol{s}(\boldsymbol{\xi}), \boldsymbol{B}(\boldsymbol{\xi})) \tag{4.16a}$$

$$\text{s.t.} \quad B_{it}^k(\boldsymbol{\xi}) \in [0,1], \quad \forall i \in \mathcal{I}_\ell, \ell \in \mathcal{L}, k \in \mathcal{K}, t \in \mathcal{T}, \tag{4.16b}$$

$$g_{ij}^r(\boldsymbol{\xi}), a_{ijk}^r(\boldsymbol{\xi}), s_\ell^r(\boldsymbol{\xi}) \geq 0, \quad \forall j \in \mathcal{J}_r, r \in \mathcal{R}, i \in \mathcal{I}_\ell, \ell \in \mathcal{L}, k \in \mathcal{K}, \tag{4.16c}$$

$$(4.2b) - (4.2i), (4.6b) - (4.6c).$$

Let $\boldsymbol{\pi} = (\boldsymbol{\pi}_1, \ldots, \boldsymbol{\pi}_8)$ be the dual variables associated with constraints (4.6c), (4.2b)-(4.2h) respectively. The *dual subproblem (DSP)* can be presented as follows:

$$\max_{\boldsymbol{\pi}} \quad \sum_{\ell \in \mathcal{L}} \left[\pi_{2\ell} \sum_{r \in \mathcal{R}} \sum_{i \in \mathcal{I}_\ell} \left(q_i^r \bar{y}_i^r + \sum_{j \in \mathcal{J}_r} c_{ij}^r \bar{\delta}_{ij}^r \right) + \pi_{3\ell} \left(D_\ell^r - \sum_{i \in \mathcal{I}_\ell} m_i \bar{y}_i^r \right) - \sum_{r \in \mathcal{R}} \sum_{i \in \mathcal{I}_\ell} \sum_{j \in \mathcal{J}_r} \bar{\delta}_{ij}^r \left(\pi_{4rij} \bar{L} + \pi_{5rij} \bar{R}_{ij}^r \right) \right.$$
$$\left. + \sum_{i \in \mathcal{I}_\ell} \sum_{k \in \mathcal{K}} \left(-\pi_{6ik} + \pi_{7ik} \sum_{r \in \mathcal{R}} \sum_{j \in \mathcal{J}_r} \tau_{ijk}^r \bar{\delta}_{ij}^r \right) \right] - \sum_{k \in \mathcal{K}} \sum_{t \in \mathcal{T}} \pi_{8kt} C_t^k, \tag{4.17a}$$

$$\text{s.t.} \quad \sum_{\ell \in \mathcal{L}} \pi_{1\ell} |\mathcal{I}_\ell| \leq 1 - \lambda, \tag{4.17b}$$

$$\pi_{2\ell} - \pi_{1\ell} \leq \frac{\lambda}{|I_\ell|}, \quad \forall \ell \in \mathcal{L}, \tag{4.17c}$$

$$\pi_{3r\ell} - p_\ell^r \pi_{2\ell} \leq 0, \quad \forall r \in \mathcal{R}, \ell \in \mathcal{L}, \tag{4.17d}$$

$$-\alpha_{ij}^r \pi_{2\ell} - \pi_{4rij} - \pi_{7ik} \leq 0, \quad \forall j \in \mathcal{J}_r, r \in \mathcal{R}, i \in \mathcal{I}_\ell, \ell \in \mathcal{L}, \tag{4.17e}$$

$$-\beta_{ij}^r \pi_{2\ell} - \pi_{4rij} - \pi_{5ijr} - \pi_{7ik} \leq 0, \quad \forall j \in \mathcal{J}_r, r \in \mathcal{R}, i \in \mathcal{I}_\ell, \ell \in \mathcal{L}, k \in \mathcal{K} \tag{4.17f}$$

$$-\pi_{6ik} + t\pi_{yik} - \pi_{8kt} \leq 0, \quad \forall i \in \mathcal{I}_\ell, \ell \in \mathcal{L}, k \in \mathcal{K}, t \in \mathcal{T}, \tag{4.17g}$$

$$\pi_{1\ell}, \pi_{3r\ell}, \pi_{4rij}, \pi_{5ijr}, \pi_{6ik}, \pi_{8kt} \geq 0, \quad \forall j \in \mathcal{J}_r, r \in \mathcal{R}, i \in \mathcal{I}_\ell, \ell \in \mathcal{L}, k \in \mathcal{K}. \tag{4.17h}$$

If formulation (4.16) is feasible, we can obtain the optimal solution $\bar{\pi}$ of DSP (4.17) and the corresponding objective value $\bar{z}_{sp}$. The Benders cut for MP (4.15) can be generated as follows:

$$\begin{aligned}\theta(\boldsymbol{\xi}) \geq & \bar{z}_{sp}(\boldsymbol{\xi}) + \sum_{\ell \in \mathcal{L}} \left[\bar{\pi}_{2\ell} \sum_{r \in \mathcal{R}} \sum_{i \in \mathcal{I}_\ell} \left(q_i^r (y_i^r - \bar{y}_i^r) + \sum_{j \in \mathcal{J}_r} c_{ij}^r (\delta_{ij}^r - \bar{\delta}_{ij}^r) \right) - \bar{\pi}_{3\ell} \sum_{i \in \mathcal{I}_\ell} m_i (y_i^r - \bar{y}_i^r) \right. \\ & \left. - \sum_{r \in \mathcal{R}} \sum_{i \in \mathcal{I}_\ell} \sum_{j \in \mathcal{J}_r} (\delta_{ij}^r - \bar{\delta}_{ij}^r) \left(\pi_{4rij} L + \pi_{5rij} R_{ij}^r \right) + \sum_{i \in \mathcal{I}_\ell} \sum_{k \in \mathcal{K}} \left(\pi_{7ik} \sum_{r \in \mathcal{R}} \sum_{j \in \mathcal{J}_r} \tau_{ijk}^r (\delta_{ij}^r - \bar{\delta}_{ij}^r) \right) \right].\end{aligned} \tag{4.18}$$

If formulation (4.16) or second-stage problem (4.2) is infeasible, we cut off the corresponding solution from MP (4.15) by adding the no-good cut (Ahmed [111], Codato and Fischetti [124]) for given $\bar{\boldsymbol{\delta}}$ (we do not need to include $\bar{\boldsymbol{y}}$ according to constraints (4.1c)) as well as adding the feasibility cut

$$\sum_{r \in \mathcal{R}} \sum_{\ell \in \mathcal{L}} \sum_{i \in \mathcal{I}_\ell} \sum_{j \in \mathcal{J}_r} \left(\delta_{ij}^r (1 - \bar{\delta}_{ij}^r) + (1 - \delta_{ij}^r) \bar{\delta}_{ij}^r \right) \geq 1, \tag{4.19a}$$

$$0 \geq \sum_{\ell \in \mathcal{L}} \left[\bar{\pi}_{2\ell} \sum_{r \in \mathcal{R}} \sum_{i \in \mathcal{I}_\ell} \left(q_i^r y_i^r + \sum_{j \in \mathcal{J}_r} c_{ij}^r \delta_{ij}^r \right) + \bar{\pi}_{3\ell} \left(D_\ell^r - \sum_{i \in \mathcal{I}_\ell} m_i y_i^r \right) - \sum_{r \in \mathcal{R}} \sum_{i \in \mathcal{I}_\ell} \sum_{j \in \mathcal{J}_r} \delta_{ij}^r \left(\bar{\pi}_{4rij} \bar{L} + \bar{\pi}_{5rij} \bar{R}_{ij}^r \right) \right.$$

$$+\sum_{i\in\mathcal{I}_\ell}\sum_{k\in\mathcal{K}}\left(-\bar{\pi}_{6ik}+\bar{\pi}_{7ik}\sum_{r\in\mathcal{R}}\sum_{j\in\mathcal{J}_r}\tau^r_{ijk}\delta^r_{ij}\right)\Bigg]-\sum_{k\in\mathcal{K}}\sum_{t\in\mathcal{T}}\bar{\pi}_{8kt}C^k_t, \tag{4.19b}$$

where $\bar{\boldsymbol{\pi}}$ is an extreme direction of the dual problem. Note that even though no-good cut (4.19a) is commonly used in binary MP, feasibility cut (4.19b) is at least equally good. Thus, during our implementation, we use feasibility cut for the warm start and no-good cut and feasibility cuts for the branch and cut procedure.

Suppose that the MP solution $(\bar{\boldsymbol{y}}, \bar{\boldsymbol{\delta}})$ is also feasible to the second-stage problem (4.2). Then we can evaluate its corresponding objective value by plugging into the second-stage problem (4.2) with valid inequalities:

$$\begin{aligned} z_e(\boldsymbol{\xi}) = \min_{\boldsymbol{g}(\boldsymbol{\xi}),\boldsymbol{a}(\boldsymbol{\xi}),\boldsymbol{s}(\boldsymbol{\xi}),\boldsymbol{B}(\boldsymbol{\xi})} & Q(\bar{\boldsymbol{y}}, \bar{\boldsymbol{\delta}}, \boldsymbol{\xi}, \boldsymbol{g}(\boldsymbol{\xi}), \boldsymbol{a}(\boldsymbol{\xi}), \boldsymbol{s}(\boldsymbol{\xi}), \boldsymbol{B}(\boldsymbol{\xi})) \\ \text{s.t.} \quad & (4.2b)-(4.2k), (4.6b)-(4.6c), (4.7a)-(4.7b), (4.11), (4.12), (4.14). \end{aligned} \tag{4.20}$$

We can obtain the optimal objective value $\bar{z}_e(\boldsymbol{\xi})$ for formulation (4.20), then the L-shaped cut for MP (4.15) can be generated as follows:

$$\theta(\boldsymbol{\xi}) \geq z_e(\boldsymbol{\xi}) + (z_e(\boldsymbol{\xi}) - lb(\boldsymbol{\xi}))\left(\sum_{r\in\mathcal{R}}\sum_{\ell\in\mathcal{L}}\sum_{i\in\mathcal{I}_\ell}\sum_{j\in\mathcal{J}_r}\left(\delta^r_{ij}(1-\bar{\delta}^r_{ij}) + (1-\delta^r_{ij})\bar{\delta}^r_{ij}\right)\right) \tag{4.21}$$

where $lb(\boldsymbol{\xi})$ is a valid lower bound of $\theta(\boldsymbol{\xi})$.

The detailed implementation can be found in Algorithm 5.

We can further warm-start Algorithm 5 by relaxing the integrality of $\boldsymbol{y}$ and $\boldsymbol{\delta}$ in MP (4.15) to generate optimality and feasibility cuts at the root node. The effectiveness of Algorithm 5 is demonstrated in Section 4.5.1.

The proposed inequalities (4.7) - (4.14) in Section 4.4 accelerate each iteration in Algo-

Algorithm 5: Decomposition Algorithm

1 Initialization: Set feasible region $\mathcal{X} = \{(\boldsymbol{y}, \boldsymbol{\delta}) : (4.1b) - (4.1d)\}$, $LB = 0, UB = \infty, \epsilon > 0$;
2 **while** $UB - LB > \epsilon$ **do**
3 Solve the OD pair/route assignment master problem (MP) (4.15), record the optimal solution $(\bar{\boldsymbol{y}}, \bar{\boldsymbol{\delta}})$ and optimal value z^*_{sp};
4 $LB = \max\{LB, z^*_{mp}\}$;
5 **for** *each realization of random parameter* $\boldsymbol{\xi}$ **do**
6 Solve the delay assignment subproblem (SP) (4.16);
7 **if** *formulation* (4.16) *is feasible* **then**
8 Record the optimal value $z^*_{sp}(\boldsymbol{\xi})$ and add Benders cut (4.18) to MP (4.15);
9 **if** *formulation* (4.20) *is feasible* **then**
10 Record the optimal value $z^*_e(\boldsymbol{\xi})$ and add L-shaped cut (4.21) to MP (4.15)
11 **else**
12 Add no-good cut (4.19a) and feasibility cut (4.19b) to MP (4.15) and go to line 3;
13 $UB = \min\{UB, \min_{v \in \mathbb{R}} \{v + \varepsilon^{-1}\mathbb{E}[z^*_e(\boldsymbol{\xi}) - v]_+\}\}$

rithm 5, improving the lower bound much faster compared to the original formulation. The convergence of the decomposition algorithm also improves a lot if we use both.

4.5 Numerical Study

In this section, we present a group of numerical results to demonstrate the strengths of different model formulations and show the effectiveness of our solution method using random instances as well as a real-world network in Seattle. We report the results on random instances and conduct sensitivity analysis in Section 4.5.1. We then apply our solution method to a real-world network in Seattle in Section 4.5.2 for more aircraft fleet management insights. In reality, the UAM service providers operating on-demand services usually file their flight plan a day or hours before the actual departure time. We are allowed to obtain the allocation plan for the whole planning horizon offline. In this case, A time limit of 3,600

seconds was set for solving each random instance and the real-world case study. All the instances were coded in Python 3.7.0 with calls to Gurobi 9.0.3 on a personal laptop with a 1.9 GHz Intel Core i7 processor and 16 GB memory.

4.5.1 Results on Random Instances

Experimental Design and Setup We consider a small network and a larger network with different numbers of nodes and test 12 random instances for the small network and 8 random instances for the larger network. The small network has 5 vertiports, $|\mathcal{K}| = 5$ bottleneck points and $|\mathcal{R}| = 4$ OD pairs, while the larger network has 10 vertiports, $|\mathcal{K}| = 8$ bottleneck points and $|\mathcal{R}| = 6$ OD pairs. Each OD pair has 3 candidate routes. We consider $|\mathcal{L}| = 3$ service providers with different numbers of aircraft and each bears an aircraft capacity of $\boldsymbol{m} = 4$. The time horizon is $|\mathcal{T}| = 50$ and the travel time between 2 nodes in the free-condition airspace is set to either 2 or 3 time units. We let the weighted scalar $\lambda = 0.5$. The aircraft relocation cost $\boldsymbol{q}$ is randomly selected from {0,1} to ensure that at most one origin vertiport among all OD pairs incurs a relocation cost of 0 if relocation is not needed. The assignment cost $\boldsymbol{c}$ is set equal to the travel time in a free condition. The ground delay cost $\boldsymbol{\alpha}$ is set to 1 and the airborne delay cost $\boldsymbol{\beta}$ is set to 3 per unit of time. The penalty cost $\boldsymbol{s}$ is set to 20 per unsatisfied passenger. The total travel delay limit is set to $\bar{L} = 10$ and the airborne delay limit is set $\bar{\boldsymbol{R}} = \mathbf{2}$. The airspace capacities of each bottleneck point per time unit are randomly generated with equal probability from two sets of different levels of airspace capacity: $\{1, 2\}$ for the low level, $\{2, 3\}$ for the high level. The passenger demand of each OD pair during the whole time horizon is generated from three different discrete uniform distributions to represent different levels of passenger demand: $\mathcal{U}(2, 6)$ for low level, $\mathcal{U}(6, 10)$ for medium level, $\mathcal{U}(10, 20)$ for high level. In the small network, the numbers of aircraft for service providers are set to 3 for the low-level passenger demand instances, 5 for

the medium-level passenger demand instances and 10 for the high-level passenger demand instances. In the larger network, the numbers of aircraft for service providers are 6 for the low-level passenger demand instances, 10 for the medium-level passenger demand instances, and 15 for the high-level passenger demand instances. We let the risk parameter $\varepsilon = 0.1$ in CVaR to minimize the worst-case outcomes.

Numerical Results We summarize the instances and report the results in Table 4.1 where a-b in the "Instance" column means the size network a and random instance b; "MILP" represents FairUAM (4.1) and "MILP.VI" represents FairUAM (4.1) with valid inequalities (4.7) - (4.14). We see that the computational time increases as the instance size (e.g., network size, number of aircraft, etc.) increases. When the number of scenarios increases, both objective value and computational time increase. MILP is only able to solve the first 5 instances to optimality. MILP.VI improves MILP's performance and can solve 80% more instances (i.e., the first 9 instances) to optimality. However, no instance in the larger network can be solved to optimality by either MILP or MILP.VI. On the contrary, Algorithm 5 can improve MILP.VI and solve 14 instances to optimality, which is 56% more instances solvable compared to MILP.VI and 180% more instances solvable compared to MILP. This is probably because using decomposition and exploring formulation structures take advantage of solving smaller and easier subproblems. We also notice that, with the same passenger demand and the same number of aircraft, smaller airspace capacity instances are often more difficult to solve since the more restrictions in the airspace are, the harder aircraft assignment can be. When the airspace capacity increases, the objective value decreases since larger airspace capacity allows more aircraft to stay in the same airspace at the same time, which leads to short delays and smaller unsatisfied passenger demand. With the same airspace capacity, higher passenger demand results in longer computational time, since either more aircraft should be assigned to OD pairs or some UAM service providers may have unsatisfied

passenger demand. Higher passenger demand also leads to a higher objective value, which is intuitive since the total operation cost of UAM service providers increases.

Table 4.1: Random Instance Setting and Results of Different Formulations and Algorithm 5

Instance	Num. of Scenarios	Airspace Capacity	Passenger Demand	MILP			MILP.VI			Algorithm 5		
				Time(s)	Gap(%)	Obj.Val	Time(s)	Gap(%)	Obj.Val	Time(s)	Gap(%)	Obj.Val
S-1	5	low	low	23	0	133.8	12	0	133.8	6	0.0	133.8
S-2			medium	67	0	285.8	33	0	285.8	12	0.0	285.8
S-3		high	medium	37	0	184.3	20	0	184.3	9	0.0	184.3
S-4			high	85	0	252.3	49	0	252.3	15	0.0	252.3
S-5	10	low	low	869	0	145.3	150	0	145.3	67	0.0	145.3
S-6			medium	3600	0.5	306.3	535	0	304.7	181	0.0	304.7
S-7		high	medium	3600	2.4	232.3	364	0	226.7	115	0.0	226.7
S-8			high	3600	2.7	352.7	1801	0	343.3	337	0.0	343.3
S-9	20	low	low	3600	2.2	189.8	2736	0	185.6	869	0.0	185.6
S-10			medium	3600	5.4	379.3	3600	0.3	359.8	2497	0.0	358.8
S-11		high	medium	3600	5.3	285.2	3600	0.8	272.3	1684	0.0	270.0
S-12			high	3600	6.8	430.0	3600	1.0	406.7	3600	0.2	403.5
L-13	10	low	low	3600	13.4	292.2	3600	3.9	264.6	666	0.0	254.3
L-14			medium	3600	17.3	340.1	3600	5.4	299.1	1631	0.0	282.9
L-15		high	medium	3600	15.6	353.3	3600	5.2	313.3	1055	0.0	296.7
L-16			high	3600	25.1	714.5	3600	8.6	603.4	3600	0.4	549.9
L-17	20	low	low	3600	38.9	441.9	3600	11.3	324.4	3600	1.3	294.9
L-18			medium	3600	46.1	717.4	3600	14.9	489.1	3600	4.4	435.4
L-19		high	medium	3600	46.9	609.6	3600	15.3	396.6	3600	7.3	362.2
L-20			high	3600	57.3	904.7	3600	21.4	681.0	3600	10.2	596.0

To better demonstrate the effectiveness of valid inequalities, besides comparing computational time and optimality gap of MILP and MILP.VI in Table 4.1, we solved instance S-4 using Algorithm 1 with and without valid inequalities (4.7) - (4.14) respectively, which are illustrated in Figure 4.3. Note that, the results for other instances are similar and Figure 4.3 is for demonstration. The computational time of instance S-4 significantly decreases from 438 seconds to 15 seconds if we apply valid inequalities. The improvement mainly comes from the symmetry-breaking ones that prevent exploring unnecessary equivalent solutions.

To demonstrate the robustness of the solutions from our model, we consider an additional risk-neutral FairUAM (4.1) where $\varepsilon = 1$ and $\rho(Z) = \mathbb{E}_{\mathbb{P}}[Z]$ to compare with our risk-averse one. We first obtained the solutions by solving two formulations with instance S-8. Then, we generated 10 new scenarios following the same procedure mentioned before for

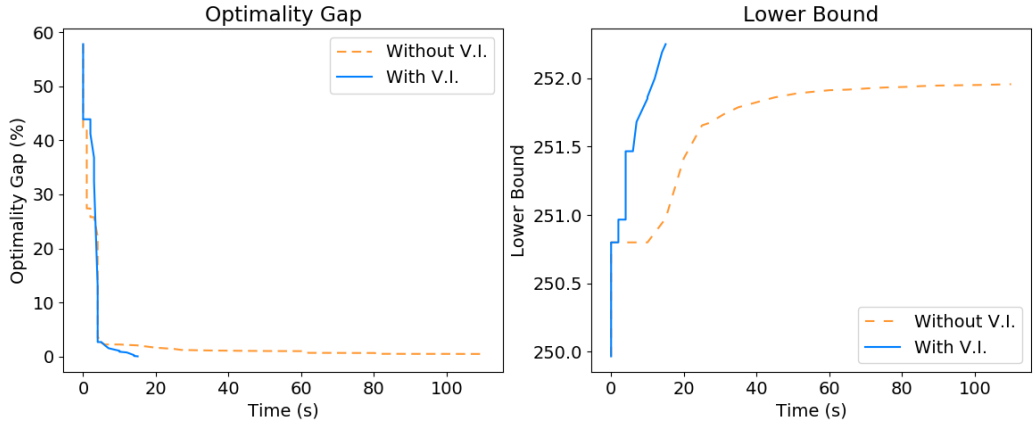

Figure 4.3: Comparison of Lower Bound and Optimality Gap with and without the Valid Inequalities

evaluation. We assumed that weather conditions or passenger demand are changing rapidly over time. Thus, we applied a truncated Gaussian noise to generate airspace capacity and passenger demand per scenario to make sure that they are nonnegative. More specifically, we let the random perturbation of airspace capacity follow a Gaussian distribution $\mathcal{N}(0, 0.1)$ truncated to be non-positive and rounded to the nearest nonnegative integer. For the random perturbation applied to passenger demand, we let it follow a Gaussian distribution $\mathcal{N}(0, 0.2)$ truncated to a nonnegative number and rounded to the nearest integer. We repeated the process 15 times to generate asymptotic 95% confidence intervals. The results are illustrated in Figure 4.4. It shows that, when the demand increases or the airspace capacity decreases, the objective value increases and the risk-averse one is more robust. It is worth mentioning that, when the airspace capacity is small (e.g., a part of bottleneck points having 0 capacity), no aircraft can depart; otherwise, it will violate the airspace capacity. In this case, both risk-neutral and risk-averse models end up with a trivial solution.

We conducted a sensitivity analysis of weighted scalar λ on instance S-8 to demonstrate the trade-off between efficiency and fairness. We let $\lambda \in \{0, 0.25, 0.5, 0.75, 1\}$. For better comparison, we illustrate the change in percentage for total cost and unfairness, where for

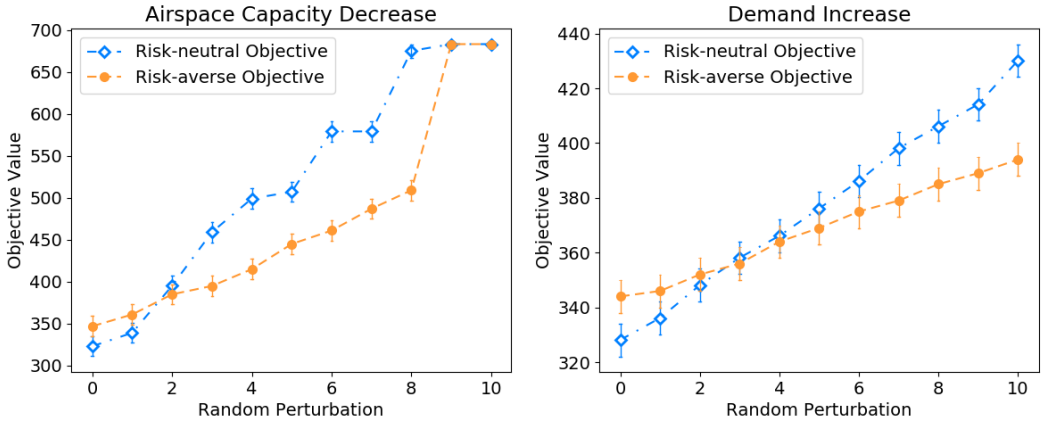

Figure 4.4: Evaluation of the Objective Value when Airspace Capacity Decreases or Demand Increases

the total cost change, we let the base case be the lowest possible cost, and for the unfairness change, we let the base case be the smallest value of the largest average company cost. We evaluate unfairness as the absolute difference between the highest and lowest average company operation costs. The result is illustrated in Figure 4.5. We see that, when the weighted scalar $\lambda = 1$, the total operation cost is the smallest; however, the solution is extremely unfair among different UAM service providers. Some service providers suffer much higher average aircraft operation cost due to delays. As the weighted scalar increases, we can reduce the unfairness dramatically with a small increase in the total operation cost. When the weighted scalar $\lambda = 0$, we make the fairest assignment for each service provider; however, as expected, the total operation cost is the highest. In summary, we recommend using an appropriate parameter λ which can help achieve a good balance between fairness and efficiency.

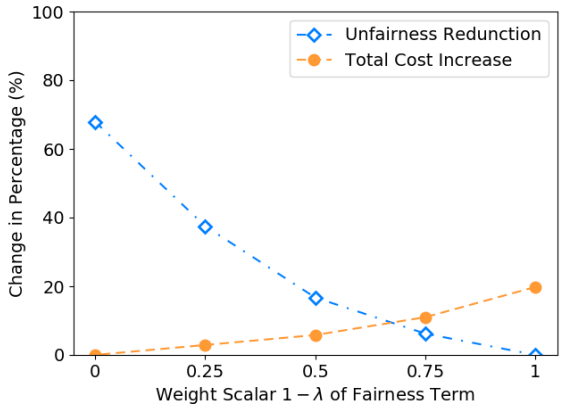

Figure 4.5: Trade-off between Fairness and Efficiency

4.5.2 Case Study on a Real-World Network

Experimental Design and Setup We consider 13 airports within 50 miles from Seattle-Tacoma International Airport (KSEA), where their airport codes are denoted as the location of vertiports. The connectivity of vertiports is shown in Figure 4.6. The airspace above each vertiport is considered an intersection point of different routes. For example, two possible routes for OD pair (KSEA, KSHN) are: (Route 1) KSEA $\rightarrow$ 2S1 $\rightarrow$ KSHN, (Route 2) KSEA $\rightarrow$ KTIW $\rightarrow$ KSHN. Aircraft assigned to these routes will enter the airspace above KSEA, 2S1, KTIW, and KSHN, considered the bottleneck points on these routes. Note that we use the same name to represent the airspace. We let the time horizon $|\mathcal{T}|$ be 60 and a single unit of time be equal to 2 minutes, that is, the planning horizon is 2 hours in total. Travel time needed between 2 nodes in the free-condition airspace is set equal to the Euclidean distance divided by the travel speed 4 miles per time unit and rounded up to the nearest integer, i.e., travel time between KBFI and KSEA (the Euclidean distance is 5.6 miles) is 2 units of time. We consider $|\mathcal{L}| = 3$ service providers, each with a different number of aircraft and having different aircraft with capacity varying from $\boldsymbol{m} \in \{3, 4, 5\}$. Each service provider corresponds to 10 OD pairs, and all 25 OD pairs are covered by at least one service provider.

If an OD pair is operated by more than one service provider, the demand is assigned evenly to each service provider. The aircraft relocation cost $\boldsymbol{q}$ is selected from $\{0, 1, 2\}$ with equal probability. The assignment cost $\boldsymbol{c}$ is set to be equal to the travel time in a free condition multiplied by the unit cost 0.5 per time unit. The ground delay cost $\boldsymbol{\alpha}$ is set to 1, and airborne delay cost $\boldsymbol{\beta}$ is set to 3 per unit of time. The penalty cost $\boldsymbol{s}$ is 20 per unsatisfied passenger. We make this assumption because one commonly used air-ground delay cost ratio in the literature is 3 (Mukherjee and Hansen [74]). We set the weighted parameter $\lambda = 0.5$ to balance the fairness and the efficiency, and risk parameter $\varepsilon = 0.1$ to hedge against the risk. We also use results from the model without fairness ($\lambda = 0, \varepsilon = 0.1$) and the risk-neutral model ($\lambda = 0.5, \varepsilon = 1$) for comparison.

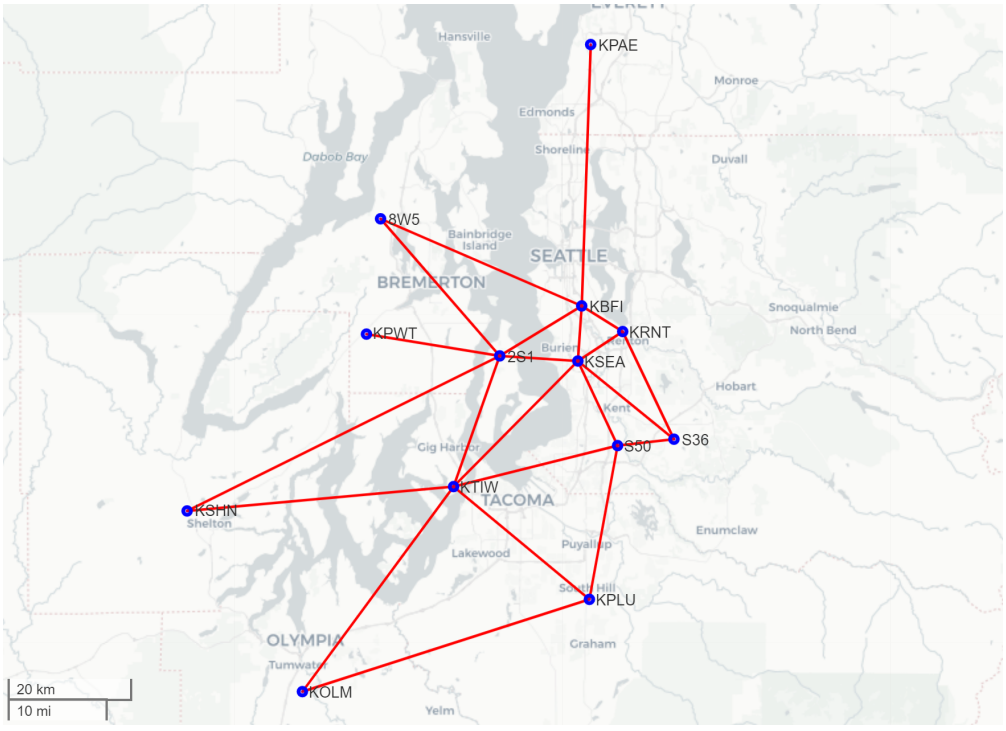

Figure 4.6: Map of 13 airports within 50 miles from KSEA

Data Input The airspace capacity of each bottleneck point was generated based on the Doppler radar map on Nov 14th, 2021, from 6 PM to 8 PM. The full capacity is set to 3

aircraft per time unit when the color is gray on the map for corresponding vertiport locations. The reduced capacity is set to 2 or 1 aircraft per time unit when the color becomes blue or green, respectively. To model the uncertain parameters, we shifted the timeline by 5 units for each scenario and applied a truncated Gaussian distribution $\mathcal{N}(0, 0.5)$ rounded to the nearest integer to generate the airspace capacity of each bottleneck point.

The passenger demand was generated based on population and airport operations data. We first collected the total population data in the corresponding area having the same zipcode for each vertiport then multiplied them by 0.02%, assuming that 0.02% of the population plan to travel during the planning horizon. We also collected the average transient general aviation operation data for each vertiport, and multiplied them by 0.02 to represent the travel needs of people not living in the corresponding area. We let the sum of these two numbers for each vertiport to represent the total passenger demand of all the OD pairs that depart from the same vertiports. For a given origin vertiport, its destination vertiports are the nearest two vertiports at least 30 miles away and within 50 miles. (An origin vertiport may have only one destination vertiport, i.e., KTIW has only one destination.) We then assigned the total passenger demand to OD pairs evenly and rounded them up to the nearest integers. For example, KSEA has two destination vertiports, KPAE (31.6 miles) and KSHN (41.9 miles). Each OD pair has a passenger demand of 13 since the total passenger demand at KSEA is 25. To model the future uncertainty, we applied a truncated Gaussian distribution $\mathcal{N}(0, 2)$ rounded to the nearest nonnegative integer to the passenger demand of each OD pair. In our numerical study, we generated 10 scenarios for this problem.

Numerical Results We ran Algorithm 5 to solve all the cases in this subsection and display the results in Table 4.2, where "Max" denotes the largest average company cost, "Ave.G" denotes the average company ground delay among different scenarios, "Ave.A"

denotes the average company airborne delay, and "Ave.S" denotes the average unsatisfied passenger demand. "Num. of Aircraft" denotes the number of aircraft of each service provider, which corresponds to the planning horizon. The computational time of all the cases is less than an hour. It is seen that increasing the number of aircraft can decrease the unsatisfied passenger demand and optimal value. And all three models yield the same unsatisfied passenger demand. This is probably because satisfying the passenger demand is prioritized in all models. Although the ratio of the cost of airborne delay and ground delay is not large, airborne delay tends to be close to zero and ground delay is always larger than zero. This is not surprising, since when the delay cannot be avoided, it is better to hold aircraft on the ground instead of letting them wait in the air. Compared to the model without fairness, the model with fairness can decrease the highest company operation cost by about 10% with a 2% increase in the optimal value. Notice that, in the fair and risk-averse model, due to fairness enforcement among different UAM service providers, those service providers with nonzero unsatisfied passenger demand are assigned to have a smaller ground delay. However, in the model without fairness, due to the lack of the fairness term, a service provider with nonzero unsatisfied passenger demand may be assigned to a large ground delay, which leads to a larger company operation cost. Furthermore, the largest ground delay in the fair and risk-averse model is always higher than that from the model without fairness. Compared to the result from the risk-neutral model, the risk-averse one yield a small increase of 5% in the total operation cost and the largest company operation cost since it is optimizing the worst scenario performance instead of average performance over all the scenarios. To further demonstrate the robustness of solutions from the two models, following the same procedure in Section 4.5.1, we generated 5 new scenarios and applied a truncated Gaussian noise to passenger demand. The result is shown in Figure 4.7, which shows that, the total operation cost increases and the risk-averse one tends to be more robust when the passenger demand increases.

Table 4.2: Results of Case Study on A Real-World Network

Case	Num. of Aircraft	Fair and Risk Averse					Without Fairness					Risk Neutral				
		Total	Company Cost				Total	Company Cost				Total	Company Cost			
			Max	Ave.G	Ave.A	Ave.S		Max	Ave.G	Ave.A	Ave.S		Max	Ave.G	Ave.A	Ave.S
1	(10,10,10)	40.4	14.6	(16,4,5)	(0,0,0)	(5,6,4)	39.7	15.8	(4,18,2)	(0,0,0)	(5,6,4)	38.3	14.2	(13,4,4)	(0,0,0)	(5,6,4)
2	(15,15,15)	17.1	6.7	(15,25,17)	(0,0,0)	(4,0,0)	16.7	7.3	(27,13,15)	(0,0,0)	(4,0,0)	16.5	6.4	(15,22,16)	(0,0,0)	(4,0,0)
3	(18,15,12)	12.5	4.2	(24,23,8)	(0,0,0)	(0,0,2)	12.2	4.9	(10,25,17)	(0,0,0)	(0,0,2)	11.9	4.1	(21,20,8)	(0,0,0)	(0,0,2)

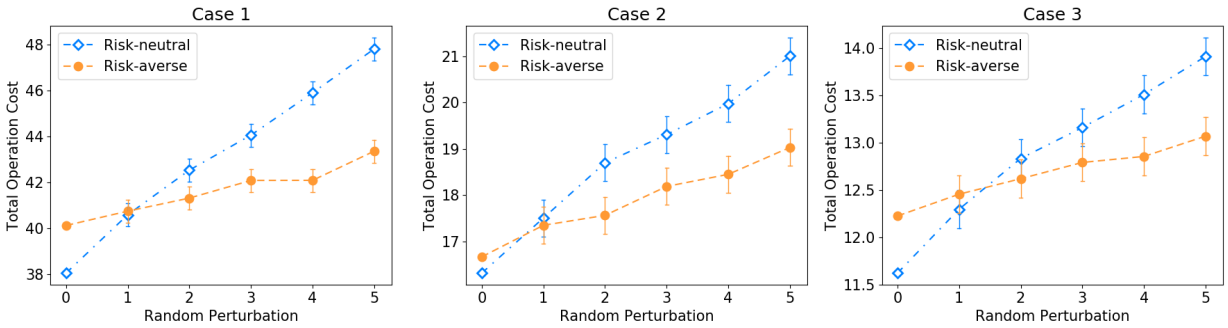

Figure 4.7: Evaluation of Total Operation Cost when Passenger Demand Increases

Managerial Insight FairUAM can provide the UAM traffic manager with an optimal UAM aircraft resource allocation plan and delay assignment without perfect information, achieving both company-level fairness and system-level efficiency. The framework accounts for the existence of uncertainties in weather information and demand fluctuation. Besides generating an optimal operation plan, our framework can also provide extra support for the UAM traffic manager to identify the busy bottleneck points, which are usually regarded as the system hotspots. With such information, UAM service providers are capable of better designing their routes in the aircraft path-planning stage before filing the flight plan to the UAM traffic manager in the future. UAM service providers can consider more candidate routes or even take detours to avoid busy bottleneck points and possible future congestion. In addition, identification of the current system hotspots can also be valuable when the UAM network is still in the blueprint or can improve the existing UAM network. Instead of improving the capability of all the bottleneck points, which is quite expensive, focusing on the busiest bottleneck points is more effective in a mature UAM operating environment

with high-density aircraft. In this case, we would like to evaluate the utilization rate of bottleneck points. The higher the utilization rate is, the busier the corresponding bottleneck point should be.

Suppose in time horizon $\mathcal{T}$, the time point that the last aircraft landing at its destination vertiport is

$$t_0 = \arg\min_{t'} \left\{ t' : \sum_{t>t', t\in\mathcal{T}} tB_{it}^k(\boldsymbol{\xi}) = 0, \forall k \in \mathcal{K} \right\}.$$

We consider the utilization rate of the bottleneck point $k \in \mathcal{K}$ between time 0 and t_0 as the ratio of the actual number of aircraft passing the bottleneck point divided by the total number of aircraft it can handle during this period, which can be represented as

$$UR_k = \frac{\sum_{t\in\mathcal{T}_0} \sum_{\ell\in\mathcal{L}} \sum_{i\in\mathcal{I}_\ell} B_{it}^k(\boldsymbol{\xi})}{\sum_{t\in\mathcal{T}_0} C_t^k}$$

where $\mathcal{T}_0 = \{0, \ldots, t_0\}$. The results are displayed in Table 4.3. We see that KSEA, KBFI, 2S1, and KTIW are the busiest bottleneck points with the highest utilization rate. This may be because these bottleneck points are located around the center of the network, and many routes pass those bottleneck points more often compared to others. When we numerically increase the total airspace capacity $\sum_{t\in\mathcal{T}_0} C_t^k$ of those bottleneck points by 10% in Case 1, we find that the optimal value can be reduced by 5%. Note that the results of Cases 2 and 3 are similar. This implies that if the traffic manager would like to further reduce total congestion or operation cost, it is a good idea to focus on these four bottleneck points. Enlarging the capability of these four bottleneck points can benefit the whole network. Note that the capacity of the system hotspots can be increased by introducing promising advanced aircraft separation assurance technologies and aircraft onboard automation (see, e.g., Kochenderfer et al. [125], Brittain et al. [126]). We further illustrated how the total operation cost and the fairness change while increasing the total capacity of these four bottleneck points, as shown

in Figure 4.8. The fairness score is defined as the ratio of the smallest average company cost to the largest average company cost such that 1 is completely fair and 0 is completely unfair. It is shown that the total operation cost decreases when the total capacity increases since the congestion level can be reduced. However, when the total capacity of these four bottleneck points is increased by over 15%, the objective value tends to stay at a similar value since the system hotspots transfer to other bottleneck points.

On the other hand, changing the number of bottleneck points on a route when designing the routes, i.e., taking a detour to avoid visiting busy airspace, can also decrease the delay. We demonstrate the impact on the total operation cost and the largest company average operation cost when some routes are redesigned to avoid busy bottleneck points (KSEA, KBFI, 2S1, KTIW) using Case 1, which is shown in Figure 4.8. We can see that the total operation cost can be reduced, while the fairness almost stays the same. This suggests that to achieve the best efficiency, it may not have to sacrifice fairness between UAM service providers. The overall efficiency can also be improved with better network and route design to obtain a win-win situation.

Table 4.3: Airspace Utilization Rate

Case	KSEA	KRNT	KBFI	2S1	S50	S36	KTIW	KPWT	KPLU	8W5	KPAE	KSHN	KOLM
1	0.33	0.14	0.25	0.31	0.17	0.08	0.25	0.11	0.19	0.17	0.11	0.31	0.17
2	0.50	0.20	0.40	0.40	0.25	0.10	0.50	0.15	0.30	0.30	0.15	0.35	0.25
3	0.55	0.25	0.50	0.60	0.30	0.15	0.45	0.15	0.35	0.30	0.20	0.20	0.25

In our FairUAM framework, a better input (e.g., more accurate weather prediction) leads to a better operation plan and less computational effort. Following the same procedure in applying the random Gaussian perturbation to airspace capacity, we demonstrate the impact of the accuracy of airspace capacity on the total operation cost and the largest average company operation cost using Case 1 as shown in Figure 4.9. We notice that by increasing the fluctuation in airspace capacity, the total operation cost increases. This raises

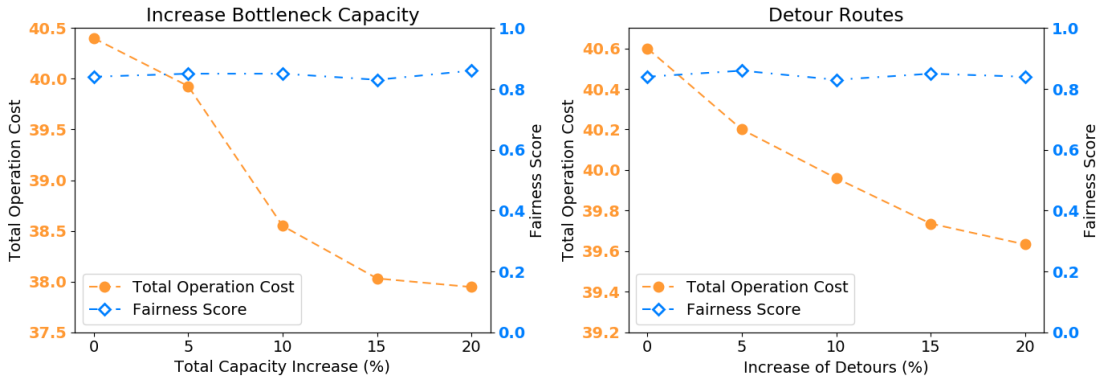

Figure 4.8: Impact on Total Operation Cost and Fairness while Increasing Total Capacity of Busy Bottleneck Points (KSEA, KBFI, 2S1, KTIW) or Taking Detours to Avoid Them

the requirement for a better weather forecast or even an online weather report for each bottleneck point. For the passenger aspect, since changes in passenger demand result in an extra computational effort or sometimes unsatisfied demand, instead of only focusing on launching the service or developing the technology, it is also important for the service providers to understand their passengers and incentivize the passengers for higher service satisfaction.

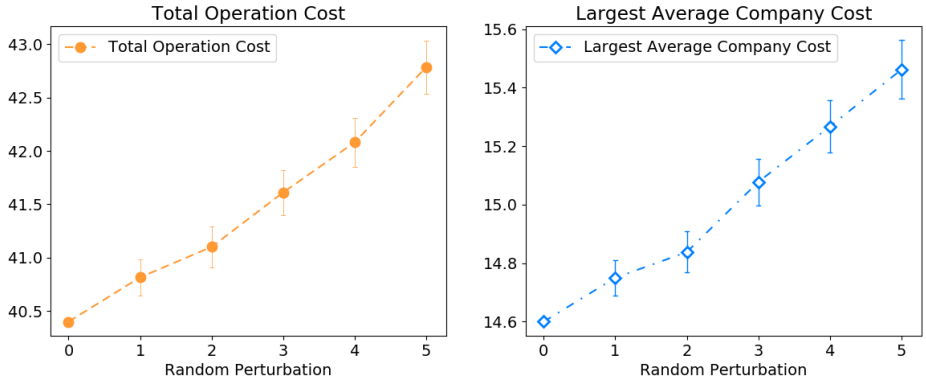

Figure 4.9: Evaluation of Total Operation Cost and Largest Average Company Cost when Airspace Capacity Changes

4.6 Conclusion

In this chapter, we study the FairUAM, which is proven to be NP-hard in a deterministic setting and NP-hard with a given route and OD pair assignment. To simplify FairUAM, we derive monotonicity properties and relax the integrality of some decision variables. To further improve the MILP formulation, we propose valid inequalities by exploring the model structures. We develop a decomposition-based algorithm to solve FairUAM. Finally, we generate random instances to demonstrate the effectiveness of the proposed method to apply it to a real-world network in Seattle. Compared to the risk-neutral model and the model without fairness consideration, FairUAM is more robust when the passenger demand or weather forecasting is subject to error and can fairly assign the aircraft and delay at the company-level. Aircraft-level fairness can also be included in FairUAM with a simple modification to the fairness term. For the managerial aspect, FairUAM not only generates the optimal operation plan but also detects the system hotspots by finding the busy bottleneck points. This information provides UAM service providers extra support for better route planning. It also provides some guidance in future UAM network design. For our future work, we would like to include network design and rerouting into consideration. The FairUAM framework can also be generalized to other resource allocation problems under demand and capacity uncertainties. For example, we can extend our framework to robot task allocation with demand and capacity uncertainties in the warehouse. We can also generalize the framework to fair vehicle allocation in disaster evacuation to minimize travel time.

Chapter 5

Fair Constrained Markovian Decision Processes Problems

5.1 Introduction

For decision-making processes under uncertainty, Markov decision processes (MDPs) have been widely used to account for current decisions and their future effects in stochastic environments (Puterman [42]). Although MDPs are considered to be proficient in optimizing longer-term goals, the absence of constraints severely impairs their practical applicability. To address this issue, constrained MDPs (CMDPs) have been proposed to find the optimal decision policy by incorporating real-world limitations into the decision-making processes. CMDPs have been proven to be highly effective in situations in the presence of hard constraints. They have been successfully applied to various domains, including infrastructure maintenance (Hu et al. [53], Durango-Cohen and Sarutipand [127]), healthcare decisions (Chen et al. [47], Ayvaci et al. [128]), path planning (Ding et al. [129], Allamaraju et al. [130]), finance (Bäuerle and Rieder [131], Ohlmann and Bean [132]), manufacturing (Ahiska and Kurtul [133], Sun and Li [134]), production (Xiang et al. [135], Ohno et al. [136]), communication (Ding et al. [137], Alsheikh et al. [138]), power system (Byon and Ding [139], Grillo et al. [140]) and so on.

Despite the broad applicability and versatility of CMDPs in providing high-quality solutions

for constrained problems across various fields, persistent concerns about individual fairness arise when optimizing the overall objective involving multiple parties. In this context, Fair CMDPs are particularly relevant, as decision-makers must consider not only the optimization of the overall outcome but also the preservation of fairness, among different parties, which, unfortunately, adds another layer of complexity to the decision-making process. Although some researchers have made progress towards incorporating long-term fairness as an extra constraint or objective component in MDPs (Wen et al. [58], Liu et al. [141], Hu and Chen [142], Hu and Zhang [143]), works on effectively balancing efficiency and fairness within CMDPs are rather limited. This evident gap emphasizes the pressing need for a more comprehensive approach that can integrate efficiency and fairness into the CMDPs framework. This motivates us to study the Fair Budget-Constrained Markov Decision Processes (FCMDP) problems which balance the overall efficiency and individual fairness subject to budget constraint.

5.1.1 Summary of Main Contributions

This chapter investigates Fair Budget-Constrained Markov Decision Processes (FCMDP) as a general mechanism to allocate limited resources among multiple agents. This allocation strategy is designed to achieve a balance between overall efficiency and individual fairness. The principal goal of the FCMDP is to establish the optimal policy for agents across the decision horizon, with a focus on minimizing the weighted sum of total cost and the highest user cost among agents. The key contributions of our FCMDP are summarized below:

(i) We develop a Mixed Integer Linear Programming (MILP) formulation for the FCMDP under a finite horizon and prove its NP-hardness, even under a single horizon. This complexity motivates us to develop effective solution methods to solve the FCMDP.

(ii) We prove that the continuous relaxation of the MILP is equivalent to the optimal Lagrangian dual.

(iii) We extend our model to consider FCMDP under the infinite horizon and develop the MILP to accommodate this extension.

(iv) We propose approximation algorithms to solve FCMDP under both finite and infinite horizons.

(v) We apply our proposed solution approaches to a real-world infrastructure maintenance problem, with data from the state of North Carolina to illustrate their managerial insights and algorithmic effectiveness.

The remainder of this chapter is organized as follows. In Section 5.2, we propose the model formulation for FCMDP and prove its NP-hardness. In Section 5.3, we derive an equivalent MILP formulation and demonstrate the equivalence between the continuous relaxation of MILP and the Lagrangian dual of the FCMDP. Section 5.4 presents the solution algorithms and Section 5.5 extends FCMDP to infinity horizon. Section 5.6 numerically demonstrates that highlight the effectiveness of our proposed formulation and algorithms. Finally, Section 5.7 concludes this chapter.

5.2 Fair Budget-Constrained MDP under a Finite Horizon

In this section, we will study a fair budget-constrained MDP (FCMDP) within a finite horizon. We first introduce the model formulation and show the NP-hardness of it. We then propose an MILP formulation for this problem.

5.2.1 Model Formulation

Let us consider a finite-horizon FCMDP involved with multiple agents. Let us use set $\mathcal{T}$ to denote the time horizon, i.e., $\mathcal{T} = \{1, 2, ..., T\}$. There are K agents involved in this decision process, i.e., we let set $\mathcal{K} := \{1, \ldots, K\}$ denote the corresponding agents. Each agent $k \in \mathcal{K}$ can be at a state $s \in \mathcal{S}_k$ where a finite set $\mathcal{S}_k$ represents all the possible states. The initial condition of an agent $k \in \mathcal{K}$ is specified by h_k, where $\sum_{s\in\mathcal{S}_k} h_k(s) = 1$. We would like to select an action $a \in \mathcal{A}_k$ from a finite set $\mathcal{A}_k$ for each agent $k \in \mathcal{K}$ at each state. For the agent $k \in \mathcal{K}$ at time $t \in \mathcal{T}$, the agency cost incurred by action $a \in \mathcal{A}_k$ is $C^t_{k,a}$, and the one period user cost with state $s \in \mathcal{S}_k$ is $U^t_{k,s}$; while $P^t_{k,a}(s, s')$ denotes the probability from state s to a new state s' under action $a \in \mathcal{A}_k$. At each time $t \in \mathcal{T}$, the expected total agency cost is limited to a certain budget level B^t. We also suppose the future cost is discounted at rate $\alpha \in (0, 1]$. For notational convenience, we let $\boldsymbol{U}^t_k = \left\{U^t_{k,s}\right\}_{s\in\mathcal{S}_k}$, $\boldsymbol{C}^t_k = \left\{C^t_{k,a}\right\}_{a\in\mathcal{A}_k}$ for each $k \in \mathcal{K}, t \in \mathcal{T}$.

For the agent $k \in \mathcal{K}$ at time $t \in \mathcal{T}$, we let $\delta^t_{k,s} \in \mathcal{A}_k$ denote its action to be taken at state $s \in \mathcal{S}_k$. For simplicity, we let $\boldsymbol{\delta}^t_k := \{\delta^t_{k,s}\}_{s\in\mathcal{S}_k}$ for each $k \in \mathcal{K}, t \in \mathcal{T}$, $\boldsymbol{\delta}^t := \{\boldsymbol{\delta}^t_k\}_{k\in\mathcal{K}}$ for each $t \in \mathcal{T}$, and let $\boldsymbol{\pi} = \{\boldsymbol{\delta}^t\}_{t\in\mathcal{T}}$ denote a policy. For the agent $k \in \mathcal{K}$ at time $t \in \mathcal{T}$, we let $\boldsymbol{P}^t_{k,\boldsymbol{\delta}^t_k}$ denote its transition matrix given that at each state $s \in \mathcal{S}_k$, the agent k will choose action $\delta^t_{k,s}$. Hence, for a given policy $\boldsymbol{\pi}$, we let $h^\top_k \boldsymbol{P}^t_{k,\boldsymbol{\pi}} = h^\top_k \boldsymbol{P}^1_{k,\boldsymbol{\delta}^1_k} \boldsymbol{P}^2_{k,\boldsymbol{\delta}^2_k} \cdots \boldsymbol{P}^t_{k,\boldsymbol{\delta}^t_k}$ denote the probability distribution of agent $k \in \mathcal{K}$'s states at time $t \in \mathcal{T}$. We let $\bar{\Pi}$ denote the set of all the possible (including those feasible and infeasible to the budget constraints) policies, and its subset $\Pi \subseteq \bar{\Pi}$, which denotes all the possible feasible policies by imposing a budget constraint at each time period, i.e.,

$$\Pi = \left\{ \boldsymbol{\pi} \in \bar{\Pi} : \sum_{k\in\mathcal{K}} h^\top_k \boldsymbol{P}^t_{k,\boldsymbol{\pi}} \boldsymbol{C}^t_k \leq B^t, \forall t \in \mathcal{T} \right\}. \tag{5.1}$$

The objective of FCMDP is to choose the best policy $\boldsymbol{\pi} = \{\boldsymbol{\delta}^t\}_{t\in\mathcal{T}}$ which optimizes the efficiency and the fairness at the same time, i.e., minimizing the weighted sum of total expected user cost and the largest expected user cost for agents. We introduce a weighted scalar ρ to balance the trade-off between efficiency and fairness. We assume that the agency cost is applied at the beginning of each year while user cost is evaluated at the end of each year. Thus, under this setting, FCMDP is formulated as below:

$$v^* = \min_{\boldsymbol{\pi}\in\Pi} \rho \sum_{k\in\mathcal{K}} \sum_{t\in\mathcal{T}} \alpha^t h_k^\top \boldsymbol{P}_{k,\boldsymbol{\pi}}^t \boldsymbol{U}_k^t + (1-\rho) \max_{k\in\mathcal{K}} \sum_{t\in\mathcal{T}} \alpha^t h_k^\top \boldsymbol{P}_{k,\boldsymbol{\pi}}^t \boldsymbol{U}_k^t. \tag{5.2}$$

We note that formulation (5.2) is NP-hard even if $\rho = 1, T = 1, |S_k| = 2, |\mathcal{A}_k| = 2$ for each $k \in \mathcal{K}$.

Proposition 5.1. *Solving FCMDP is, in general, NP-hard.*

Proof: Let us first consider the NP-hard problem - optimization over knapsack constraint which asks

(optimization over knapsack constraint) Given n items with weight w_i and value v_i for each $i \in [n]$, what is the maximum profit if at most W weight of items should be picked?

The knapsack problem can be formulated as below:

$$\max_{\boldsymbol{x}\in\{0,1\}^n} \left\{ \sum_{i\in[n]} v_i x_i : \sum_{i\in[n]} w_i x_i \le W \right\}. \tag{5.3}$$

Next, we will construct a special case of formulation (5.2) as below: suppose $T = 1, \alpha = 1, K = n, B^1 = W, \rho = 1$ and for each $k \in \mathcal{K}$, we have $S_k = \{0, 1\}, \mathcal{A}_k = \{0, 1\}, h_k(s) = 0.5$

for each $s \in \mathcal{S}_k$ and

$$U^1_{k,s} = \begin{cases} 2v_k & \text{if } s = 1 \\ 0 & \text{if } s = 0 \end{cases}, \quad C^1_{k,a} = \begin{cases} 2w_k & \text{if } a = 1 \\ 0 & \text{if } a = 0 \end{cases}$$

and the transition probability is

$$P_{k,a}(s, s') = \begin{cases} 1 & \text{if } a = s = s' \\ 0 & \text{otherwise} \end{cases}$$

for each $a \in \mathcal{A}_k, s \in \mathcal{S}_k, s' \in \mathcal{S}_k$. Therefore, under this setting, formulation (5.2) is exactly equivalent to formulation (5.3), which is an NP-hard problem. □

This result suggests that there might not exist an efficient polynomial algorithm to solve FCMDP (5.2). Therefore, in the next sections, we focus on developing exact and approximate algorithms to solve it.

5.2.2 An MILP Formulation

In this subsection, we will derive a MIP formulation for formulation (5.2). To begin with, let us define the decision variables as follows. For each time $t \in \mathcal{T}$, $z^t_{k,a,s} = 1$ if the action a is accessible in state s for agent k; 0, otherwise. For each agent $k \in \mathcal{K}$, suppose that variable $x^t_{k,s}$ denotes its probability to stay at state $s \in \mathcal{S}_k$ at time $t \in \mathcal{T}$. For notationally convenience, we let $x^0_{k,s} = h_k(s)$ for each $k \in \mathcal{K}$ and $s \in \mathcal{S}_k$, and let $\mathbf{z}^t := \{z^t_{k,a,s}\}_{k,a,s}, \mathbf{x}^t := \{x^t_{k,s}\}_{k,s}$ and $\mathbf{x} = \{\mathbf{x}^t\}_{t\in\mathcal{T}}, \mathbf{z} = \{\mathbf{z}^t\}_{t\in\mathcal{T}}$.

With these notations, FCMDP (5.2) is equivalent to the following mixed integer nonconvex

program

$$v^* = \min_{\mathbf{x},\mathbf{z}} \quad \rho \sum_{k\in\mathcal{K}} \sum_{t\in\mathcal{T}} \sum_{s\in\mathcal{S}} \alpha^t U^t_{k,s} x^t_{k,s} + (1-\rho) \max_{k\in\mathcal{K}} \sum_{t\in\mathcal{T}} \sum_{s\in\mathcal{S}} \alpha^t U^t_{k,s} x^t_{k,s}, \tag{5.4a}$$

$$\text{s.t.} \quad \sum_{s\in\mathcal{S}_k} \sum_{a\in\mathcal{A}_k} x^{t-1}_{k,s} P^t_{k,a}(s,s') z^t_{k,a,s} = x^t_{k,s'}, \forall s' \in \mathcal{S}_k, k \in \mathcal{K}, t \in \mathcal{T}, \tag{5.4b}$$

$$\sum_{k\in\mathcal{K}} \sum_{s\in\mathcal{S}_k} \sum_{a\in\mathcal{A}_k} x^{t-1}_{k,s} z^t_{k,a,s} C^t_{k,a} \leq B_t, \forall t \in \mathcal{T}, \tag{5.4c}$$

$$\sum_{a\in\mathcal{A}_k} z^t_{k,a,s} = 1, \forall k \in \mathcal{K}, s \in \mathcal{S}_k, t \in \mathcal{T}, \tag{5.4d}$$

$$x^0_{k,s} = h_k(s), \forall s \in \mathcal{S}_k, k \in \mathcal{K}, \tag{5.4e}$$

$$0 \leq x^t_{k,s} \leq 1, \forall k \in \mathcal{K}, s \in \mathcal{S}_k, t \in \mathcal{T}, \tag{5.4f}$$

$$z^t_{k,a,s} \in \{0,1\}, \forall k \in \mathcal{K}, s \in \mathcal{S}_k, a \in \mathcal{A}_k, t \in \mathcal{T}, \tag{5.4g}$$

where constraints (5.4b) enforce the transition conditions for the probability distribution at current stage $t \in \mathcal{T}$, constraints (5.4c) represent the budget constraints for user costs, constraints (5.4d) demonstrate that at each time $t \in \mathcal{T}$, only one action can be chosen for a particular state s and agent k, constraints (5.4e) ensure the initial conditions, constraints (5.4f) and (5.4g) define the boundaries of decision variables.

5.3 Linearization and Relaxation Schemes

In this section, we study different relaxation schemes and their corresponding mathematical programs to solve formulation (5.2) and linearize the nonlinear terms in formulation (5.4).

5.3.1 Continuous Relaxation

First of all, we relax the deterministic policy into randomized policy, i.e., at each time t, each agent $k \in \mathcal{K}$ with its state $s \in \mathcal{S}_k$ could choose a subset of actions with respect to a probability distribution. We show that formulation (5.2) is equivalent to a linear program formulation. In fact, for each $t \in \mathcal{T}$, we relax the integrality of $z^t_{k,a,s}$ to be the proportion that action a is accessible in state s for agent k.

$$v^{\mathrm{R}} = \min_{\mathbf{x},\mathbf{z}} \quad \rho \sum_{k\in\mathcal{K}} \sum_{t\in\mathcal{T}} \sum_{s\in\mathcal{S}} \alpha^t U^t_{k,s} x^t_{k,s} + (1-\rho) \max_{k\in\mathcal{K}} \sum_{t\in\mathcal{T}} \sum_{s\in\mathcal{S}} \alpha^t U^t_{k,s} x^t_{k,s}, \tag{5.5a}$$

$$\text{s.t.} \quad 0 \le z^t_{k,a,s} \le 1, \forall k \in \mathcal{K}, s \in \mathcal{S}_k, a \in \mathcal{A}_k, t \in \mathcal{T}, \tag{5.5b}$$

$$(5.4\text{b}) - (5.4\text{f}).$$

Note that formulation (5.5) is a nonlinear program due to the bilinear terms in formulation (5.4b) and formulation (5.4c). However, we can reformulate it as a linear program (LP) by variable substitution. Let us define $y^t_{k,a,s} = x^{t-1}_{k,s} z^t_{k,a,s}$, $\mathbf{y}^t := \{y^t_{k,a,s}\}_{k,a,s}$ and $\mathbf{y} = \{\mathbf{y}^t\}_{t\in\mathcal{T}}$ with additional constraints

$$\sum_{a\in\mathcal{A}_k} y^t_{k,a,s} = x^{t-1}_{k,s}, \forall k \in \mathcal{K}, s \in \mathcal{S}_k, t \in \mathcal{T}. \tag{5.6}$$

By replacing variables $\{\mathbf{z}^t\}_{t\in\mathcal{T}}$ with $\{\mathbf{y}^t\}_{t\in\mathcal{T}}$, we can rewrite formulation (5.5):

$$v^{\mathrm{LP}} = \min_{\mathbf{x},\mathbf{y}} \quad \rho \sum_{k\in\mathcal{K}} \sum_{t\in\mathcal{T}} \sum_{s\in\mathcal{S}} \alpha^t U^t_{k,s} x^t_{k,s} + (1-\rho) \max_{k\in\mathcal{K}} \sum_{t\in\mathcal{T}} \sum_{s\in\mathcal{S}} \alpha^t U^t_{k,s} x^t_{k,s}, , \tag{5.7a}$$

$$\text{s.t.} \quad \sum_{s\in\mathcal{S}_k} \sum_{a\in\mathcal{A}_k} P^t_{k,a}(s,s') y^t_{k,a,s} = x^t_{k,s'}, \forall s' \in \mathcal{S}_k, k \in \mathcal{K}, t \in \mathcal{T}, \tag{5.7b}$$

$$\sum_{k\in\mathcal{K}}\sum_{s\in\mathcal{S}_k}\sum_{a\in\mathcal{A}_k} y^t_{k,a,s}C^t_{k,a} \le B_t, \forall t\in\mathcal{T}, \tag{5.7c}$$

$$\sum_{s\in\mathcal{S}_k}\sum_{a\in\mathcal{A}_k} y^t_{k,a,s} = 1, \forall k\in\mathcal{K}, t\in\mathcal{T}, \tag{5.7d}$$

$$0 \le y^t_{k,a,s} \le 1, \forall k\in\mathcal{K}, s\in\mathcal{S}_k, a\in\mathcal{A}_k, t\in\mathcal{T}, \tag{5.7e}$$

(5.4e), (5.4f), (5.6),

where constraints (5.7b)-(5.7e) corresponds to constraints (5.4b)-(5.4d), (5.4g), respectively. Note that we can linearize the piecewise maximum in the objective function (5.7a) with epigraphical variable.

Indeed, we can show that formulations (5.7) and (5.5) yield the same optimal value.

Theorem 5.2. *Formulation* (5.7) *is equivalent to formulation* (5.5)*, i.e.* $v^{\mathrm{LP}} = v^{\mathrm{R}}$.

Proof: Let $(\widehat{\mathbf{x}}, \widehat{\mathbf{z}})$ be a feasible solution to formulation (5.5). Define $\widehat{\mathbf{y}}$ as $\widehat{y}^t_{k,a,s} = \widehat{x}^{t-1}_{k,s}\widehat{z}^t_{k,a,s}$ for each $k\in\mathcal{K}, s\in\mathcal{S}_k, a\in\mathcal{A}_k, t\in\mathcal{T}$. Then clearly $(\widehat{\mathbf{x}}, \widehat{\mathbf{y}})$ is feasible to formulation (5.7). Hence, $v^{\mathrm{LP}} \ge v^{\mathrm{R}}$.

On the other hand, suppose $(\widehat{\mathbf{x}}, \widehat{\mathbf{z}})$ is feasible to formulation (5.7). Then define $\widehat{\mathbf{z}}$ as $\widehat{z}^t_{k,a,s} = \frac{\widehat{y}^t_{k,a,s}}{\widehat{x}^{t-1}_{k,s}}$ for each $k\in\mathcal{K}, s\in\mathcal{S}_k, a\in\mathcal{A}_k, t\in\mathcal{T}$, where by convention, we let $0\cdot\infty = 0$. Then we see that $(\widehat{\mathbf{x}}, \widehat{\mathbf{z}})$ satisfy all the constraints in formulation (5.5), i.e. $(\widehat{\mathbf{x}}, \widehat{\mathbf{z}})$ is feasible to formulation (5.5). Hence, $v^{\mathrm{LP}} \le v^{\mathrm{R}}$. □

By the fact that $\{\mathbf{z}^t\}_{t\in\mathcal{T}}$ are binary variables, we can introduce new variables to represent these bilinear terms and use McCormick inequalities (McCormick [109]) to linearize them . Recall that $y^t_{k,a,s} = x^{t-1}_{k,s}z^t_{k,a,s}$ and $\mathbf{y}^t = \{y^t_{k,a,s}\}_{k,a,s}$, which can be linearized as

$$0 \le y^t_{k,a,s} \le x^{t-1}_{k,s},\ y^t_{k,a,s} \le z^t_{k,a,s},\ y^t_{k,a,s} \ge z^t_{k,a,s} - 1 + x^{t-1}_{k,s}, \forall k\in\mathcal{K}, s\in\mathcal{S}_k, a\in\mathcal{A}_k, t\in\mathcal{T}. \tag{5.8}$$

We further introduce an epigraph variable E and fairness constraints for the fairness part in formulation (5.4a) to linearize the maximum operator such that

$$\sum_{t\in\mathcal{T}}\sum_{s\in\mathcal{S}}\alpha^t U^t_{k,s}x^t_{k,s} \leq E, \forall k \in \mathcal{K}. \tag{5.9}$$

Then formulation (5.4a) is equivalent to

$$\min_{\mathbf{x},\mathbf{z}} \rho\sum_{k\in\mathcal{K}}\sum_{t\in\mathcal{T}}\sum_{s\in\mathcal{S}}\alpha^t U^t_{k,s}x^t_{k,s} + (1-\rho)E.$$

Note that formulations (5.5a) and (5.7a) can be rewritten in the same way.

Hence, we conclude that

Proposition 5.3. *Formulation* (5.4) *is equivalent to the following mixed integer linear program (MILP):*

$$v^* = \min_{\mathbf{x},\mathbf{z},\mathbf{y}}\Bigg\{\rho\sum_{k\in\mathcal{K}}\sum_{t\in\mathcal{T}}\sum_{s\in\mathcal{S}}\alpha^t U^t_{k,s}x^t_{k,s} + (1-\rho)E : \\ (5.4d)-(5.4g), (5.6), (5.7b)-(5.7e), (5.8), (5.9)\Bigg\}, \tag{5.10}$$

However, formulation (5.10) can be challenging to solve considering that the number of binary variables can easily scale up and inequalities (5.8) do not help too much. Indeed, let us denote

$$v^{\text{Rel}} = \min_{\mathbf{x},\mathbf{z},\mathbf{y}}\Bigg\{\rho\sum_{k\in\mathcal{K}}\sum_{t\in\mathcal{T}}\sum_{s\in\mathcal{S}}\alpha^t U^t_{k,s}x^t_{k,s} + (1-\rho)E : \\ (5.4d)-(5.4f), (5.5b), (5.6), (5.7b)-(5.7e), (5.8), (5.9)\Bigg\}, \tag{5.11}$$

which relax the integrality of $\{\mathbf{z}^t\}_{t\in\mathcal{T}}$. Then we can show that it does not improve the

continuous relaxation bound v^{R}.

Proposition 5.4. $v^{\mathrm{Rel}} = v^{\mathrm{R}}$.

Proof: Since formulation (5.11) contains all the constraints in formulation (5.7), thus it is sufficient to show that $v^{\mathrm{Rel}} \leq v^{\mathrm{LP}} = v^{\mathrm{R}}$. Let $(\widehat{\mathbf{x}}, \widehat{\mathbf{y}})$ be a feasible solution to formulation (5.7). Let us define $\widehat{\mathbf{z}}$ as $\widehat{z}^t_{k,a,s} = \widehat{y}^t_{k,a,s} / \widehat{x}^{t-1}_{k,s}$ for each $k \in \mathcal{K}, s \in \mathcal{S}_k, a \in \mathcal{A}_k, t \in \mathcal{T}$, where by convention, we let $0 \cdot \infty = 0$.

We only need to show that $(\widehat{\mathbf{x}}, \widehat{\mathbf{z}}), \widehat{\mathbf{y}})$ is feasible to formulation (5.11). Clearly, $(\widehat{\mathbf{x}}, \widehat{\mathbf{z}})$ is feasible to formulations (5.4d) -(5.4f) and (5.5b), and $(\widehat{\mathbf{x}}, \widehat{\mathbf{y}})$ is feasible to formulations (5.6), (5.7b) -(5.7e). By the construction of $\widehat{\mathbf{z}}$, inequalities (5.8) are also satisfied. Thus, $v^{\mathrm{Rel}} \leq v^{\mathrm{LP}} = v^{\mathrm{R}}$. This completes the proof. □

5.3.2 Lagrangian Relaxation

In this section, we apply the Lagrangian relaxation approach to solve formulation (5.2). We relax the budget constraints in formulation (5.2) with Lagrangian multipliers $\boldsymbol{\lambda} := \{\alpha^t \lambda^t\}$ and fairness constraints with Lagrangian multipliers $\boldsymbol{\mu} := \{\mu^k\}$. Thus, the relaxed MDP is

$$\begin{aligned} v^{\mathrm{LR}} = \sup_{\boldsymbol{\lambda}, \boldsymbol{\mu}} L(\boldsymbol{\lambda}, \boldsymbol{\mu}) := \min_{\boldsymbol{\pi} \in \bar{\Pi}} \quad & \sum_{k \in \mathcal{K}} h_k^\top \sum_{t \in \mathcal{T}} \alpha^t \boldsymbol{P}^t_{k,\boldsymbol{\pi}} \left((\rho + \mu^k) \boldsymbol{U}^t_k + \lambda^t \boldsymbol{C}^t_{k,\boldsymbol{\pi}} \right) \\ & + E \left(1 - \rho - \sum_{k \in \mathcal{K}} \mu^k \right) - \sum_{t \in \mathcal{T}} B^t \alpha^t \lambda^t, \end{aligned} \tag{5.12}$$

Since E is arbitrary, we can let

$$1 - \rho - \sum_{k \in \mathcal{K}} \mu^k = 0. \tag{5.13}$$

Then formulation (5.12) can be rewritten as

$$v^{\mathrm{LR}} = \sup_{\boldsymbol{\lambda},\boldsymbol{\mu}:(5.13)} -\sum_{t\in\mathcal{T}} B^t\alpha^t\lambda^t + \sum_{k\in\mathcal{K}} L_k(\boldsymbol{\lambda},\boldsymbol{\mu}) := \min_{\boldsymbol{\pi}_k\in\bar{\Pi}_k} h_k^\top \sum_{t\in\mathcal{T}} \alpha^t \boldsymbol{P}_{k,\boldsymbol{\pi}}^t \left((\rho+\mu^k)\boldsymbol{U}_k^t + \lambda^t \boldsymbol{C}_{k,\boldsymbol{\pi}}^t\right) \tag{5.14}$$

where that $\bar{\Pi}$ denotes all of possible (including feasible and infeasible) policies without budget constraints and hence can be decomposed across agents (i.e., $\bar{\Pi} = \bar{\Pi}_1 \times \ldots \times \bar{\Pi}_K$). Note that for any given Lagrangian multipliers $\{\boldsymbol{\lambda},\boldsymbol{\mu}\}$, $L_k(\boldsymbol{\lambda},\boldsymbol{\mu})$ can be solved by value iteration or policy iteration for a regular finite horizon MDP. Then we can use the subgradient method to optimize over $\boldsymbol{\lambda}$ and $\boldsymbol{\mu}$. This approach has been studied by Hu et al. [53] for bridge maintenance optimization problems.

It can be shown that the optimal value of the Lagrangian relaxation approach is exactly the same as v^{R}.

Theorem 5.5. $v^{\mathrm{R}} = v^{\mathrm{LR}}$.

Proof: First of all, by standard Lagrangian duality theorem (Wolsey and Nemhauser [144]), we know that $v^{\mathrm{R}} = v^{\mathrm{LP}} \leq v^{\mathrm{LR}}$. Thus, we only need to show that $v^{\mathrm{R}} \geq v^{\mathrm{LR}}$.

Next, we prove the following claim.

Claim 3. Suppose $f : \mathbb{R}^{n_1} \to \mathbb{R}_+$ and $g : \mathbb{R}^{n_2} \to \mathbb{R}_+$ are linear functions. Then, for any two nonempty sets $X \subseteq \mathbb{R}^{n_1}, Y \subseteq \mathbb{R}^{n_2}$, we have $\Phi := \mathrm{conv}\{(x,y,t) : f(x)g(y) \leq t, (x,y) \in X \times Y\} \supseteq \Psi := \{(x,y,t) : f(x)g(y) \leq t, (x,y) \in \mathrm{conv}(X) \times \mathrm{conv}(Y)\}$.

Proof: Let $(\widehat{\boldsymbol{x}},\widehat{\boldsymbol{y}},t) \in \Psi$, then, there exists $\{\bar{\boldsymbol{x}}^{l_1}\} \subseteq X, \{\lambda_{l_1}\}$ and $\{\bar{\boldsymbol{y}}^{l_2}\} \subseteq Y, \{\mu_{l_2}\}$ with $\sum_{l_1}\lambda_{l_1} = 1, \sum_{l_2}\mu_{l_2} = 1$ and $\lambda_{l_1}, \mu_{l_2} \in [0,1]$, such that $\widehat{x} = \sum_{l_1}\lambda_{l_1}\bar{\boldsymbol{x}}^{l_1}, \widehat{y} = \sum_{l_2}\mu_{l_2}\bar{\boldsymbol{y}}^{l_2}$ and

$t \geq f(\widehat{\boldsymbol{x}})g(\widehat{\boldsymbol{y}})$. Let $\bar{t}_{l_1,l_2} = f(\bar{\boldsymbol{x}}^{l_1})g(\bar{y}^{l_2})$. Since $(\bar{\boldsymbol{x}}^{l_1}, \bar{\boldsymbol{y}}^{l_2}) \in X \times Y$ for each l_1, l_2, thus

$$(\widehat{\boldsymbol{x}}, \widehat{\boldsymbol{y}}, \sum_{l_1}\sum_{l_2} \lambda_{l_1}\mu_{l_2}\bar{t}_{l_1,l_2}) = \sum_{l_1}\sum_{l_2} \lambda_{l_1}\mu_{l_2}(\bar{\boldsymbol{x}}^{l_1}, \bar{\boldsymbol{y}}^{l_2}, \bar{t}_{l_1,l_2}) \in \Phi.$$

Thus, $(\widehat{\boldsymbol{x}}, \widehat{\boldsymbol{y}}, t) \in \Phi$ since $\sum_{l_1}\sum_{l_2} \lambda_{l_1}\mu_{l_2}\bar{t}_{l_1,l_2} = f(\widehat{\boldsymbol{x}})g(\widehat{\boldsymbol{y}}) \leq t$. ◇

Now we are ready to show that $v^{\text{LP}} \geq v^{\text{LR}}$. First of all, we reformulate formulation (5.4) into a more compact form by projection out $\mathbf{x}$ variables with formulation (5.4b) as

$$v^* = \min_{\mathbf{z},E} \quad \rho \sum_{k\in\mathcal{K}}\sum_{s\in\mathcal{S}_k}\sum_{a\in\mathcal{A}_k}\prod_{t\in\mathcal{T}} g^t_{k,a,s}(z^t_{k,a,s}) + (1-\rho)E \tag{5.15a}$$

$$\text{s.t.} \quad \sum_{s\in\mathcal{S}_k}\sum_{a\in\mathcal{A}_k}\prod_{t\in\mathcal{T}} g^t_{k,a,s}(z^t_{k,a,s}) \leq E, \forall k \in \mathcal{K}, \tag{5.15b}$$

$$\sum_{k\in\mathcal{K}}\sum_{s\in\mathcal{S}_k}\sum_{a\in\mathcal{A}_k}\prod_{\tau\in[t]} f^\tau_{k,a,s}(z^\tau_{k,a,s}) \leq B_t, \forall t \in \mathcal{T}, \tag{5.15c}$$

$$(5.4\text{d}), (5.4\text{g}),$$

where $g^t_{k,a,s}(\cdot), f^t_{k,a,s}(\cdot)$ are nonnegative valued affine functions. Under this setting, formulation (5.14) is equivalent to

$$v^{\text{LR}} = \sup_{\boldsymbol{\lambda},\mu:(5.13)} -\sum_{t\in\mathcal{T}} B^t\alpha^t\lambda^t + \min_{\mathbf{z}:(5.4\text{d}),(5.4\text{g}),} \sum_{k\in\mathcal{K}}(\rho+\mu^k)\sum_{s\in\mathcal{S}_k}\sum_{a\in\mathcal{A}_k}\prod_{t\in\mathcal{T}} g^t_{k,a,s}(z^t_{k,a,s}) + \sum_{t\in\mathcal{T}}\lambda^t\sum_{k\in\mathcal{K}}\sum_{s\in\mathcal{S}_k}\sum_{a\in\mathcal{A}_k}\prod_{\tau\in[t]} f^\tau_{k,a,s}(z^\tau_{k,a,s}).$$

Thus, by the primal characterization of the Lagrangian dual (Magnanti et al. [145]), we have

$$v^{\text{LR}} = \min_{\mathbf{z},E,\sigma,\boldsymbol{\gamma},\boldsymbol{\zeta}} \{\sigma : (\mathbf{z}, E, \sigma, \{\gamma_t\}, \{\zeta_k\}) \in \mathcal{R}, \gamma_t \leq B_t, \forall t \in \mathcal{T}, \zeta_k \leq E, \forall k \in \mathcal{K}\},$$

where

$$\mathcal{R} := \text{conv}\Big\{(\mathbf{z}, E, \sigma, \{\gamma_t\}, \{\zeta_k\}) : \sigma \geq \rho \sum_{k\in\mathcal{K}} \sum_{s\in\mathcal{S}_k} \sum_{a\in\mathcal{A}_k} \prod_{t\in\mathcal{T}} g^t_{k,a,s}(z^t_{k,a,s}) + (1-\rho)E,$$
$$\gamma_t \geq \sum_{k\in\mathcal{K}} \sum_{s\in\mathcal{S}_k} \sum_{a\in\mathcal{A}_k} \prod_{\tau\in[t]} f^\tau_{k,a,s}(z^\tau_{k,a,s}), \forall t \in \mathcal{T},$$
$$\zeta_k \geq \sum_{s\in\mathcal{S}_k} \sum_{a\in\mathcal{A}_k} \prod_{t\in\mathcal{T}} g^t_{k,a,s}(z^t_{k,a,s}), \forall k \in \mathcal{K},$$
$$(5.4d), (5.4g)\Big\}.$$

Note that

$$\text{conv}\{\{z^t_{k,a,s}\}_{k,a,s,t} : (5.4d), (5.4g)\} = \prod_{k,s,t} \text{conv}\{\{z^t_{k,a,s}\}_{k,a,s,t} : (5.4d), (5.4g)\}$$

because of separability of indices k, s, t in constraints (5.4d) and(5.4g), and for each k, s, t, we have

$$\text{conv}\{\{z^t_{k,a,s}\}_a : (5.4d), (5.4g)\} = \{\{z^t_{k,a,s}\}_{a\in\mathcal{A}_k} : (5.4d), (5.5b)\}$$

due to the total unimodularity of the assignment matrix.

Hence, by Claim 3, we have

$$\mathcal{R} \supseteq \bar{\mathcal{R}} = \text{conv}\Big\{(\mathbf{z}, E, \sigma, \{\gamma_t\}, \{\zeta_k\}) : \sigma \geq \rho \sum_{k\in\mathcal{K}} \sum_{s\in\mathcal{S}_k} \sum_{a\in\mathcal{A}_k} \prod_{t\in\mathcal{T}} g^t_{k,a,s}(z^t_{k,a,s}) + (1-\rho)E,$$
$$\gamma_t \geq \sum_{k\in\mathcal{K}} \sum_{s\in\mathcal{S}_k} \sum_{a\in\mathcal{A}_k} \prod_{\tau\in[t]} f^\tau_{k,a,s}(z^\tau_{k,a,s}), \forall t \in \mathcal{T},$$
$$\zeta_k \geq \sum_{s\in\mathcal{S}_k} \sum_{a\in\mathcal{A}_k} \prod_{t\in\mathcal{T}} g^t_{k,a,s}(z^t_{k,a,s}), \forall k \in \mathcal{K},$$
$$(5.4d), (5.5b)\Big\}.$$

Hence,

$$
\begin{aligned}
v^{\mathrm{LR}} \leq \bar{v} &:= \min_{\mathbf{z},E,\sigma,\boldsymbol{\gamma},\boldsymbol{\zeta}} \left\{\sigma : (\mathbf{z}, E, \sigma, \{\gamma_t\}, \{\zeta_k\}) \in \bar{\mathcal{R}}, \gamma_t \leq B_t, \forall t \in \mathcal{T}, \zeta_k \leq E, \forall k \in \mathcal{K}\right\} \\
&= \min_{\mathbf{z},E} \left\{ \rho \sum_{k\in\mathcal{K}} \sum_{s\in\mathcal{S}_k} \sum_{a\in\mathcal{A}_k} \prod_{t\in\mathcal{T}} g^t_{k,a,s}(z^t_{k,a,s}) + (1-\rho)E : (5.4\mathrm{d}), (5.5\mathrm{b}), (5.15\mathrm{b}), (5.15\mathrm{c}) \right\}.
\end{aligned}
$$

We complete the proof by noting that $\bar{v}$ is exactly equal to v^{R} defined in formulation (5.5) by projecting out variable $\mathbf{x}$. □

This theorem suggests that instead of solving formulation (5.14), which can be complicated, it is equivalent to solving the linear programming formulation (5.11) with the same optimal value. And apparently, formulation (5.11) can be solved more easily by off-the-shelf solvers.

This result also shows that when there is no budget constraint or none of the budget constraints are tight, then a randomized policy is optimal.

Corollary 5.6. *Suppose that $B_t = \infty$ for all $t \in \mathcal{T}$, then $v^* = v^{\mathrm{R}}$.*

Proof: If $B_t = \infty$ for all $t \in \mathcal{T}$, then the budget constraints are redundant, thus $v^* = v^{\mathrm{LR}}$. By Theorem 5.5, we have $v^* = v^{\mathrm{LR}} = v^{\mathrm{R}}$. □

5.4 An Effective Heuristic Solution Algorithm

An optimal policy for small to medium-sized instances of the FCMDP can be attained within acceptable solution times by solving the MILP (5.10) using commercial solvers such as Gurobi. However, obtaining an optimal solution for larger instances becomes considerably more challenging due to the exponential growth in the number of binary variables. It is noteworthy that when the continuous relaxation of the MILP (5.10) can yield a lower bound

that has a small gap compared to the optimal objective value of the MILP (5.10), it can be considered as a good approximation of the MILP (5.10). However, even if we can construct a restricted support in accordance with the solution of the continuous relaxation, there is no guarantee that an integral policy can be generated based on this restricted support. In other words, the solution of the continuous relaxation of the MILP (5.10) may not serve as a Bernoulli distribution to generate random policies that are feasible to MILP (5.10).

To address this challenge, we propose a heuristic algorithm based on the binary search. To incorporate the budget constraints into the objective, we introduce penalty coefficient ω_t for each budget constraint in stage $t \in \mathcal{T}$, normalized by dividing B_t. The algorithm conducts a binary search on ω_t for each $t \in \mathcal{T}$ to find suitable values. In each iteration, we solve the unconstrained MDP with a modified objective function:

$$\min_{\mathbf{z}} \left\{ \rho \sum_{k\in\mathcal{K}} \sum_{t\in\mathcal{T}} \sum_{s\in\mathcal{S}} \alpha^t U^t_{k,s} x^t_{k,s} + (1-\rho)E + \sum_{t\in\mathcal{T}} \omega_t \sum_{k\in\mathcal{K}} \sum_{s\in\mathcal{S}_k} \sum_{a\in\mathcal{A}_k} x^{t-1}_{k,s} z^t_{k,a,s} C^t_{k,a}, \right.$$

to find the best policy for the unconstrained MDP. If the policy obtained is feasible for the original problem, specifically, the following conditions hold:

$$\eta_t = \frac{1}{B_t} \sum_{k\in\mathcal{K}} \sum_{s\in\mathcal{S}_k} \sum_{a\in\mathcal{A}_k} x^{t-1}_{k,s} z^t_{k,a,s} C^t_{k,a} \leq 1, \forall t \in \mathcal{T},$$

we update the upper bound of ω_t with its current value for $\forall t \in \mathcal{T}$. However, if $\eta_t > 1$ for any $\omega_t, t \in \mathcal{T}$, we update the lower bound of ω_t with its current value. This procedure is summarized in Algorithm 6.

In the following section, we will numerically illustrate the performance of the Heuristic Algorithm 6.

Algorithm 6: A Heuristic Algorithm with Binary Search

Initialization: let $\varepsilon > 0, i = 0, N_m > 0, \phi = \infty$, u_t, l_t be the upper and lower bound for ω_t for $\forall t \in \mathcal{T}$;

while $i < N_m$ *and* $\sum_{t\in\mathcal{T}}(u_t - l_t) > \varepsilon$ **do**

  Let $\omega_t = \frac{1}{2}(u_t + l_t), \forall t \in \mathcal{T}$ and solve the unconstrained MDP

$$\bar{\mathbf{z}} \in \arg\min_{\mathbf{z}} \left\{ \rho \sum_{k\in\mathcal{K}} \sum_{t\in\mathcal{T}} \sum_{s\in\mathcal{S}} \alpha^t U^t_{k,s} x^t_{k,s} + (1-\rho)E + \sum_{t\in\mathcal{T}} \omega_t \sum_{k\in\mathcal{K}} \sum_{s\in\mathcal{S}_k} \sum_{a\in\mathcal{A}_k} x^{t-1}_{k,s} z^t_{k,a,s} C^t_{k,a} : \right.$$
$$\left. (5.4d) - (5.4g), (5.6), (5.7b), (5.7d), (5.7e), (5.8), (5.9) \right\};$$

  Obtain $\eta_t, \forall t \in \mathcal{T}$;

  if $\eta_t \leq 1, \forall t \in \mathcal{T}$ **then**

    Let $u_t = \omega_t$ and $\phi = \min\left\{\phi, \rho \sum_{k\in\mathcal{K}} \sum_{t\in\mathcal{T}} \sum_{s\in\mathcal{S}} \alpha^t U^t_{k,s} x^t_{k,s} + (1-\rho)E\right\}$;

  else

    for $t \in \mathcal{T}$ **do**

      if $u_t - l_t \leq \frac{1}{|\mathcal{T}|}\varepsilon$ **then**

        Let $l_t = u_t$

      else if $\eta_t > 1$ **then**

        Let $l_t = \omega_t$;

  $i \leftarrow i + 1$

5.5 An extension: Fair Budget-Constrained MDP under Infinite Horizon

In this section, we assume that $T = \infty$, and for each $t \in \mathcal{T}$, the transition matrix is $\mathbf{P^t} := \mathbf{P}$, user cost is $\mathbf{U}^t = \mathbf{U}$, while there is only one budget constraint with agency cost $\mathbf{C}^t = \mathbf{C}$ and budget $B_t := B$. Then according to Hawkins [45], Blackwell [146], there exists a stationary policy which optimizes formulation (5.2). In particular, in this section, we consider a stationary deterministic policy.

Let $\{V_{k,s}\}_{k\in\mathcal{K}, s\in\mathcal{S}_k}$ denote the optimal value of the agent $k \in \mathcal{K}$ at state $s \in \mathcal{S}_k$, $\{\beta_{k,s}\}_{k\in\mathcal{K}, s\in\mathcal{S}_k}$

denote the stationary distribution and $\chi_{k,a,s} = 1$ if action a is accessible in state s for agent k and 0 otherwise. Let set

$$X = \left\{ \boldsymbol{\chi} : \begin{array}{ll} \displaystyle\sum_{k\in\mathcal{K}}\sum_{s\in\mathcal{S}_k}\sum_{a\in\mathcal{A}_k} \beta_{k,s} C_{k,a}\chi_{k,a,s} \leq B, & (5.16a) \\ \displaystyle\sum_{a\in\mathcal{A}_k} \chi_{k,a,s} = 1, \forall k \in \mathcal{K}, s \in \mathcal{S}_k, & (5.16b) \\ \displaystyle\sum_{s\in S_k}\sum_{a\in\mathcal{A}_k} \beta_{k,s} P_{k,a}(s,s')\chi_{k,a,s} = \beta_{k,s'}, \forall k \in \mathcal{K}, s' \in \mathcal{S}_k, & (5.16c) \\ \displaystyle\sum_{s\in S_k} \beta_{k,s} = 1, \forall k \in \mathcal{K}, & (5.16d) \\ \chi_{k,a,s} \in \{0,1\}, \forall k \in \mathcal{K}, s \in \mathcal{S}_k, a \in \mathcal{A}_k. & (5.16e) \end{array} \right\}$$

Let $\zeta_{k,a,s} = \beta_{k,s}\chi_{k,a,s}$ for each $k \in \mathcal{K}, s \in \mathcal{S}_k, a \in \mathcal{A}_k$. Then by projecting out variables $\{\beta_{k,s}\}_{k\in\mathcal{K},s\in\mathcal{S}_k}$, we can reformulate formulation (5.16) as a mixed integer linear set below

$$X = \left\{ \boldsymbol{\chi} : \begin{array}{ll} \displaystyle\sum_{k\in\mathcal{K}}\sum_{s\in\mathcal{S}_k}\sum_{a\in\mathcal{A}_k} C_{k,a}\zeta_{k,a,s} \leq B, & (5.17a) \\ \displaystyle\sum_{a\in\mathcal{A}_k} \chi_{k,a,s} = 1, \forall k \in \mathcal{K}, s \in \mathcal{S}_k, & (5.17b) \\ \displaystyle\sum_{s\in S_k}\sum_{a\in\mathcal{A}_k} P_{k,a}(s,s')\zeta_{k,a,s} = \sum_{a\in\mathcal{A}_k} \zeta_{k,a,s'}, \forall k \in \mathcal{K}, s' \in \mathcal{S}_k, & (5.17c) \\ \displaystyle\sum_{s\in S_k}\sum_{a\in\mathcal{A}_k} \zeta_{k,a,s} = 1, \forall k \in \mathcal{K}, & (5.17d) \\ 0 \leq \zeta_{k,a,s} \leq \chi_{k,a,s}, \forall k \in \mathcal{K}, s \in \mathcal{S}_k, a \in \mathcal{A}_k, & (5.17e) \\ (5.16b), (5.16e). & \end{array} \right\}$$

Then the infinite-horizon FCMDP (5.2) can be formulated as

$$\min_{\boldsymbol{\chi}\in X}\min_{\mathbf{V}}\Bigg\{\rho\sum_{k\in\mathcal{K}}\sum_{s\in\mathcal{S}_k}h_k(s)V_{k,s}+(1-\rho)\max_{k\in\mathcal{K}}\sum_{s\in\mathcal{S}_k}h_k(s)V_{k,s}:\\ V_{k,s}\geq\alpha\sum_{s'\in\mathcal{S}}P_{k,a}(s,s')V_{k,s'}+\sum_{s'\in\mathcal{S}}\alpha P_{k,a}(s,s')U_{k,s'}\chi_{k,a,s}-M_{k,a,s}(1-\chi_{k,a,s}),\\ V_{k,s}\geq 0,\forall k\in\mathcal{K},s\in\mathcal{S}_k,a\in\mathcal{A}_k\Bigg\},\tag{5.18}$$

which is an MILP and $\{M_{k,a,s}\}_{k,a,s}$ are large numbers.

Note that $\{M_{k,a,s}\}_{k,a,s}$ can be chosen to be equal to the optimal value of the following problem:

$$\min_{\tilde{\mathbf{V}},w}\left\{w: w\geq\tilde{V}_{k,s},\tilde{V}_{k,s}\geq\sum_{s'\in\mathcal{S}}\alpha P_{k,a}(s,s')\left(\tilde{V}_{k,s'}+U_{k,s'}\right),\forall k\in\mathcal{K},s\in\mathcal{S}_k,a\in\mathcal{A}_k\right\}.\tag{5.19}$$

Alternatively, we can improve the value of $\{M_{k,a,s}\}_{k,a,s}$ by solving optimization problem iteratively, i.e., for each (k,a,s), we maximize

$$\max_{\boldsymbol{\chi}\in\text{Rel(X)}}\sum_{s'\in\mathcal{S}}\alpha P_{k,a}(s,s')V_{k,s'}+\sum_{s'\in\mathcal{S}}\alpha P_{k,a}(s,s')U_{k,s'}\chi_{k,a,s}-V_{k,s},\tag{5.20a}$$

$$\text{s.t.}\quad V_{k,s}\geq\sum_{s'\in\mathcal{S}}\alpha P_{k,a}(s,s')V_{k,s'}+\sum_{s'\in\mathcal{S}}\alpha P_{k,a}(s,s')U_{k,s'}\chi_{k,a,s}-M_{k,a,s}(1-\chi_{k,a,s}),\\ \forall k\in\mathcal{K},s\in\mathcal{S}_k,a\in\mathcal{A}_k,\tag{5.20b}$$

$$V_{k,s}\geq 0,\forall k\in\mathcal{K},s\in\mathcal{S}_k,\tag{5.20c}$$

where in Rel(X), we relax the binary variable to be continuous. We update $M_{k,a,s}$ by the optimal value to FCMDP (5.20).

5.6 Numerical Study

In this section, we numerically illustrate the performance of our formulation and the efficacy of the exact and approximation algorithms using hypothetical and real-world instances. Particularly, we apply these algorithms to a real-world bridge maintenance problem in North Carolina. In the context of the maintenance problem, all the decisions are made upfront, prior to the actual execution of operations. In our numerical study, the duration of each stage is set to be a year. To solve each instance, we set a time limit of 3,600 seconds. All the instances were programmed using Python 3.7.0, with calls to Gurobi 9.0.3, on a personal laptop equipped with a 1.9 GHz Intel Core i7 processor and 16 GB of memory.

5.6.1 Results on Hypothetical Instances

We generated the testing hypothetical instances with varying numbers of agents and stages. Each agent possesses six states to represent their conditions, ranging from the best to the worst. Each state carries a user cost, randomly generated from a uniform distribution spanning 0 to 100,000. It is worth noting that the best state has the lowest user cost, while the worst state has the highest user cost for each agent at a given stage. At each stage, the decision-maker can choose one of three actions for an agent: do-nothing, modest action, and the best effort. The do-nothing action incurs zero agency cost. Conversely, the modest action has an agency cost generated from a uniform distribution between 0 and 50,000, while the best effort action's agency cost is generated from a uniform distribution between 50,000 and 100,000, for each agent at each stage. The initial conditions for each agent are randomly selected from the 6 states. The budget allocated for each stage is set as the number of agents times a randomly generated value from a uniform distribution between 10,000 and 60,000. Transition probabilities are randomly generated based on the principle that an agent would

be more likely to transition from a poor condition to a good one if the best effort action were taken, as compared to the modest action. However, if the do-nothing action were chosen, the agent's condition would either stay the same or be worse.

We first numerically illustrate the strength of the MILP (5.10) and its continuous relaxation. We would like to highlight that the continuous relaxation of the MILP (5.10), in essence, is the random policy. To ensure that the efficiency term, represented by the total expected user cost, is on a similar scale as the fairness term, denoted by the maximum expected user cost for agents, we set the weighted scalar ρ to be 0.5 divided by the number of agents so that the efficiency and fairness terms are of the same magnitude. Besides, the discount factor α is set to 0.9. To enhance distinction among different instances, we normalize the objective value by the number of stages. The results are shown in Table 5.1. We denote the objective value as "Obj," the largest user cost among all the agents as "Largest", which is normalized by the number of stages. "Average" represents the total expected user cost, which is normalized by both the number of agents and the number of stages, i.e., average user cost among agents. The optimality gap is represented by "Opt.Gap" when the MILP cannot be solved to optimality. Furthermore, "Gap" indicates the difference between the objective value obtained from the continuous relaxation and the MILP divided by the continuous relaxation value. We see that the MILP can be solved to optimality for all the instances with 10 stages, and the instances with 20 stages are more challenging to solve. For instances 9 and 10, Gurobi failed even to find a feasible solution. We also note that the gap between the continuous relaxation and the MILP is rather small. This suggests that in situations where solving larger instances becomes computationally expensive or finding a solution within the time limit is impossible, the continuous relaxation serves as a reliable approximation for the optimal objective value. It is worth mentioning that the average user cost among agents is considerably lower than the largest user cost. This discrepancy implies the existence of a

cost imbalance among agents, highlighting the importance of taking fairness into account.

Table 5.1: Results of MILP (5.10) and Continuous Relaxation/Randomized Policy

Instance	Num. Agents	Num. Stages	MILP					Continuous Relaxation / Randomized Policy				
			Obj	Time (s)	Largest	Average	Opt.Gap (%)	Obj	Time (s)	Largest	Average	Gap (%)
1	10	10	20309.1	116.3	25950.4	14667.7	0.00	20246.1	0.3	25934.8	14557.5	0.31
2	20	10	19303.9	163.9	25856.4	12751.4	0.00	19295.1	0.6	25848.1	12742.1	0.05
3	50	10	21004.3	215.0	29283.5	12725.1	0.00	20999.1	1.9	29283.5	12714.7	0.02
4	100	10	21210.2	334.7	29310.5	13109.8	0.00	21207.9	5.3	29310.5	13105.3	0.01
5	200	10	23086.0	530.8	34101.5	12070.4	0.00	23083.2	15.0	34101.5	12064.8	0.01
6	10	20	13396.6	3600.0	17434.8	9358.5	0.00	13362.8	0.7	17442.8	9282.8	0.25
7	20	20	12785.4	3600.0	17395.7	8175.2	0.01	12780.1	2.9	17391.5	8168.6	0.04
8	50	20	13712.7	3600.0	19179.1	8246.4	0.02	13705.3	8.8	19179.1	8231.6	0.05
9	100	20	/	/	/	/	/	14107.0	11.4	19757.7	8456.3	/
10	200	20	/	/	/	/	/	15414.4	88.8	22993.4	7835.3	/

We also tested Algorithm 6, as illustrated in Table 5.2. The term "Best LB" represents the best lower bound obtained for each instance, while "Gap" denotes the difference between the objective value obtained from Algorithm 6 and the best lower bound divided by the best lower bound. The results show that Algorithm 6 can find near-optimal solutions with much less time, compared to solving MILP directly. Besides, the relative gap between the objective value obtained from Algorithm 6 and the best lower bound of most instances remains below 5% for most instances. These findings highlight the effectiveness of Algorithm 6 in finding good-quality feasible solutions, especially for solving large-sized instances. By leveraging this heuristic algorithm, we can solve larger instances and obtain high-quality solutions within affordable computational limits.

Table 5.2: Results of Algorithm 6

Instance	Best LB	Obj	Time (s)	Largest	Average	Gap (%)
1	20309.1	20555.7	15.3	25975.2	15136.3	1.21
2	19303.9	19568.5	24.3	25821.7	13315.2	1.37
3	21004.3	21015.0	67.2	26103.3	15926.8	0.05
4	21210.2	21500.6	161.7	26302.4	16698.7	1.37
5	23086.0	23523.4	234.2	31917.9	15128.9	1.89
6	13362.8	13927.4	86.9	17537.9	10316.9	4.23
7	12780.1	13206.1	150.4	18239.1	8173.0	3.33
8	13705.3	14332.0	408.8	18825.0	9839.1	4.57
9	14107.0	15245.7	967.4	20521.7	9969.8	8.07
10	15414.4	16137.1	2073.5	23438.9	8835.3	4.69

We conduct the sensitivity analysis on the discount factor α and the weighted scalar ρ for instance 4, which is shown in Table 5.3, Table 5.4, and Figure 5.1. The discount factor α was varied from 0.1 to 1, and the weighted scalar ρ was set to be 0.5 divided by the number of agents. In order to show their importance, we solved the instance using every given discount factor and then evaluated the objective function without a discount factor by applying the same solution to the following formulation:

$$\rho \sum_{k\in\mathcal{K}} \sum_{t\in\mathcal{T}} \sum_{s\in\mathcal{S}} U^t_{k,s} x^t_{k,s} + (1-\rho) \max_{k\in\mathcal{K}} \sum_{t\in\mathcal{T}} \sum_{s\in\mathcal{S}} U^t_{k,s} x^t_{k,s}.$$

This allows us to assess the influence of the discount factor on the objective function. We observe that the objective value without a discount factor increases while the discount factor α decreases. This is because a smaller discount factor emphasizes more on the recent decisions, and a larger discount factor focuses more on long-run performances. It is important to note that there is no evident monotonicity when evaluating only the average user cost without a discount factor nor the largest user cost without a discount factor. Fluctuations of these terms may happen when the discount factor α changes, since we are optimizing both efficiency and fairness simultaneously.

Table 5.3: Impact of Discount Factor

Discount	MILP			Evaluation w/o α		
Factor α	Obj	Largest	Average	Obj	Largest	Average
1	35380.2	49976.3	20784.0	35380.2	49976.3	20784.0
0.9	21210.2	29310.5	13109.8	35384.3	49976.3	20792.2
0.8	13641.6	18680.0	8603.2	35940.1	51154.9	20725.4
0.7	9187.4	12482.2	5892.6	35948.0	51154.9	20741.0
0.6	6389.8	8639.7	4139.9	35960.8	51154.9	20766.8
0.5	4501.7	6077.8	2925.7	35980.7	51202.9	20758.4
0.4	3138.0	4240.8	2035.2	35989.8	51154.9	20824.7
0.3	2168.5	2988.5	1348.5	36174.6	51203.0	21146.3
0.2	1348.5	1892.0	805.0	38477.5	52409.3	24545.6
0.1	633.9	903.4	364.3	44696.4	57998.4	31394.5

We set the discount factor α to be 0.9, and varied the weighted scalar ρ from 0 to 1, divided

by the number of agents. To illustrate the impact on fairness and efficiency, we used the percentage change for the average user cost and unfairness, where for the average user cost, we let the baseline be the lowest possible average user cost attained when $\rho = 1$. For the unfairness, we let the base case be the smallest value of the largest user cost, achieved when $\rho = 0$. We evaluated unfairness as the absolute difference between the highest and lowest largest user cost. The results, illustrated in Figure 5.1, reveal that by reducing the weighted scalar, fairness can be improved by 37% with a 16% decrease in efficiency. Moreover, it is noteworthy that as the weighted scalar ρ decreases, the disparity between the largest and smallest user costs diminishes significantly. These results underscore the possibility of achieving significant gains in fairness while maintaining a relatively high level of efficiency.

Table 5.4: Impact of Weighted Scalar

Weighted Scalar ρ	Obj	Largest	Smallest	Average
1	12353.9	32535.9	1030.8	12353.9
0.75	17255.4	30505.4	3350.5	12838.7
0.5	21210.2	29310.5	7888.5	13109.8
0.25	23588.8	26835.9	8702.0	13847.5
0	23750.5	23750.5	10047.5	14376.5

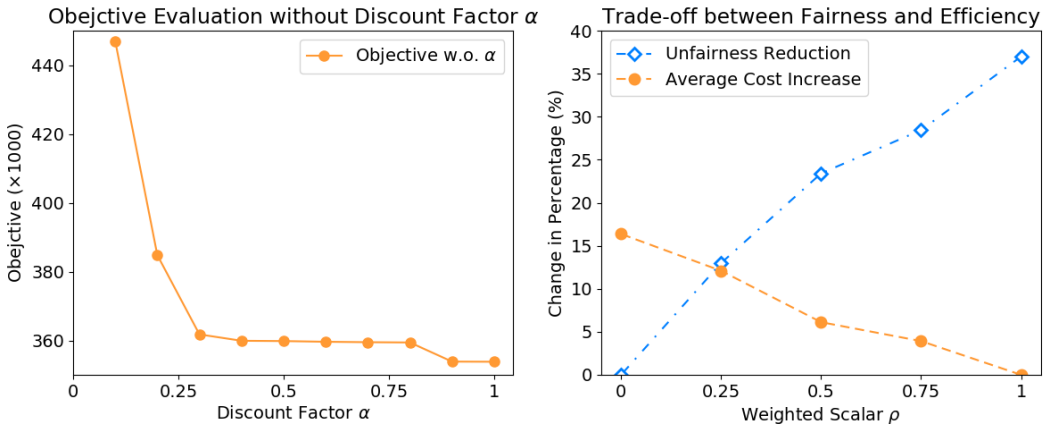

Figure 5.1: Impact of Discount Factor α and Weighted Scalar ρ

5.6.2 Case Study on A Bridge Maintenance Problem

In this case study, we focus on the long-term maintenance of 696 bridges in North Carolina over a 20-year horizon, where each year is denoted as a stage and each bridge is an agent. We use six distinct states to indicate the varying conditions of each bridge. Each state carries a corresponding user cost ranging from 0 to 100,000 dollars specific to a particular bridge. At every stage, three candidate actions can be taken for each bridge: repairs, preventive maintenance, or doing-nothing. Among these, the repair action has the highest agency cost, and no action incurs zero agency cost, irrespective of the bridge's state at each stage. The initial condition of each bridge is categorized within the six states. A budget for the total agency cost for all bridges in each stage is set in advance of the planning horizon. The transition probability between states adheres to the principle that a bridge is more likely to transition from a poor condition to a good one if a repair action is taken, as opposed to preventive maintenance. If doing-nothing action were taken, a bridge would either maintain its current condition or potentially worsen. As the size of this case study is very large, we employed Algorithm 6 to solve it.

We considered the discount factor $\alpha = 0.9$ and weight scalar $\rho \in \{0, 0.5, 1\}$. Besides, we examine three different budget levels: limited, moderate, and abundant. The results are shown in Table 5.5. It is evident that increasing the budget can lead to a decrease in the objective value, as an abundant budget provides the decision-maker with the ability to repair bridges or conduct preventive maintenance more frequently than any limited budget allows. Notably, there exists a trade-off between fairness and efficiency due to a limited budget. Similar trends are observed in cases with a moderate budget. In contrast, instances with an abundant budget demonstrate more favorable outcomes, offering the potential to achieve substantial improvements in fairness while maintaining a relatively high level of efficiency. We also observe that, when considering both fairness and efficiency, the largest

user cost among bridges significantly exceeds the average user cost, highlighting a systematic imbalance among bridges. However, by focusing solely on fairness among bridges, the largest user cost decreases by 40% on average, but it only results in a slight increase of 14% on average in the average user cost. This indicates that the decision-maker can achieve a fair policy without significantly compromising overall efficiency. These findings not only show the trade-off between fairness and efficiency, but also underscore the impact of budget levels on decision-making.

Table 5.5: Results of Case Study on Bridge Maintenance

Budget	$\rho = 0.0$			$\rho = 0.5$			$\rho = 1.0$		
($\times 10^6$)	Obj	Largest	Average	Obj	Largest	Average	Obj	Largest	Average
9	38647.6	38647.6	18297.6	34587.8	52515.2	16660.3	15804.8	74389.3	15804.8
18	26351.5	26351.5	15418.1	24485.5	34113.0	14857.9	13320.7	41157.0	13320.7
36	22801.1	22801.1	13660.2	21097.6	29587.8	12607.3	11503.0	35877.6	11503.0

5.7 Conclusion

In this chapter, we study the Fair Constrained Markov Decision Process (FCMDP). We first prove that solving FCMDP is NP-hard even when there is a single stage, two states, and two actions for each agent. We then provide a Mixed Integer Linear Programming (MILP) formulation for the FCMDP. We further establish the equivalence between the continuous relaxation of this MILP, Randomized FCMDP, and the Lagrangian dual of the original problem. For large-scale FCMDP instances, we develop an effective heuristic algorithm capable of obtaining near-optimal solutions. To validate the effectiveness of the proposed algorithms, we generate hypothetical instances and also apply the heuristic algorithm to a real-world bridge maintenance problem in North Carolina. It reveals that by incorporating fairness considerations in addition to efficiency, we can significantly decrease the imbalance among agents while incurring only a slight increase in the average user cost. This finding

indicates that the decision-makers can achieve a fair policy that benefits all agents without aggressively compromising overall efficiency. In our future work, we intend to incorporate the uncertainty in transition probability and develop techniques to hedge against the risk of parametric uncertainties. Our FCMDP framework is also promising to address multistage resource allocation problems. For instance, our framework can be effectively applied to task allocation issues within fulfillment centers where the number of induct or eject stations is limited. This framework can be generalized to wireless communication problems with limited bandwidth and multiple users, thereby enabling a fair allocation of bandwidth.

Chapter 6

Conclusion

In this dissertation, we present theoretical results and algorithms designed for fair and risk-averse resource allocation problems in transportation under uncertainty. We address the challenges in those problems and derive MILP formulations. To further strengthen the MILP formulations, we delve into the problem structure and propose valid inequalities as necessitated. To solve these problems with maximum efficiency, we design decomposition algorithms and approximation algorithms. The scope of our frameworks is broadened to address resource allocation issues within various transportation systems, including public transportation, Urban Air Mobility, and multistage facility maintenance.

In the first section, we study DrFRAM under type-∞ Wasserstein ambiguity set, which is the first one focusing on fair multi-type transit resource allocation under passenger arrival and alighting rates uncertainty. DrFRAM is proved to be NP-hard even with two types of buses. We derive the monotonicity properties of the DrFRAM and linearize the nonlinear components. We develop stronger MILP formulation and valid inequalities to design efficient scenario decomposition methods. No-one-left based approximation algorithm is also proposed for solving DrFRAM to near-optimality. Finally, we numerically demonstrate the effectiveness of the proposed approaches, which outperform the sampling average approximation method.

In the second section, we develop a novel formulation for FairUAM to allocate aircraft from multiple UAM service providers under passenger demand and airspace capacity uncertainties.

FairUAM is proven to be NP-hard with only one UAM service provider or even with the aircraft allocation. The monotonicity properties derived make it possible for us to simplify the FairUAM model. Six families of valid inequalities are proposed to significantly improve the solution time. Finally, we numerically demonstrate the effectiveness of the proposed method using generated instances and apply it to a case study of a real-world network.

In the third section, we establish a MILP formulation for the FCMDP under a finite horizon and demonstrate its NP-hardness, even in single-stage instances. We demonstrate the equivalence between the continuous relaxation of the MILP and the optimal Lagrangian dual. We accommodate the MILP to extend our model to infinite horizons and propose exact and approximation algorithms to solve FCMDP. Finally, we apply our proposed solution approach to a real-world infrastructure maintenance problem in North Carolina to illustrate their practical effectiveness.

Based on the foundation of our present framework and numerical demonstrations, potential extensions attract our exploration in the future, addressing the prevailing fairness and risk-averse concerns in these areas. Our framework is able to adapt to a variety of transportation-related issues with fairness concerns and demand uncertainties. These include the challenges of truck platooning, shared mobility, and so on. Beyond the sphere of transportation, our frameworks could be expanded to address task allocation issues where resources are limited and demand uncertain, such as allocating warehouse robots or vehicles during disaster evacuations.

Bibliography

[1] Carlos F Daganzo and Yanfeng Ouyang. *Public transportation systems: Principles of system design, operations planning and real-time control*. World Scientific, 2010.

[2] Avishai Ceder. *Public transit planning and operation: Modeling, practice and behavior*. CRC press, 2016.

[3] Steven Chien and Paul Schonfeld. Optimization of grid transit system in heterogeneous urban environment. *Journal of Transportation Engineering*, 123(1):28–35, 1997.

[4] Joaquin De Cea and Enrique Fernández. Transit assignment for congested public transport systems: an equilibrium model. *Transportation science*, 27(2):133–147, 1993.

[5] Luca Quadrifoglio, Randolph W Hall, and Maged M Dessouky. Performance and design of mobility allowance shuttle transit services: bounds on the maximum longitudinal velocity. *Transportation science*, 40(3):351–363, 2006.

[6] JF Guan, Hai Yang, and Sumedha Chandana Wirasinghe. Simultaneous optimization of transit line configuration and passenger line assignment. *Transportation Research Part B: Methodological*, 40(10):885–902, 2006.

[7] Mansoureh Jeihani, Lei Zhang, Anam Ardeshiri, Arash Amiri, Arefeh Nasri, Kiana Roshan Zamir, Babak Baghaei, et al. Development of a framework for transit-oriented development (tod). Technical report, Maryland. State Highway Administration, 2013.

[8] Valérie Guihaire and Jin-Kao Hao. Transit network design and scheduling: A global review. *Transportation Research Part A: Policy and Practice*, 42(10):1251–1273, 2008.

[9] Daniel Hörcher and Alejandro Tirachini. A review of public transport economics. *Economics of Transportation*, 25:100196, 2021.

[10] Seyed Mohammad Nourbakhsh and Yanfeng Ouyang. A structured flexible transit system for low demand areas. *Transportation Research Part B: Methodological*, 46(1): 204–216, 2012.

[11] Yanfeng Ouyang, Seyed Mohammad Nourbakhsh, and Michael J Cassidy. Continuum approximation approach to bus network design under spatially heterogeneous demand. *Transportation Research Part B: Methodological*, 68:333–344, 2014.

[12] Peng Will Chen and Yu Marco Nie. Connecting e-hailing to mass transit platform: Analysis of relative spatial position. *Transportation Research Part C: Emerging Technologies*, 77:444–461, 2017.

[13] Christina Iliopoulou and Konstantinos Kepaptsoglou. Integrated transit route network design and infrastructure planning for on-line electric vehicles. *Transportation Research Part D: Transport and Environment*, 77:178–197, 2019. ISSN 1361-9209. doi: https://doi.org/10.1016/j.trd.2019.10.016. URL https://www.sciencedirect.com/science/article/pii/S1361920919305000.

[14] Mojtaba Abdolmaleki, Neda Masoud, and Yafeng Yin. Transit timetable synchronization for transfer time minimization. *Transportation Research Part B: Methodological*, 131:143–159, 2020.

[15] Azucena Román-De la Sancha, Juan M Mayoral, and Luis I Román. A novel approach for transit transfer stations design optimization in densely populated cities. *Procedia computer science*, 130:1013–1018, 2018.

[16] Timothy C Matisziw, Alan T Murray, and Changjoo Kim. Strategic route extension in transit networks. *European journal of operational research*, 171(2):661–673, 2006.

[17] Jian Gang Jin, Kwong Meng Teo, and Amedeo R Odoni. Optimizing bus bridging services in response to disruptions of urban transit rail networks. *Transportation Science*, 50(3):790–804, 2016.

[18] Richa Agarwal and Özlem Ergun. Ship scheduling and network design for cargo routing in liner shipping. *Transportation Science*, 42(2):175–196, 2008.

[19] Arthur Mahéo, Philip Kilby, and Pascal Van Hentenryck. Benders decomposition for the design of a hub and shuttle public transit system. *Transportation Science*, 53(1): 77–88, 2019.

[20] Luyu Liu, Harvey J Miller, and Jonathan Scheff. The impacts of covid-19 pandemic on public transit demand in the united states. *Plos one*, 15(11):e0242476, 2020.

[21] Baichuan Mo, Kairui Feng, Yu Shen, Clarence Tam, Daqing Li, Yafeng Yin, and Jinhua Zhao. Modeling epidemic spreading through public transit using time-varying encounter network. *Transportation Research Part C: Emerging Technologies*, 122: 102893, 2021.

[22] Gongyu Chen, Xinyu Fei, Huiwen Jia, Xian Yu, and Siqian Shen. An optimization-and-simulation framework for redesigning university campus bus system with social distancing. *arXiv preprint arXiv:2010.10630*, 2020.

[23] Konstantinos Gkiotsalitis and Oded Cats. Optimal frequency setting of metro services in the age of covid-19 distancing measures. *Transportmetrica A: Transport Science*, pages 1–23, 2021.

[24] Hongyuan Yang and Marco Nie. Optimizing operational strategies for mass transit systems in response to a global pandemic. *Available at SSRN 3721007*, 2020.

[25] Parker D Vascik and R John Hansman. Evaluation of key operational constraints affecting on-demand mobility for aviation in the los angeles basin: ground infrastructure, air traffic control and noise. In *17th AIAA Aviation Technology, Integration, and Operations Conference*, page 3084, 2017.

[26] Dimas Numan Fadhil. A gis-based analysis for selecting ground infrastructure locations for urban air mobility. *inlangen]. Master's Thesis, Technical University of Munich*, 2018.

[27] Matthew Daskilewicz, Brian German, Matthew Warren, Laurie A Garrow, Sreekar-Shashank Boddupalli, and Thomas H Douthat. Progress in vertiport placement and estimating aircraft range requirements for evtol daily commuting. In *2018 Aviation Technology, Integration, and Operations Conference*, page 2884, 2018.

[28] Suchithra Rajendran and Joshua Zack. Insights on strategic air taxi network infrastructure locations using an iterative constrained clustering approach. *Transportation Research Part E: Logistics and Transportation Review*, 128:470–505, 2019.

[29] Srushti Rath and Joseph YJ Chow. Air taxi skyport location problem with single-allocation choice-constrained elastic demand for airport access. *Journal of Air Transport Management*, 105:102294, 2022.

[30] Laurie A Garrow, Brian J German, and Caroline E Leonard. Urban air mobility: A comprehensive review and comparative analysis with autonomous and electric ground transportation for informing future research. *Transportation Research Part C: Emerging Technologies*, 132:103377, 2021.

[31] Suchithra Rajendran and Sharan Srinivas. Air taxi service for urban mobility: A critical review of recent developments, future challenges, and opportunities. *Transportation research part E: logistics and transportation review*, 143:102090, 2020.

[32] David P Thipphavong, Rafael Apaza, Bryan Barmore, Vernol Battiste, Barbara Burian, Quang Dao, Michael Feary, Susie Go, Kenneth H Goodrich, Jeffrey Homola, et al. Urban air mobility airspace integration concepts and considerations. In *2018 Aviation Technology, Integration, and Operations Conference*, page 3676, 2018.

[33] Eric R Mueller, Parmial H Kopardekar, and Kenneth H Goodrich. Enabling airspace integration for high-density on-demand mobility operations. In *17th AIAA Aviation Technology, Integration, and Operations Conference*, page 3086, 2017.

[34] Imke C Kleinbekman, Mihaela A Mitici, and Peng Wei. evtol arrival sequencing and scheduling for on-demand urban air mobility. In *2018 IEEE/AIAA 37th Digital Avionics Systems Conference (DASC)*, pages 1–7. IEEE, 2018.

[35] Suda Bharadwaj, Steven Carr, Natasha Neogi, Hasan Poonawala, Alejandro Barberia Chueca, and Ufuk Topcu. Traffic management for urban air mobility. In *NASA Formal Methods Symposium*, pages 71–87. Springer, 2019.

[36] Syed Arbab Mohd Shihab, Peng Wei, Daniela Sofia Jurado Ramirez, Rodrigo Mesa-Arango, and Christina Bloebaum. By schedule or on demand?-a hybrid operation concept for urban air mobility. In *AIAA Aviation 2019 Forum*, page 3522, 2019.

[37] Syed Arbab Mohd Shihab, Peng Wei, Jie Shi, and Nanpeng Yu. Optimal evtol fleet dispatch for urban air mobility and power grid services. In *AIAA Aviation 2020 Forum*, page 2906, 2020.

[38] Satadru Roy, Mark T Kotwicz Herniczek, Caroline Leonard, Ayush Jha, Nathan Wang,

Brian German, and Laurie Garrow. A multi-commodity network flow approach for optimal flight schedules for an airport shuttle air taxi service. In *AIAA Scitech 2020 Forum*, page 0975, 2020.

[39] Suda Bharadwaj, Tichakorn Wongpiromsarn, Natasha Neogi, Joseph Muffoletto, and Ufuk Topcu. Minimum-violation traffic management for urban air mobility. In *NASA Formal Methods Symposium*, pages 37–52. Springer, 2021.

[40] Zhiqiang Wu and Yu Zhang. Integrated network design and demand forecast for on-demand urban air mobility. *Engineering*, 7(4):473–487, 2021.

[41] Zhengyi Wang, Daniel Delahaye, Jean-Loup Farges, and Sameer Alam. Complexity optimal air traffic assignment in multi-layer transport network for urban air mobility operations. *Transportation Research Part C: Emerging Technologies*, 142:103776, 2022.

[42] Martin L Puterman. *Markov decision processes: discrete stochastic dynamic programming*. John Wiley & Sons, 1994.

[43] Kamal Golabi, Ram B Kulkarni, and George B Way. A statewide pavement management system. *Interfaces*, 12(6):5–21, 1982.

[44] Eitan Altman. *Constrained Markov decision processes*, volume 7. CRC Press, 1999.

[45] Jeffrey Thomas Hawkins. *A Langrangian decomposition approach to weakly coupled dynamic optimization problems and its applications*. PhD thesis, Massachusetts Institute of Technology, 2003.

[46] Daniel Adelman and Adam J Mersereau. Relaxations of weakly coupled stochastic dynamic programs. *Operations Research*, 56(3):712–727, 2008.

[47] Qiushi Chen, Turgay Ayer, and Jagpreet Chhatwal. Optimal m-switch surveillance policies for liver cancer in a hepatitis c–infected population. *Operations Research*, 66 (3):673–696, 2018.

[48] Nedialko B Dimitrov and David P Morton. Combinatorial design of a stochastic Markov decision process. In *Operations Research and Cyber-Infrastructure*, pages 167–193. Springer, 2009.

[49] John Gittins. A dynamic allocation index for the sequential design of experiments. *Progress in statistics*, pages 241–266, 1974.

[50] Peter Whittle. Restless bandits: Activity allocation in a changing world. *Journal of applied probability*, 25(A):287–298, 1988.

[51] John C Gittins and David M Jones. A dynamic allocation index for the discounted multiarmed bandit problem. *Biometrika*, 66(3):561–565, 1979.

[52] Hadi Hosseini, Jesse Hoey, and Robin Cohen. A coordinated mdp approach to multi-agent planning for resource allocation, with applications to healthcare. *arXiv preprint arXiv:1407.1584*, 2014.

[53] Xiaofei Hu, Carlos Daganzo, and Samer Madanat. A reliability-based optimization scheme for maintenance management in large-scale bridge networks. *Transportation Research Part C: Emerging Technologies*, 55:166–178, 2015.

[54] Constantine Caramanis, Nedialko B Dimitrov, and David P Morton. Efficient algorithms for budget-constrained markov decision processes. *Automatic Control, IEEE Transactions on*, 59(10):2813–2817, 2014.

[55] Frits De Nijs, Erwin Walraven, Mathijs De Weerdt, and Matthijs Spaan. Constrained

multiagent markov decision processes: A taxonomy of problems and algorithms. *Journal of Artificial Intelligence Research*, 70:955–1001, 2021.

[56] Frits de Nijs and Peter J Stuckey. Risk-aware conditional replanning for globally constrained multi-agent sequential decision making. In *Proceedings of the 19th International Conference on Autonomous Agents and MultiAgent Systems*, pages 303–311, 2020.

[57] Guangyao Shi, Nare Karapetyan, Ahmad Bilal Asghar, Jean-Paul Reddinger, James Dotterweich, James Humann, and Pratap Tokekar. Risk-aware uav-ugv rendezvous with chance-constrained markov decision process. In *2022 IEEE 61st Conference on Decision and Control (CDC)*, pages 180–187. IEEE, 2022.

[58] Min Wen, Osbert Bastani, and Ufuk Topcu. Algorithms for fairness in sequential decision making. In *International Conference on Artificial Intelligence and Statistics*, pages 1144–1152. PMLR, 2021.

[59] Karan N Chadha, Ankur A Kulkarni, and Jayakrishnan Nair. Efficiency fairness tradeoff in battery sharing. *Operations Research Letters*, 49(3):377–384, 2021.

[60] Xinwei Chen, Tong Wang, Barrett W Thomas, and Marlin W Ulmer. Same-day delivery with fair customer service. *European journal of operational research*, 308(2): 738–751, 2023.

[61] Warren B Powell and Huseyin Topaloglu. Stochastic programming in transportation and logistics. *Handbooks in operations research and management science*, 10:555–635, 2003.

[62] Zhi-Chun Li, William HK Lam, and SC Wong. The optimal transit fare structure

under different market regimes with uncertainty in the network. *Networks and Spatial Economics*, 9(2):191–216, 2009.

[63] Michael Fernandes, Logan Walls, Sean Munson, Jessica Hullman, and Matthew Kay. Uncertainty displays using quantile dotplots or cdfs improve transit decision-making. In *Proceedings of the 2018 CHI Conference on Human Factors in Computing Systems*, pages 1–12, 2018.

[64] Zhi-Chun Li, William HK Lam, and Agachai Sumalee. Modeling impact of transit operator fleet size under various market regimes with uncertainty in network. *Transportation Research Record*, 2063(1):18–27, 2008.

[65] Xiao Fu and William HK Lam. A network equilibrium approach for modelling activity-travel pattern scheduling problems in multi-modal transit networks with uncertainty. *Transportation*, 41(1):37–55, 2014.

[66] Younes Hamdouch, WY Szeto, and Y Jiang. A new schedule-based transit assignment model with travel strategies and supply uncertainties. *Transportation Research Part B: Methodological*, 67:35–67, 2014.

[67] Yuval Hadas and Matan Shnaiderman. Public-transit frequency setting using minimum-cost approach with stochastic demand and travel time. *Transportation Research Part B: Methodological*, 46(8):1068–1084, 2012.

[68] Karmel S Shehadeh. Distributionally robust optimization approaches for a stochastic mobile facility fleet sizing, routing, and scheduling problem. *Transportation Science*, 2022.

[69] Kati Moug, Huiwen Jia, and Siqian Shen. A shared mobility based framework for

evacuation planning and operations under forecast uncertainty. *IISE Transactions*, (just-accepted):1–33, 2022.

[70] Ashish Kulshrestha, Yingyan Lou, and Yafeng Yin. Pick-up locations and bus allocation for transit-based evacuation planning with demand uncertainty. *Journal of Advanced Transportation*, 48(7):721–733, 2014.

[71] Kun An and Hong K Lo. Two-phase stochastic program for transit network design under demand uncertainty. *Transportation Research Part B: Methodological*, 84:157–181, 2016.

[72] Jinpeng Liang, Jianjun Wu, Ziyou Gao, Huijun Sun, Xin Yang, and Hong K Lo. Bus transit network design with uncertainties on the basis of a metro network: A two-step model framework. *Transportation Research Part B: Methodological*, 126:115–138, 2019.

[73] Gyugeun Yoon and Joseph YJ Chow. Contextual bandit-based sequential transit route design under demand uncertainty. *Transportation Research Record*, 2674(5):613–625, 2020.

[74] Avijit Mukherjee and Mark Hansen. A dynamic rerouting model for air traffic flow management. *Transportation Research Part B: Methodological*, 43(1):159–171, 2009.

[75] Moein Ganji, David J Lovell, Michael O Ball, and Alex Nguyen. Resource allocation in flow-constrained areas with stochastic termination times. *Transportation research record*, 2106(1):90–99, 2009.

[76] Shubham Gupta and Dimitris J Bertsimas. Multistage air traffic flow management under capacity uncertainty: a robust and adaptive optimization approach. 2011.

[77] Kai Wang and Alexandre Jacquillat. A stochastic integer programming approach to air traffic scheduling and operations. *Operations Research*, 68(5):1375–1402, 2020.

[78] Virginie Gabrel, Cécile Murat, and Aurélie Thiele. Recent advances in robust optimization: An overview. *European journal of operational research*, 235(3):471–483, 2014.

[79] Hamed Rahimian and Sanjay Mehrotra. Distributionally robust optimization: A review. *arXiv preprint arXiv:1908.05659*, 2019.

[80] Wenjuan Hou, Tao Fang, Zhi Pei, and Qiao-Chu He. Integrated design of unmanned aerial mobility network: A data-driven risk-averse approach. *International Journal of Production Economics*, 236:108131, 2021.

[81] An Yan and Bill Howe. Fairness in practice: a survey on equity in urban mobility. *A Quarterly bulletin of the Computer Society of the IEEE Technical Committee on Data Engineering*, 42(3), 2020.

[82] Dimitris Bertsimas, Vivek F Farias, and Nikolaos Trichakis. On the efficiency-fairness trade-off. *Management Science*, 58(12):2234–2250, 2012.

[83] Jun Chen, Long Chen, and Dengfeng Sun. Air traffic flow management under uncertainty using chance-constrained optimization. *Transportation Research Part B: Methodological*, 102:124–141, 2017.

[84] Olga Rodionova, Heather Arneson, Banavar Sridhar, and Antony Evans. Efficient trajectory options allocation for the collaborative trajectory options program. In *2017 IEEE/AIAA 36th Digital Avionics Systems Conference (DASC)*, pages 1–10. IEEE, 2017.

[85] Sadeque Hamdan, Ali Cheaitou, Oualid Jouini, Zied Jemai, Imad Alsyouf, and Maamar Bettayeb. On fairness in the network air traffic flow management with rerouting.

In *2018 9th International Conference on Mechanical and Aerospace Engineering (ICMAE)*, pages 100–105. IEEE, 2018.

[86] Sadeque Hamdan, Ali Cheaitou, Oualid Jouini, Tobias Andersson Granberg, Zied Jemai, Imad Alsyouf, Maamar Bettayeb, and Billy Josefsson. Central authority–controlled air traffic flow management: An optimization approach. *Transportation Science*, 56(2):299–321, 2022.

[87] Mercedes Pelegrín, Claudia d'Ambrosio, Rémi Delmas, and Youssef Hamadi. Urban air mobility: From complex tactical conflict resolution to network design and fairness insights. 2021.

[88] Pengcheng Wu, Junfei Xie, Yanchao Liu, and Jun Chen. Risk-bounded and fairness-aware path planning for urban air mobility operations under uncertainty. *Aerospace Science and Technology*, 127:107738, 2022.

[89] Christopher Chin, Karthik Gopalakrishnan, Maxim Egorov, Antony Evans, and Hamsa Balakrishnan. Efficiency and fairness in unmanned air traffic flow management. *IEEE Transactions on Intelligent Transportation Systems*, 22(9):5939–5951, 2021.

[90] Mehdi Bennaceur, Rémi Delmas, and Youssef Hamadi. Passenger-centric urban air mobility: Fairness trade-offs and operational efficiency. *Transportation Research Part C: Emerging Technologies*, 136:103519, 2022.

[91] Daniel Kuhn, Peyman Mohajerin Esfahani, Viet Anh Nguyen, and Soroosh Shafieezadeh-Abadeh. Wasserstein distributionally robust optimization: Theory and applications in machine learning. In *Operations Research & Management Science in the Age of Analytics*, pages 130–166. INFORMS, 2019.

[92] Bozidar Radunovic and Jean-Yves Le Boudec. A unified framework for max-min and

min-max fairness with applications. *IEEE/ACM Transactions on networking*, 15(5): 1073–1083, 2007.

[93] Jianbo Du, Liqiang Zhao, Jie Feng, and Xiaoli Chu. Computation offloading and resource allocation in mixed fog/cloud computing systems with min-max fairness guarantee. *IEEE Transactions on Communications*, 66(4):1594–1608, 2017.

[94] Rui Gao and Anton J Kleywegt. Distributionally robust stochastic optimization with Wasserstein distance. *arXiv preprint arXiv:1604.02199*, 2016.

[95] Jose Blanchet, Karthyek Murthy, and Nian Si. Confidence regions in Wasserstein distributionally robust estimation. *arXiv preprint arXiv:1906.01614*, 2019.

[96] Peyman Mohajerin Esfahani and Daniel Kuhn. Data-driven distributionally robust optimization using the Wasserstein metric: Performance guarantees and tractable reformulations. *Mathematical Programming*, 171(1-2):115–166, 2018.

[97] Jose Blanchet and Karthyek Murthy. Quantifying distributional model risk via optimal transport. *Mathematics of Operations Research*, 44(2):565–600, 2019.

[98] Grani A Hanasusanto and Daniel Kuhn. Conic programming reformulations of two-stage distributionally robust linear programs over Wasserstein balls. *Operations Research*, 66(3):849–869, 2018.

[99] Zhi Chen, Daniel Kuhn, and Wolfram Wiesemann. Data-driven chance constrained programs over Wasserstein balls. *arXiv preprint arXiv:1809.00210*, 2018.

[100] Weijun Xie. On distributionally robust chance constrained programs with Wasserstein distance. *Mathematical Programming*, pages 1–41, 2019.

[101] Soroosh Shafieezadeh Abadeh, Viet Anh Nguyen, Daniel Kuhn, and Peyman Mohajerin Mohajerin Esfahani. Wasserstein distributionally robust kalman filtering. In *Advances in Neural Information Processing Systems*, pages 8474–8483, 2018.

[102] Jose Blanchet, Yang Kang, and Karthyek Murthy. Robust Wasserstein profile inference and applications to machine learning. *Journal of Applied Probability*, 56(3):830–857, 2019.

[103] Zhi Chen and Weijun Xie. Sharing the value-at-risk under distributional ambiguity. *Available at SSRN 3400033*, 2019.

[104] Dimitris Bertsimas, Shimrit Shtern, and Bradley Sturt. A data-driven approach for multi-stage linear optimization. *Available at Optimization Online*, 2018.

[105] Nicolas Fournier and Arnaud Guillin. On the rate of convergence in Wasserstein distance of the empirical measure. *Probability Theory and Related Fields*, 162(3-4):707–738, 2015.

[106] Nicolás Garcia Trillos and Dejan Slepčev. On the rate of convergence of empirical measures in ∞ transportation distance. *Canadian Journal of Mathematics*, 67(6): 1358–1383, 2015.

[107] Weijun Xie. Tractable reformulations of two-stage distributionally robust linear programs over the type-∞ Wasserstein ball. *Operations Research Letters*, 48(4):513–523, 2020.

[108] Weijun Xie, Jie Zhang, and Shabbir Ahmed. Distributionally robust bottleneck combinatorial problems: Uncertainty quantification and robust decision making. *Mathematical Programming*, pages 1–44, 2021.

[109] Garth P McCormick. Computability of global solutions to factorable nonconvex programs: Part I- convex underestimating problems. *Mathematical programming*, 10(1): 147–175, 1976.

[110] Egon Balas. Disjunctive programming. *Annals of discrete mathematics*, 5:3–51, 1979.

[111] Shabbir Ahmed. A scenario decomposition algorithm for 0–1 stochastic programs. *Operations Research Letters*, 41(6):565–569, 2013.

[112] Kevin Ryan, Shabbir Ahmed, Santanu S Dey, Deepak Rajan, Amelia Musselman, and Jean-Paul Watson. Optimization-driven scenario grouping. *INFORMS Journal on Computing*, 32(3):805–821, 2020.

[113] Akshay Gupte, Shabbir Ahmed, Myun Seok Cheon, and Santanu Dey. Solving mixed integer bilinear problems using milp formulations. *SIAM Journal on Optimization*, 23 (2):721–744, 2013.

[114] United Nations. *World Urbanization Prospects 2018*, 2018. Available at https://population.un.org/wup/Download/ (last accessed date: October 27, 2022).

[115] David Schrank, Luke Albert, Bill Eisele, Tim Lomax, et al. Urban mobility report 2021. 2021.

[116] M Grazia Speranza. Trends in transportation and logistics. *European Journal of Operational Research*, 264(3):830–836, 2018.

[117] George Price, Douglas Helton, Kyle Jenkins, Mike Kvicala, Steve Parker, and Russell Wolfe. Urban air mobility operational concept (opscon) passenger-carrying operations. 2020. Available at https://ntrs.nasa.gov/citations/20205001587 (last accessed date: October 27, 2022).

[118] Robin Lineberger, Aijaz Hussain, and Vincent Rutgers. Change is in the air: The elevated future of mobility: What's next on the horizon? 2018. Available at https://www2.deloitte.com/content/dam/Deloitte/us/Documents/energy-resources/di-the-elevated-future-of-mobility.pdf (last accessed date: October 27, 2022).

[119] R Tyrrell Rockafellar, Stanislav Uryasev, et al. Optimization of conditional value-at-risk. *Journal of risk*, 2:21–42, 2000.

[120] Ronald L Graham. Bounds for certain multiprocessing anomalies. *Bell system technical journal*, 45(9):1563–1581, 1966.

[121] JA Hoogeveen, Steef L van de Velde, and Bart Veltman. Complexity of scheduling multiprocessor tasks with prespecified processor allocations. *Discrete Applied Mathematics*, 55(3):259–272, 1994.

[122] J.F. Benders. Partitioning procedures for solving mixed-variables programming problems. *Numerische Mathematik*, 4(1):238–252, 1962.

[123] Gilbert Laporte and François V Louveaux. The integer l-shaped method for stochastic integer programs with complete recourse. *Operations research letters*, 13(3):133–142, 1993.

[124] Gianni Codato and Matteo Fischetti. Combinatorial benders' cuts for mixed-integer linear programming. *Operations Research*, 54(4):756–766, 2006.

[125] Mykel J Kochenderfer, Jessica E Holland, and James P Chryssanthacopoulos. Next-generation airborne collision avoidance system. Technical report, Massachusetts Institute of Technology-Lincoln Laboratory Lexington United States, 2012.

[126] Marc Brittain, Xuxi Yang, and Peng Wei. A deep multi-agent reinforcement learning approach to autonomous separation assurance. *arXiv preprint arXiv:2003.08353*, 2020.

[127] Pablo L Durango-Cohen and Pattharin Sarutipand. Maintenance optimization for transportation systems with demand responsiveness. *Transportation Research Part C: Emerging Technologies*, 17(4):337–348, 2009.

[128] Mehmet US Ayvaci, Oguzhan Alagoz, and Elizabeth S Burnside. The effect of budgetary restrictions on breast cancer diagnostic decisions. *Manufacturing & Service Operations Management*, 14(4):600–617, 2012.

[129] Xu Chu Ding, Alessandro Pinto, and Amit Surana. Strategic planning under uncertainties via constrained markov decision processes. In *2013 IEEE International Conference on Robotics and Automation*, pages 4568–4575. IEEE, 2013.

[130] Rakshit Allamaraju, Hassan Kingravi, Allan Axelrod, Girish Chowdhary, Robert Grande, Jonathan P How, Christopher Crick, and Weihua Sheng. Human aware uas path planning in urban environments using nonstationary mdps. In *2014 IEEE International Conference on Robotics and Automation (ICRA)*, pages 1161–1167. IEEE, 2014.

[131] Nicole Bäuerle and Ulrich Rieder. *Markov decision processes with applications to finance*. Springer Science & Business Media, 2011.

[132] Jeffrey W Ohlmann and James C Bean. Resource-constrained management of heterogeneous assets with stochastic deterioration. *European Journal of Operational Research*, 199(1):198–208, 2009.

[133] S Sebnem Ahiska and Emre Kurtul. Modeling and analysis of a product substitu-

tion strategy for a stochastic manufacturing/remanufacturing system. *Computers & Industrial Engineering*, 72:1–11, 2014.

[134] Zeyi Sun and Lin Li. Potential capability estimation for real time electricity demand response of sustainable manufacturing systems using Markov decision process. *Journal of cleaner production*, 65:184–193, 2014.

[135] Yisha Xiang, C Richard Cassady, Tongdan Jin, and Cai Wen Zhang. Joint production and maintenance planning with machine deterioration and random yield. *International Journal of Production Research*, 52(6):1644–1657, 2014.

[136] Katsuhisa Ohno, Toshitaka Boh, Koichi Nakade, and Takayoshi Tamura. New approximate dynamic programming algorithms for large-scale undiscounted Markov decision processes and their application to optimize a production and distribution system. *European Journal of Operational Research*, 249(1):22–31, 2016.

[137] Xuchu Ding, Stephen L Smith, Calin Belta, and Daniela Rus. Optimal control of Markov decision processes with linear temporal logic constraints. *IEEE Transactions on Automatic Control*, 59(5):1244–1257, 2014.

[138] Mohammad Abu Alsheikh, Dinh Thai Hoang, Dusit Niyato, Hwee-Pink Tan, and Shaowei Lin. Markov decision processes with applications in wireless sensor networks: A survey. *IEEE Communications Surveys & Tutorials*, 17(3):1239–1267, 2015.

[139] Eunshin Byon and Yu Ding. Season-dependent condition-based maintenance for a wind turbine using a partially observed Markov decision process. *IEEE Transactions on Power Systems*, 25(4):1823–1834, 2010.

[140] Samuele Grillo, Antonio Pievatolo, and Enrico Tironi. Optimal storage scheduling

using Markov decision processes. *IEEE Transactions on Sustainable Energy*, 7(2): 755–764, 2016.

[141] Lydia T Liu, Sarah Dean, Esther Rolf, Max Simchowitz, and Moritz Hardt. Delayed impact of fair machine learning. In *International Conference on Machine Learning*, pages 3150–3158. PMLR, 2018.

[142] Lily Hu and Yiling Chen. A short-term intervention for long-term fairness in the labor market. In *Proceedings of the 2018 World Wide Web Conference*, pages 1389–1398, 2018.

[143] Yaowei Hu and Lu Zhang. Achieving long-term fairness in sequential decision making. In *Proceedings of the AAAI Conference on Artificial Intelligence*, volume 36, pages 9549–9557, 2022.

[144] Laurence A Wolsey and George L Nemhauser. *Integer and combinatorial optimization*. John Wiley & Sons, 1988.

[145] Thomas L Magnanti, Jeremy F Shapiro, and Michael H Wagner. Generalized linear programming solves the dual. *Management science*, 22(11):1195–1203, 1976.

[146] David Blackwell. Discounted dynamic programming. *The Annals of Mathematical Statistics*, 36(1):226–235, 1965.

[147] Erick Delage and Yinyu Ye. Distributionally robust optimization under moment uncertainty with application to data-driven problems. *Operations research*, 58(3):595–612, 2010.

Appendices

Appendix A

Appendix of Chapter 3

A.1 Summary Statistics of Data

Blacksburg Transit operates 17 routes that cover different areas of the town. We notice that most stops have small passenger arrival and alighting rates, while a few stops have larger values. Buses are almost empty most of the time but may be crowded when a big group of passengers gets onto the bus at some stops. The detailed summary of statistics of 17 routes is described in Table A.1.

Table A.1: Summary of Statistics of the Blacksburg Transit Data

Route	Loop Time (min)	Num of Stops	Current Headway (min)	Number of Passengers on Bus			Passenger Arrival Rate			Proportion of Passengers Alighting		
				Average	Max	Min	Average	Max	Min	Average	Max	Min
CAS	20.0	10.0	20.0	1.1	10.0	0.0	0.5	3.0	0.0	0.1	1.0	0.0
CRC	45.0	32.0	15.0	4.8	60.0	0.0	0.5	4.0	0.0	0.1	1.0	0.0
CBD	30.0	15.0	30.0	2.6	17.0	0.0	0.5	4.0	0.0	0.0	1.0	0.0
HXP	30.0	23.0	15.0	2.7	25.0	0.0	0.5	3.0	0.0	0.1	1.0	0.0
HWA	30.0	18.0	10.0	1.9	14.0	0.0	0.7	5.0	0.0	0.2	1.0	0.0
HWB	30.0	20.0	10.0	3.2	18.0	0.0	0.9	4.0	0.0	0.1	1.0	0.0
HDG	30.0	30.0	15.0	2.6	27.0	0.0	0.6	4.0	0.0	0.2	1.0	0.0
MSS	60.0	40.0	15.0	5.3	65.0	0.0	0.7	12.0	0.0	0.1	1.0	0.0
TOM	30.0	26.0	15.0	2.5	28.0	0.0	0.5	6.0	0.0	0.0	1.0	0.0
UMS	20.0	11.0	10.0	1.3	11.0	0.0	0.6	5.0	0.0	0.2	1.0	0.0
MSN	60.0	37.0	15.0	5.8	67.0	0.0	0.6	8.0	0.0	0.1	1.0	0.0
PHD	30.0	25.0	15.0	2.2	25.0	0.0	0.6	7.0	0.0	0.1	1.0	0.0
PRB	30.0	29.0	30.0	2.4	29.0	0.0	0.6	17.0	0.0	0.1	1.0	0.0
PRO	30.0	15.0	15.0	0.9	9.0	0.0	0.6	7.0	0.0	0.2	1.0	0.0
MSA	30.0	35.0	30.0	3.9	35.0	0.0	0.4	3.0	0.0	0.0	1.0	0.0
TTT	60.0	15.0	60.0	2.7	26.0	0.0	0.8	16.0	0.0	0.2	1.0	0.0
UCB	30.0	17.0	15.0	2.6	17.0	0.0	0.6	2.0	0.0	0.1	1.0	0.0

A.2 Testing Integrality of L_{ij}

We tested six small instances to compare the objective value of MILP formulations with the integer $\boldsymbol{L}$ as well as the objective value of MILP with relaxing the integrality of $\boldsymbol{L}$, where the number of bus routes I is 5 and the number of scenarios N is 6. There are $K = 3$ types of buses with nominal capacities $c_1 = 60, c_2 = 80, c_3 = 120$. Each route has $10 \sim 40$ stops. We let $\boldsymbol{\eta} = (4, 6, 3), \delta = 0.25, \omega = 5, \theta = 0, \gamma = 100$. The passenger arrival rates were assumed to follow uniform distributions with the minimum value ranging from 2 to 20 and the maximum one from 22 to 40, and the proportion of passengers alighting from the bus was randomly generated from triangular distributions with the lower limit ranging from 0 to 0.2, the upper limit range from 0.6 to 1, and the mode ranging from 0.45 to 0.55. The results are shown in Table A.2. By relaxing the integrality of $\boldsymbol{L}$, the solution time decreases around 15%, which is not very significant since our model is for strategic planning purposes. However, we see that the objective value by relaxing passenger number to be continuous can decrease by around 14%, which can be quite significant and cause misleading decisions. Relaxing the integrality of $\boldsymbol{L}$ can result in a misleading solution as shown in Table A.3, where different routes have different bus assignments. Dominant routes in each scenario (i.e., the ones having the largest weighted sum of bus utilization and passenger abandon rates) are also different. Since there is no big improvement in the solution time, we believe that keeping integer $\boldsymbol{L}$ is necessary for the sake of solution quality.

A.3 Reformulation of the Model (3.1) with Moment Ambiguity Set

Table A.2: Objective Value of MILP with Integer $\boldsymbol{L}$ and MILP with Continuous $\boldsymbol{L}$

Instance	Integer $\boldsymbol{L}$		Continuous $\boldsymbol{L}$		Relative
	Obj.Val	Time	Obj.Val	Time	Difference(%)
1	1.148	11.0	0.948	10.3	17.4
2	1.241	16.4	1.034	13.5	16.7
3	1.178	22.9	1.022	20.9	13.3
4	1.106	22.5	0.986	17.1	10.8
5	1.104	18.8	0.978	14.2	11.5
6	1.330	13.3	1.163	12.0	12.5

Table A.3: Bus assignment of MILP with Integer $\boldsymbol{L}$ and MILP with Continuous $\boldsymbol{L}$

	Integer $\boldsymbol{L}$				Continuous $\boldsymbol{L}$			
Obj.Val	0.942				0.916			
Route	Dominant Scenario	Bus 1	Bus 2	Bus 3	Dominant Scenario	Bus 1	Bus 2	Bus 3
1	2			1				1
2				2	1-6		4	
3	1, 3-6		3				2	
4			3					2
5		3				4		

A.3. Reformulation of the Model (3.1) with Moment Ambiguity Set

Let us consider the following moment ambiguity set (Delage and Ye [147])

$$\mathcal{P}(\Xi, \boldsymbol{\mu}_0, \boldsymbol{\Sigma}_0) = \left\{ \mathbb{P} \in \mathcal{M} \left| \begin{array}{l} P(\boldsymbol{\xi} \in \Xi) = 1, \\ (\mathbb{E}[\boldsymbol{\xi}] - \boldsymbol{\mu}_0)^T \boldsymbol{\Sigma}_0^{-1} (\mathbb{E}[\boldsymbol{\xi}] - \boldsymbol{\mu}_0) \leq 0, \\ \mathbb{E}[(\boldsymbol{\xi} - \boldsymbol{\mu}_0)(\boldsymbol{\xi} - \boldsymbol{\mu}_0)^T] \preceq \boldsymbol{\Sigma}_0 \end{array} \right. \right\}, \tag{A.1}$$

where $\boldsymbol{\mu}_0$ is the unbiased estimate of mean, $\boldsymbol{\Sigma}_0$ is the upper bound of the covariance matrix, $\mathcal{M}$ denotes the set of all the possible nonnegative measures. Given any $(\boldsymbol{n}, \boldsymbol{x}) \in \mathcal{X} = \{(\boldsymbol{n}, \boldsymbol{x}) : (3.1b) - (3.1f)\}$, according to lemma 1 in Delage and Ye [147], the optimal value of the inner supremum problem

$$\sup_{\mathbb{P} \in \mathcal{P}(\Xi, \boldsymbol{\mu}_0, \boldsymbol{\Sigma}_0)} \mathbb{E}_{\mathbb{P}} \left[\mathcal{Q}\left(\boldsymbol{n}, \boldsymbol{x}, \tilde{\boldsymbol{\xi}}\right) \right]$$

is equal to the optimal value of the following problem:

$$\min_{s,t,\boldsymbol{H} \succeq 0, \boldsymbol{q}} \quad s + t \tag{A.2a}$$

$$\text{s.t.} \quad r \geq \mathcal{Q}(\boldsymbol{n}, \boldsymbol{x}, \boldsymbol{\xi}) - \boldsymbol{\xi}^T \boldsymbol{H} \boldsymbol{\xi} - \boldsymbol{\xi} \boldsymbol{q}, \quad \forall \boldsymbol{\xi} \in \Xi, \tag{A.2b}$$

$$t \geq \left(\boldsymbol{\Sigma}_0 + \boldsymbol{\mu}_0 \boldsymbol{\mu}_0^T\right) \cdot \boldsymbol{H} + \boldsymbol{\mu}_0^T \boldsymbol{q}. \tag{A.2c}$$

Therefore, model (3.1) under the moment ambiguity set $\mathcal{P}$ is equivalent to solve

$$\min_{s,t,\boldsymbol{H} \succeq 0, \boldsymbol{q}} \{s + t : (A.2b), (A.2c)\}. \tag{A.3}$$

However, the separation over constraints (A.2b) is rather difficult, since $\mathcal{Q}(\boldsymbol{n}, \boldsymbol{x}, \boldsymbol{\xi})$ is highly nonconvex and nonlinear in $\boldsymbol{\xi}$.